SEISMIC EVALUATION OF PILE GROUPS

by

Hüseyin Afşin BEKER

B.S. in Civil Engineering, Yıldız Technical University, 1999

Submitted to the Kandilli Observatory and

Earthquake Research Institute in partial fulfillment of

the requirements for the degree of

Master of Science

in

Earthquake Engineering

Bogazici University Library

39001102311092

Boğaziçi University

2003

ACKNOWLEDGEMENTS

First I would like to thank my thesis supervisor Assoc.Prof.Dr. Bilge Siyahi for her guidance through preparing this thesis. Also I would like to thank Prof. Dr. Mustafa Erdik, Prof. Dr. Nuray Aydınoğlu and Prof. Dr. Özal Yüzügüllü for their valuable information during the courses.

I want to express my deepest gratitude to my family for their support throughout my life.

I would like to sincerely thank to MS EQE Ali Yalçın Salkın for his guidance and help, not only as a friend but also as a member of my family.

Also I would like to thank the following people for their help; Kemal Beyen, Yavuz Kaya, Hakan Akman, M.Ergenekon Selçuk, Utku Celep and Göktürk Önem.

ĞAZİÇİ
ERSİTESİ
PHANESİ
657309

ABSTRACT

In certain regions of the country, designing deep foundations to withstand seismic loading is a reality. Seismic loading of structures and foundations reach a critical state as the laterally applied force increases. Especially liquefaction is the major effect on laterally loaded piles. So firstly, the liquefaction potential of the site has been evaluated to make the best seismic assessment, as studied in the following chapter.

Since, liquefaction potential analysis is highly complex and is based on numerous variables such as moment magnitude, epicentrical distance, PGA, thickness of soil layers, overburden pressure and duration of motion etcetera. Most of the potential analysis methods are empirically based on the statistical measurements of known past earthquakes. Thus, firstly the liquefaction potential analysis of the site is evaluated by means of these methods.

Secondly, the effects of liquefaction-induced lateral spreading on piles have been studied. Then, after a brief information is given about the structure, which is chosen as the model, the capacity estimations of the piles and the superstructure are acquired.

Then soil, piles and the superstructure are modeled together in the SAP2000 computer program. Liquefaction-induced lateral spreading, spectral analysis (for TSC-98) and non-linear time-history analysis, with three different earthquake records (two of them are simulated), are examined.

Finally, the results of the most critically forced structural elements are illustrated and then compared both by the structural capacity and between the different methods of solutions used. This study also gives a general knowledge about the sufficiency of the Turkish Seismic Code for buildings within the vicinity of an active fault line.

ÖZET

Ülkenin çoğu bölgesinde, derin temellerin dizaynında, sismik yatay kuvvetleri göz önünde bulundurmak bir zorunluluktur. Özellikle, zemin sıvılaşması kazıklı temellere etkiyen yatay yüklerin arasında en önemlisidir. Bu yüzden ilk bölümde, kazıklı temellerin sismik hesabı yapılırken, öncelikle söz konusu bölgenin sıvılaşma potansiyeli hesaplandı.

Zemin sıvılaşma potansiyelinin hesabı, son derece kompleks ve çok fazla bilinmeyene dayalı olduğu için (Örn. Depremin büyüklüğü, episantıra olan uzaklığı, pik ivme değeri, zemin tabakalarının kalınlığı ve depremin süresi vs.) potansiyel analiz hesaplarının tamamına yakını geçmiş büyük depremlerin istatistiksel verilerini baz alan ampirik formüllere dayalıdır. O yüzden, bu çalışmada öncelikle sıvılaşma potansiyel analizi yapıldı.

İkinci olarak, sıvılaşmadan mütevelli yatay sürülmenin kazıklar üzerindeki etkisi araştırıldı. Bu analizleri uygulamak üzere seçilen model yapı hakkında verilen özet bir bilgiden sonra, hem altyapının (kazıklar) hem de üst yapının kapasite hesaplarına geçildi.

Daha sonra, zemin, kazıklar ve üst yapı birlikte SAP2000 yapısal analiz programında modellendi. Yatay sürülme, Türkiye Deprem Yönetmeliği'ne göre spektral analiz ve zaman-tanım aralığında çözüm metotlarına dayalı olarak, yapı üç farklı analiz yöntemiyle çözümlendi.

Son olarak bu sonuçlar, en kritik kesitler için değerlendirildi ve analiz yöntemlerinin kazıklı bina çözümleri için detaylı bir karşılaştırılması elde edilmiş oldu. Bu çalışmada ayrıca, faya yakın bölgelerde TDY-98'e göre spektral analiz yaparken dikkat edilmesi gereken hususlar değerlendirildi.

TABLE OF CONTENTS

LIST OF FIGURES

LIST OF TABLES

1. INTRODUCTION

Deep foundations consisting of driven or cast-in-place piles are conventionally employed to transfer axial structural loads through soft soils to stronger bearing strata at a depth. The demand on these elements arises, where making a deep footing design costs are considerably expensive. These foundation elements may also be subject to cyclic lateral loads caused by earthquake, wind, wave or ship impact.

The advantages of piles on soft soils have been widely understood especially after 1964 Niigata earthquake, and 1999 Kocaeli earthquake in Turkey, because both of these earthquakes caused severe structural damages and life-loss due to the stability problems. The weak soils especially, which tend to liquefy, demand deep foundations that prevent the structure from cyclic mobility or lateral flow of the base, which is also known as liquefaction. Thus, extra precautions must be considered during the design procedure at the sites, such as at the vicinity of an active faulting, or having a high potential of liquefaction.

However, as a matter of foundation engineering, soil liquefaction has been the major cause of damage to pile foundations in many of the past strong earthquakes, because liquefaction and/or strain-softening potential in soft soils can impose additional demands on pile foundation systems. Especially, the numerous well-documented case histories of damaged piles due to liquefaction in the 1995 Kobe earthquake have triggered intensive research on the subject in an effort to better understand the soil-pile interaction in liquefied soils and to improve the seismic design of piles.

As a result, while the evaluation of a structure design in a seismic zone, the substructure's conditions must be taken into account as well as the superstructure due to the cooperated response of structure and the foundation. And this is an example study of aseismic evaluation of pile foundations associated with the superstructure.

2. LIQUEFACTION PHENOMENA

Liquefaction is one of the most important, interesting, complex, and controversial topics in geotechnical engineering. Its devastating effects sprang to the attention of geotechnical engineers in a three-month period in 1964 when the Good Friday earthquake (M_w=9.2) in Alaska was followed by the Niigata earthquake (Ms=7.5) in Japan. Both earthquakes produced spectacular examples of liquefaction-induced damage, including slope failures, bridge and building foundation failures, and flotation of buried structures. In the 30 years since these two earthquakes, liquefaction has been studied by hundreds of researchers around the world. Much has been learned, but the road has not been smooth. Different terminologies, procedures and methods of analysis have been proposed, and a prevailing approach has been slow to emerge.

In recent years, many of these differences have been reconciled by the realization that their causes were due, in large part, to semantics. The term liquefaction has been used to describe a number of different, though related phenomena. Rather than trying to trace the convoluted development of the current state of knowledge regarding liquefaction, this chapter will present a basic framework for the conceptual understanding of liquefaction-related soil behavior and use it to describe various methods by which liquefaction hazards can be evaluated. To do this, the chapter introduces some new terminology to distinguish between phenomena that have frequently been lumped together under the heading of *liquefaction. The* new terminology allows these phenomena to be illustrated in a way that simplifies understanding of their mechanics and the manner in which they contribute to earthquake damage.

Terminology

The term *liquefaction,* originally coined by Mogami and Kubo (1953), has historically been used in conjunction with a variety of phenomena that involve soil deformations caused by monotonic, transient or repeated disturbance of saturated cohesionless soils under undrained conditions. The generation of excess pore pressure under undrained loading conditions is a hallmark of all liquefaction phenomena. The tendency for dry cohesionless soils to densify under both static and cyclic loading is well known. When cohesionless soils are saturated, however, rapid loading occurs under undrained conditions, so tendency for densification causes excess pore pressures to increase and effective stresses to decrease (Kramer, 1996).

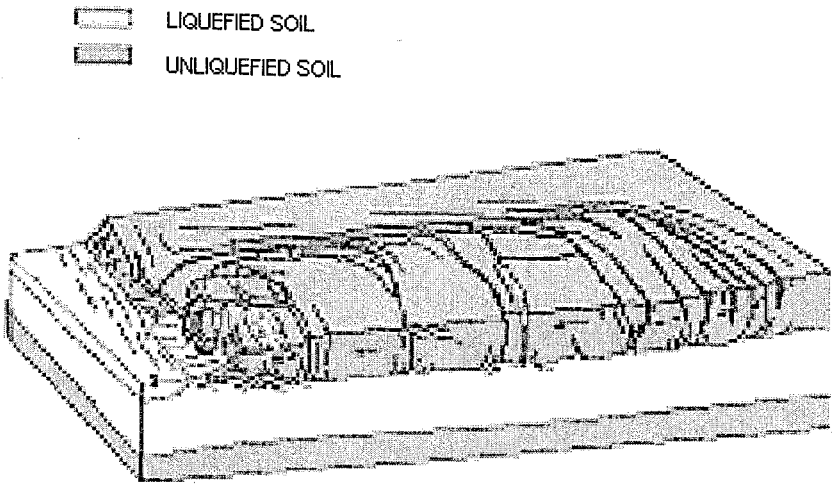

Figure 2-1 Schematic Description of a Lateral Spread Resulting from Soil Liquefaction (NRC, 1985)

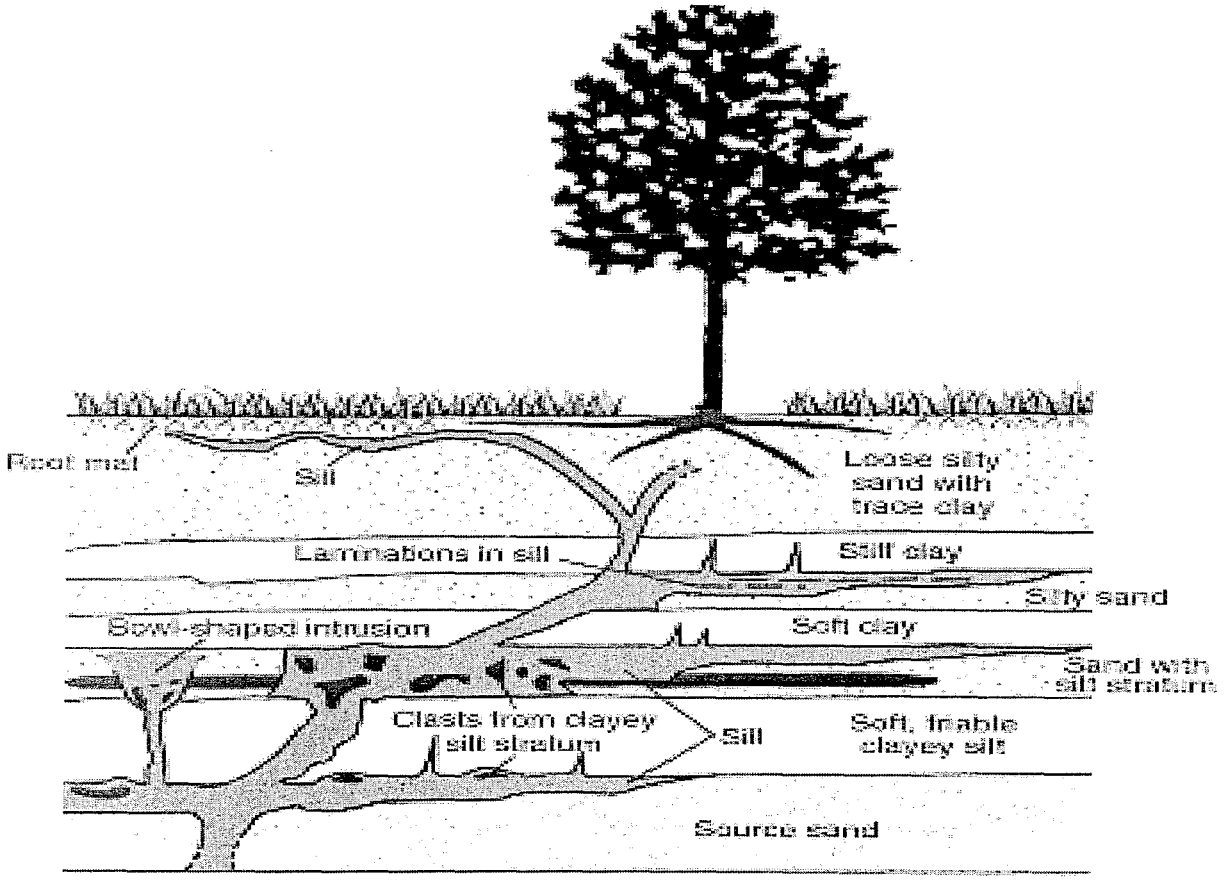

Figure 2-2 The Schematic Section of the Sand's Venting to the Surface (Kramer, 1996)

2.1. Types of Liquefaction

Liquefaction phenomena that result from this process can be divided into two main groups: *flow liquefaction* and *cyclic mobility*. Both flow liquefaction and cyclic mobility are very important, and any evaluation of liquefaction hazards should carefully consider both. In the field, flow liquefaction occurs much less frequently than cyclic mobility but its effects are usually far more severe. Cyclic mobility, on the other hand, can occur under a much broader range of soil and site conditions than flow liquefaction; its effects can range from insignificant to highly damaging. In the following, the generic term *liquefaction* will be taken to include both flow liquefaction and cyclic mobility.

2.1.1. Flow Liquefaction

This can occur when the static shear stress in a liquefiable soil layer is greater than the steady state strength of the soil. It can produce devastating flow slide failures during or after earthquake shaking. Flow liquefaction can occur only in loose soils.

Figure 2-3 A Small Flow Slide along the Shore of Lake Merced in San Francisco in 1957 (Kramer, 1996)

2.1.2. Cyclic Mobility

This can occur when the static shear stress is less than the steady-state strength and the cyclic shear stress is large enough. The steady-state strength is exceeded from moment to moment. Deformations produced by cyclic mobility develop incrementally but can become stable by the end of a strong and/or long duration earthquake. Cyclic mobility can occur in both loose and dense soils. Deformation decreases remarkably with increased density.

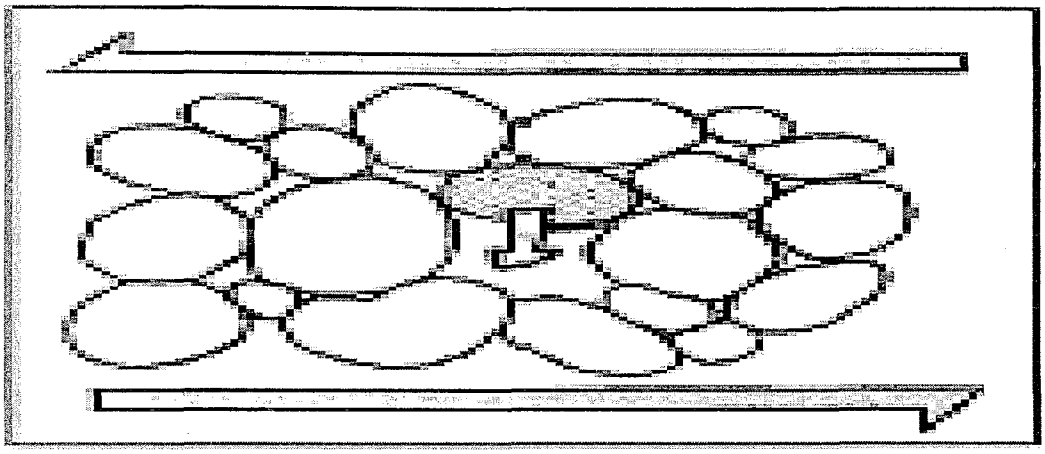

Figure 2-4 Schematic Illustration of the Shear Effect on Cohesionless Soils (NRC, 1985)

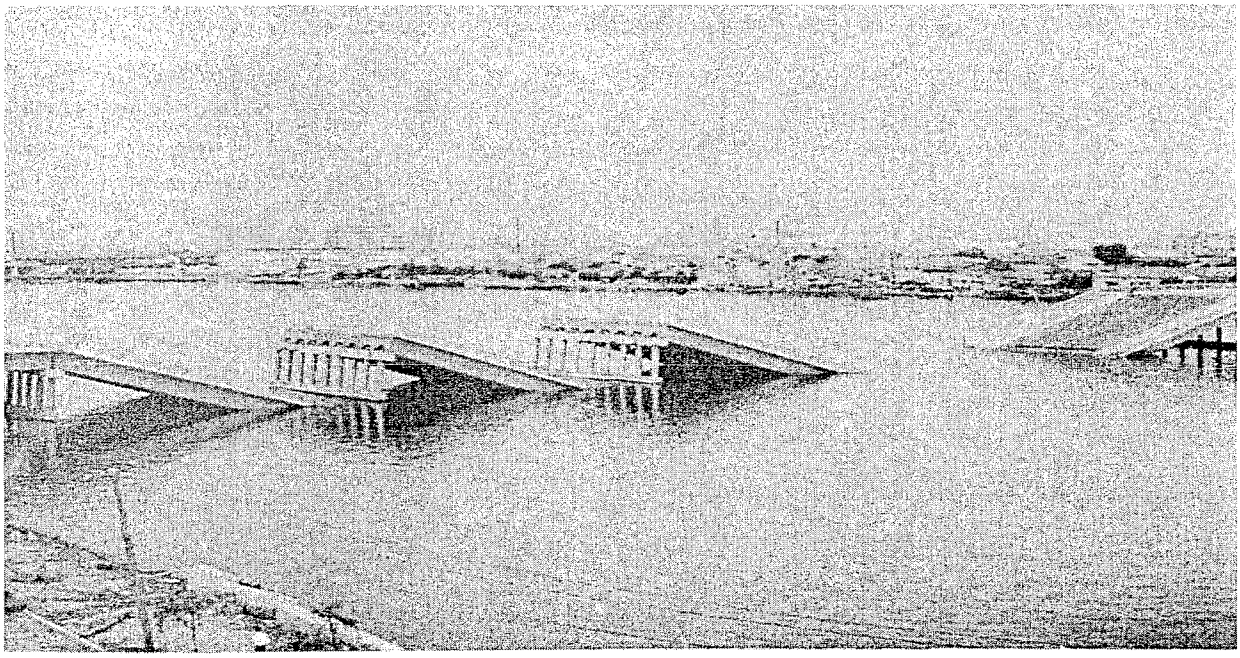

Figure 2-5 The Showa Bridge Following The 1964 Niigata Earthquake

Lateral Spreading Caused Bridge Pier Foundations to Move and Rotate Sufficiently for Simply Supported Bridge Spans to Fall (USGS Collection)

2.2. Effects of Liquefaction

The effects of liquefaction are different for different liquefaction phenomena. Although flow liquefaction is capable of producing the most spectacular effects, cyclic mobility can also produce extensive damage.

Liquefaction can dramatically alter the amplitude and frequency content of ground surface motions. As the build up of excess pore pressure causes a layer of liquefiable soil to soften, ground surface displacements may increase even when ground surface accelerations decrease. Ground oscillation may produce chaotic permanent movement of fractured blocks of surficial soil.

Ground surface settlement can develop during and/or after earthquakes due to the densification of dry or saturated sands. Settlement of dry sand occurs immediately, but settlement of saturated sands may not develop until well after earthquake shaking has ended. The magnitude of post earthquake settlement depends on the density of the sand, and on the amplitude and duration of shaking.

Figure 2-6 Liquefaction Failures in 1964 Niigata Earthquake (Steinbrugge Collection)

Figure 2-7 Liquefaction-Induced Settlement of Adjacent Buildings and the Uplift of the Sewage System Pipe (NZSEE, 1999)

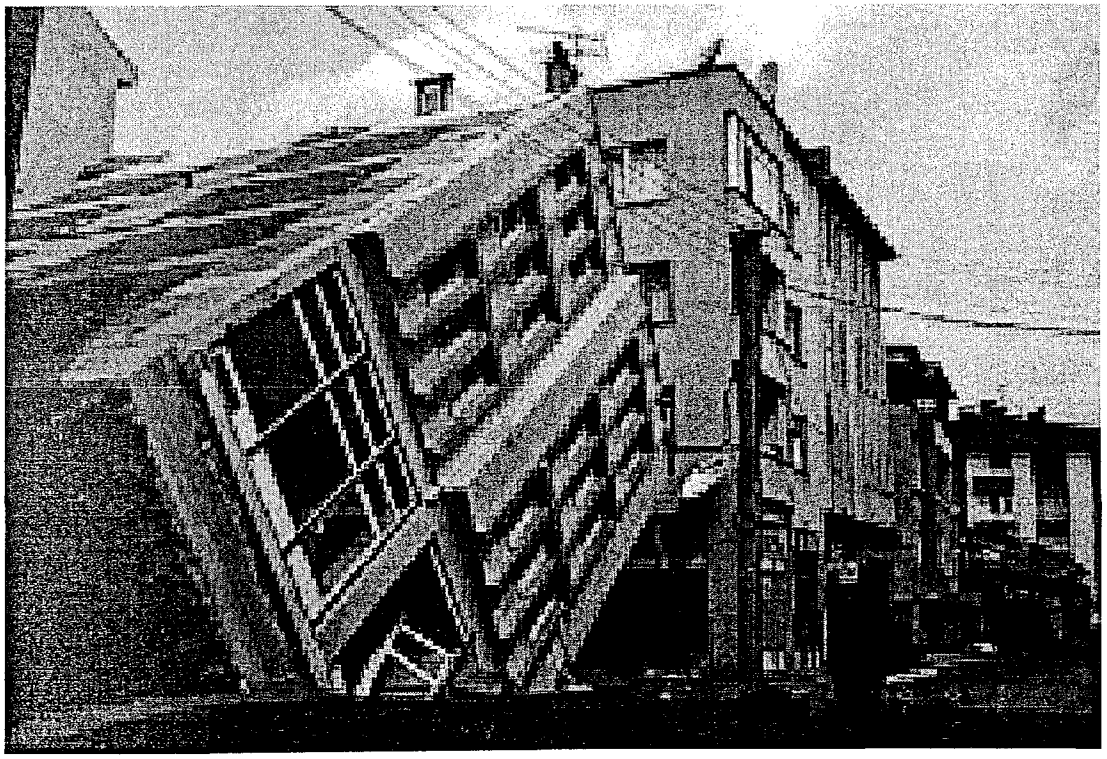

Figure 2-8 Tilted and Collapsed Buildings in Adapazarı (NZSEE, 1999)

2.3. Liquefaction Potential Analysis

The factors affecting liquefaction of sands have been extensively investigated in the past. The understanding of phenomenon has advanced to a degree that analytical procedures have been formulated to predict liquefaction at a particular site.

In 1971, Seed and Idriss presented a simplified method for evaluation of the potential for liquefaction. Seed et al. continued a series of studies and their results have been published widely. Methods for evaluation of the potential for liquefaction, by using various soil parameters, have been used in the past. However, the method of using values of blow count from the SPT has become a well-accepted procedure (Seed & Idriss, 1971).

In 1985, the Committee on earthquake engineering of National Research Council (NRC, 1985) summarized the results from all recent research and recommended a standard procedure, primarily based on the studies by Seed & Idriss, for evaluation of liquefaction potential. Today, liquefaction analysis becomes a required task for buildings or structures located in a seismic area.

2.3.1. Seed – Idriss's CSR vs. SPT Method

This empirical approach has been used for approximately 25 years to evaluate liquefaction potential in soil. It has been widely used on many projects by DSOD engineers to evaluate both embankments and foundations. CPT and Becker Hammer data is used in addition to the traditional and more commonly used SPT blow counts. The method is well liked because it is simple, relies on no undisturbed sampling or laboratory testing, and has a large body of field data to support the ensuing calculations. The major drawback is the number of correction factors that must be applied to the raw blow count data before liquefaction computations can be made. Correction factors can cumulatively change field blow counts by as much as 100 percent. While all correction factors have been logically devised, there is no certainty that they are all quantitatively valid.

2.3.1.1. Determination of CSR

Once the liquefaction resistance is known at a certain depth, the average Cyclic Shear Stress generated by an earthquake must be estimated as indicated on the right side of the flow chart. The representative horizontal shear stress is computed with a simplified equation suggested by Seed and Idriss (1971) and expressed in terms of the Cyclic Stress Ratio (CSR) given by Seed & Idriss (1983-1985)

$$CSR = 0.65 \times a_{max}/g \times \sigma_{vo}/\sigma_{vo}' \times r_d$$

$$r_d = 1.0 + 1.6 \times 10^{-6} (z^4 - 42z^3 + 105z^2 - 4200z^1)$$

Where,

r_d: *Stress reduction factor*

σ_{vo}: *Total vertical overburden stress [kN/m^2]*

σ_{vo}': *Effective vertical overburden stress [kN/m^2]*

a_{max}: *PGA of a probable earthquake [m / s^2]*

z: *Depth of the soil layer from the ground surface [m]*

2.3.1.2. Liquefaction Potential Analysis for M_w=7.5

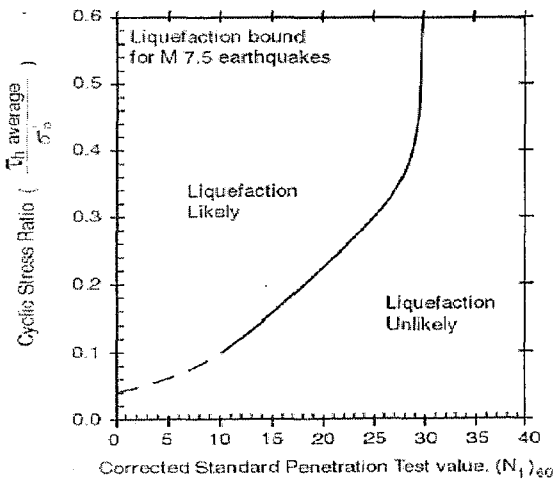

EXPLANATION

τ_h average	Average earthquake-induced horizontal cyclic shear stress.
σ'_o	Initial vertical effective overburden stress.
$(N_1)_{60}$	Standard Penetration Test blow count measured in field, modified to blow count resistance at vertical effective stress of 1 ton/ft^2 (97.5 k Pa) and 60 percent of the theoretical free-fall energy.

Peak acceleration, a_{max}, is given by the following relationship in Seed *et al.* (1985):

$$\text{Cyclic Stress Ratio} = 0.65 \cdot \frac{a_{max}}{g} \cdot \frac{\sigma_o}{\sigma'_o} \cdot r_d$$

where σ_o = total overburden stress at the depth of interest, σ'_o is the initial vertical effective stress there, g is the acceleration due tc gravity, and r_d is a stress reduction factor decreasing from 1 at the ground surface to 0.9 at the depth of 10 m.

Figure 2-9 Potential Analysis of Liquefaction for CSR vs. SPT

Seed & Idriss Method Showing Curve for Evaluation of the Potential Occurrence of Liquefaction with Accompanying Venting of Sand or Appreciable Ground Cracks for Sites on

Level Ground and a M_w= 7.5 Earthquake. Curve is for Clean Deposits. Points Above and to the Left of the Curve Have a High Potential for Liquefaction. Modified From Youd and Noble (1997)

2.3.1.3. Liquefaction Potential Analysis For Various M_w Values

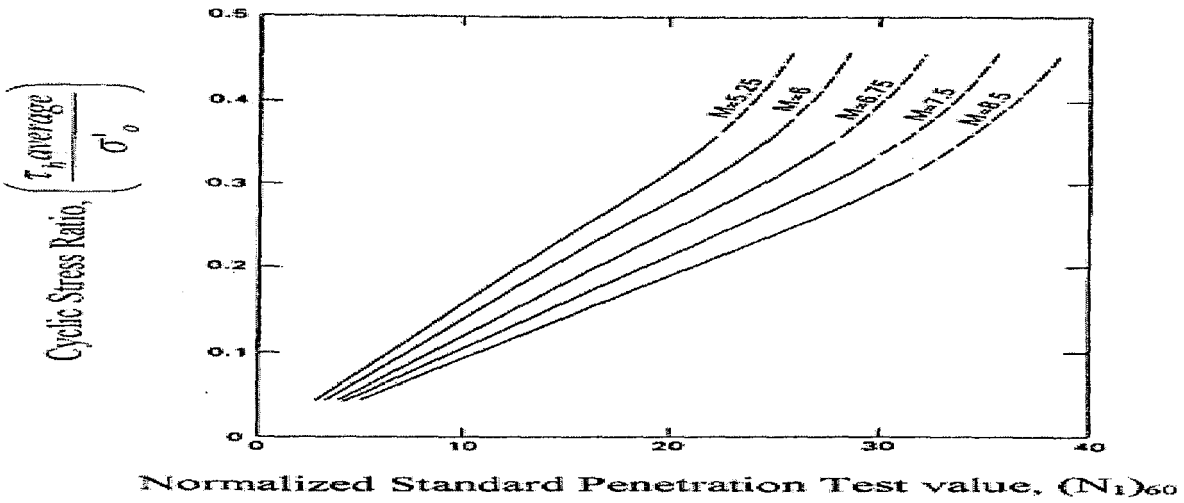

Figure 2-10 Seed & Idriss (1971) Curves for Various Values of Earthquake Magnitude The Curves Differ Very Little for the Same Value of Moment Magnitude

2.3.1.4. SPT vs. Epicentrical Distance Method

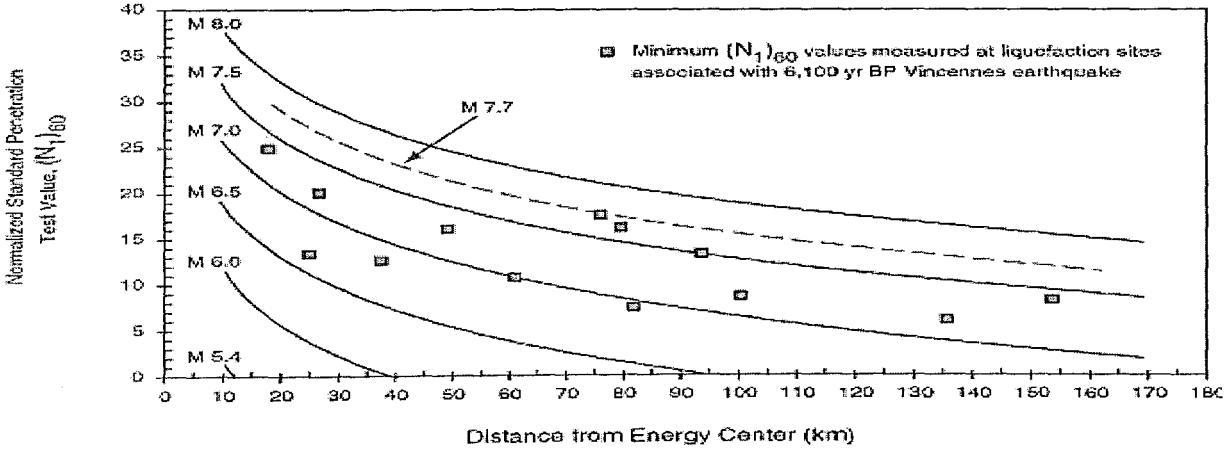

Figure 2-11 Minimum Field-Measured Values of Normalized SPT N_{60} as a Function of R

2.3.1.5. Liquefaction Potential Analysis for Various Fine Percentages

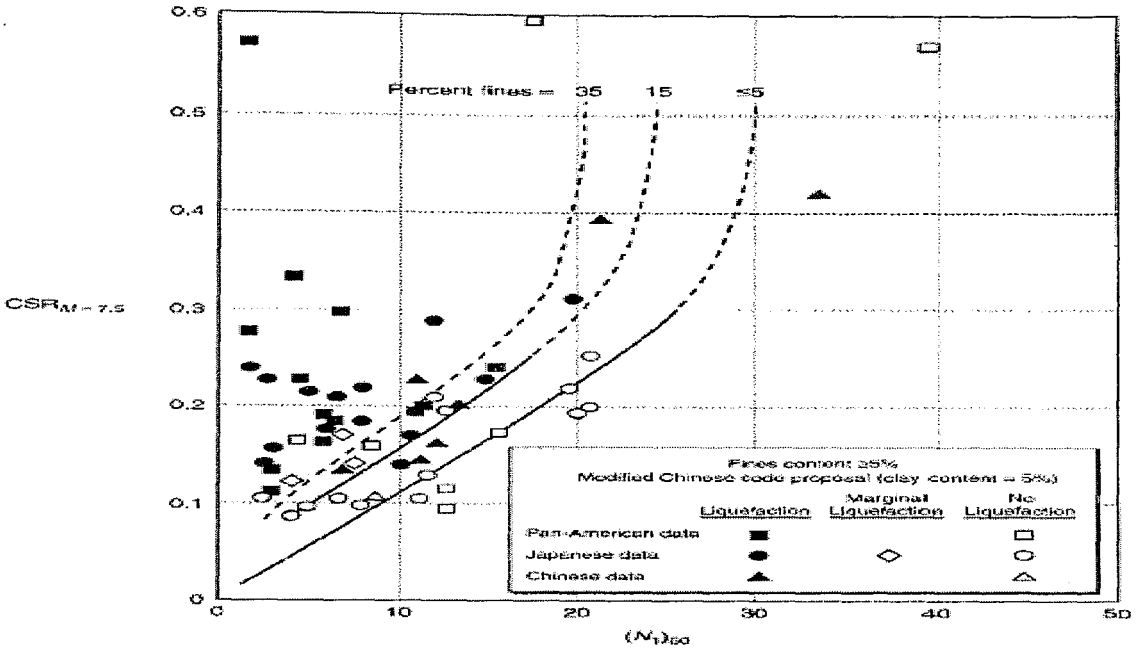

Figure 2-12 Relationship Between Cyclic Shear Stress Ratio and *N* For $M_w = 7.5$

2.3.2. Obermeier et al.'s M_w vs. Epicentrical Distance Method

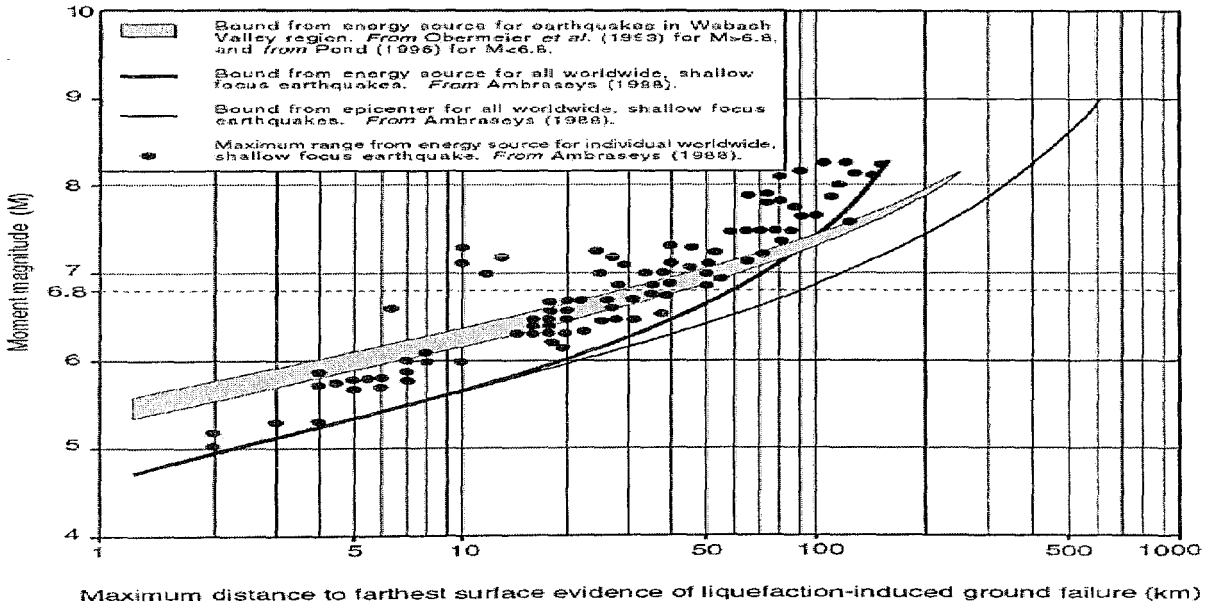

Figure 2-13 M_w vs. R of Liquefaction Effects (for Near-Field Regions R<50 km)

2.3.3. Youd and Idriss's CSR vs. SPT Method

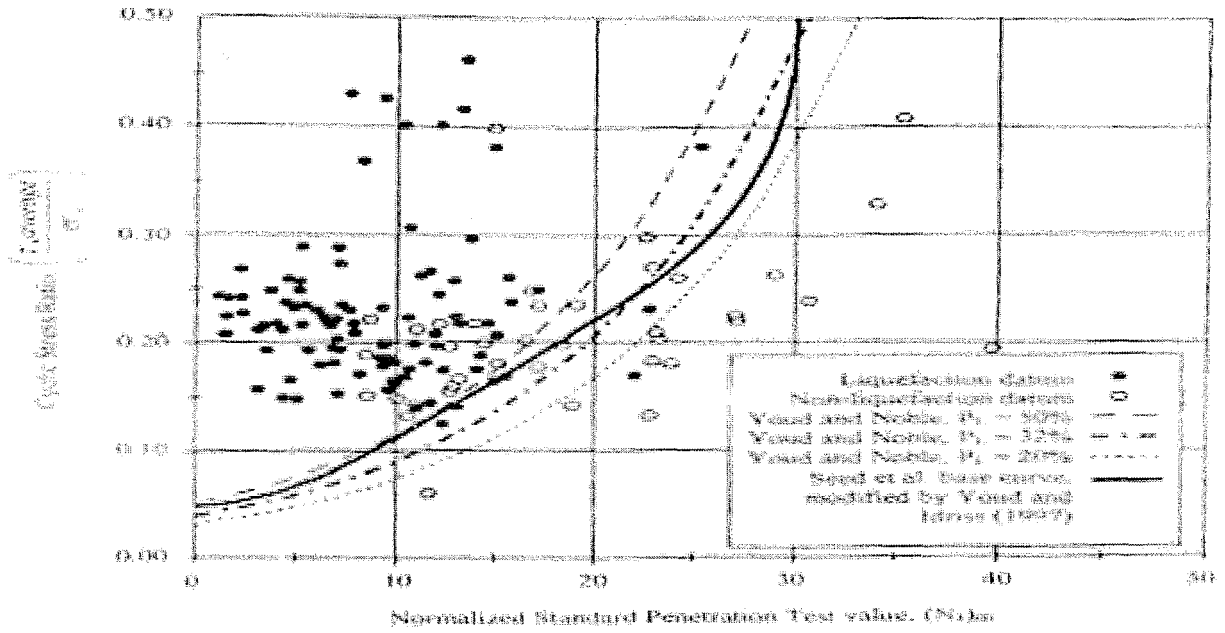

Figure 2-14 Probabilistic Liquefaction Resistance Curves for N_{60}' vs. CSR for Various P_L

2.4. Liquefaction and Lateral Spreading

When liquefaction takes place in sandy deposits during earthquakes, the ground often undergoes a large amount of permanent deformation as a result of lateral flow, even though the ground is nearly flat. In fact, Hamada et al. (1986) reported deformations as much as several meters. Permanent deformation has been observed even following the main shock and during a period of no shocks or ones of small intensity. The lateral flow is due to the action of gravity-induced shear stress, which exceeds the residual shear strength of the liquefied soil.

According to studies by Ishihara and Takeuchi (1991), there are three major ground conditions where lateral spreading can occur. The conditions are: (1) flat ground in front of a surcharge such as dikes and embankments; (2) flat ground behind a water front such as rivers, lakes and sea; and (3) slightly sloping ground. Liquefaction-induced lateral spreading can add large lateral forces on piles, which may or may not be able to remain stable.

The magnitude of the lateral forces on piles induced by lateral spreading can be predicted by techniques shown further. Relevant factors are: properties of the liquefied soil, distribution of

soil displacement, and the velocity of the lateral flow. A dramatic example of lateral spreading from Turkey in the figure below.

Figure 2-15 Lateral Spreading and Settlement Example from Gölcük (NRC,1985)

2.4.1. The Effects of Lateral Spreading on Piles

Based on the observed ground-deformation pattern using pre-earthquake and post-earthquake aerial photographs, Hamada et al. (1986) developed and empirical equation for estimating horizontal displacement of ground resulting from liquefaction-induced lateral spreading. Bartlett and Youd (1995) developed a similar, but more comprehensive model, that takes into account the magnitude of earthquake, topographical data, geological data, and soil factors. If such an estimate reveals that the lateral spreading occurs during the post-earthquake, the slowly deformed soil mass will add pressure on the existing piles. As explained earlier, the actual force on the pile is dependent on the relative displacement between the pile and soil. The procedures discussed above for analyzing the behavior of piles, based on relative displacement, can be implemented to predict the net earth pressure on piles and to investigate the stability of the pile foundation.

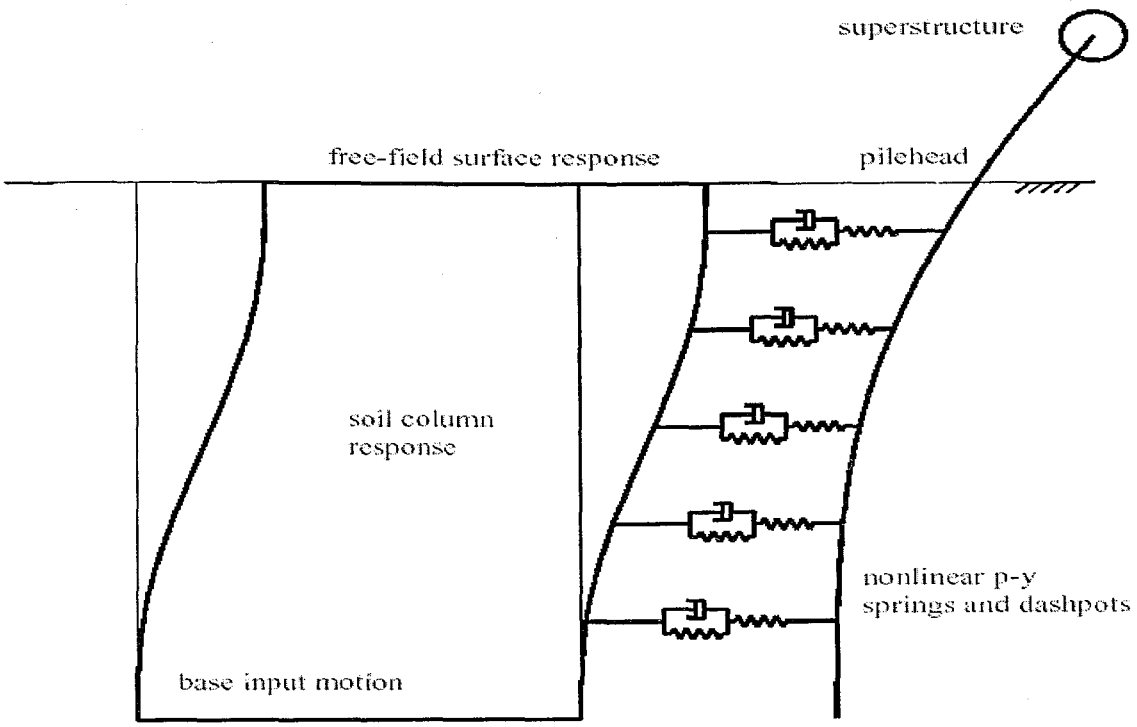

Figure 2-16 Schematic Illustration of the Effects of Lateral Spreading on Piles

3. PILES AND PILE GROUPS IN SOILS TEND TO LIQUEFY

This chapter presents a practical method for the design of pile foundations in deposits containing liquefiable soils during earthquake. If the soil has been liquefied but not inducing lateral spreading, the discrete model (the p-y method) can be used to analyze the behavior of piles by employing the residual strength of soils in the liquefied layer. However, the severe condition is for piles to resist the lateral spreading triggered by liquefied soils. This chapter introduces an analytical solution to take into account the effect of the soil movement on the behavior of piles during the post liquefaction period. Two cases were analyzed in this chapter and considerable insight into the interaction of piles and liquefied soil is discussed.

3.1. Introduction

One of the most dramatic causes of damage to structures during earthquakes has been the development of liquefaction in deposits of saturated sand. High pore water pressure arises due to ground vibration and the resulting upward flow of water frequently turns sand into a quick or liquefied condition. This chapter investigates the behavior of piles in deposits of liquefied soil, which is moving laterally. Prior to a discussion of the ability of piles to sustain lateral loading, a presentation is given on the liquefaction of soils and the way to estimate the residual strength of such liquefied soils.

Liquefaction of saturated sands has occurred during a number of earthquakes, but nowhere have the effects been more dramatic than in the town of Niigata, Japan. The earthquake induced extensive liquefaction of deposits sand in low-lying areas of the town. Thousands of buildings collapsed or suffered major damage as a result of the loss of resistance of the sand. After Niigata, liquefaction has been reported at numerous other earthquakes around the world, including the recent one at Kobe, Japan. In some cases upward flow of water from the ground continues for as much as 30 minutes after ground motions have stopped.

Seed discussed two main problems confronting foundation engineers when confronted with a situation where soil liquefaction may occur: (1) determining the stress conditions required to

trigger liquefaction and (2) determining the consequences of liquefaction in terms of potential sliding and potential deformation. Some methods can be used to avoid loss of strength of sand in the vicinity of the foundation; the methods include installation of stone columns, and densification of the loose sand by dynamic compaction. However, the cost of ground improvement is high and an alternative approach may be to allow liquefaction to occur in the soil. Then the problems for design become the determination of the potential for sliding and the possible deformations that may result. The solution of such problems requires the measurement of the strength and deformational characteristics of the liquefied soil. Then design may proceed with the view to confront the worse possible conditions.

The solution to the entire problem of the seismic response of a pile foundation during the earthquake is not addressed in this chapter; rather, this chapter introduces a simplified solution to study the effect of the soil movement on the behavior of piles at the end of the earthquake. By applying existing static loading at the pile top along with a certain "static" free-field soil displacement developed in the post-liquefaction period, the pile response can be predicted for the worse condition.

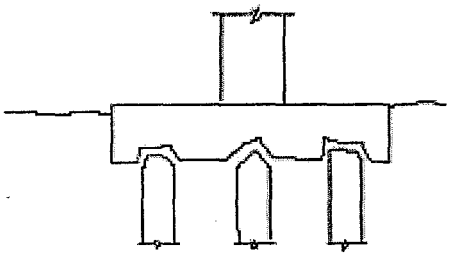

PILE PULLOUT FROM CAP

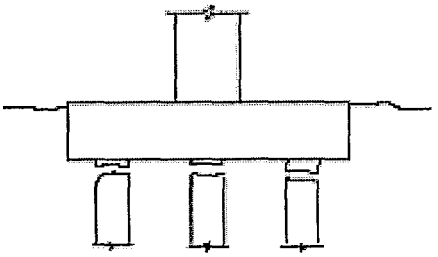

PILE FAILURE AT HEAD IN FLEXURE AND/OR SHEAR

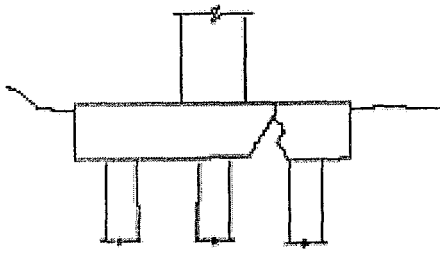

PILE CAP FAILURE

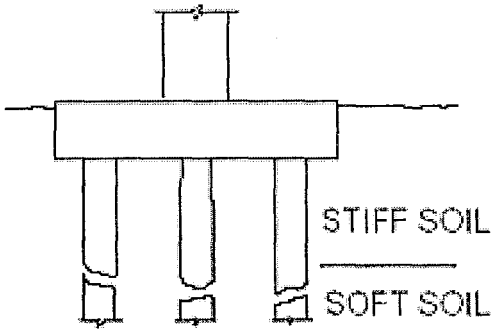

PILE FLEXURE/SHEAR FAILURE AT STIFFNESS CONTRAST

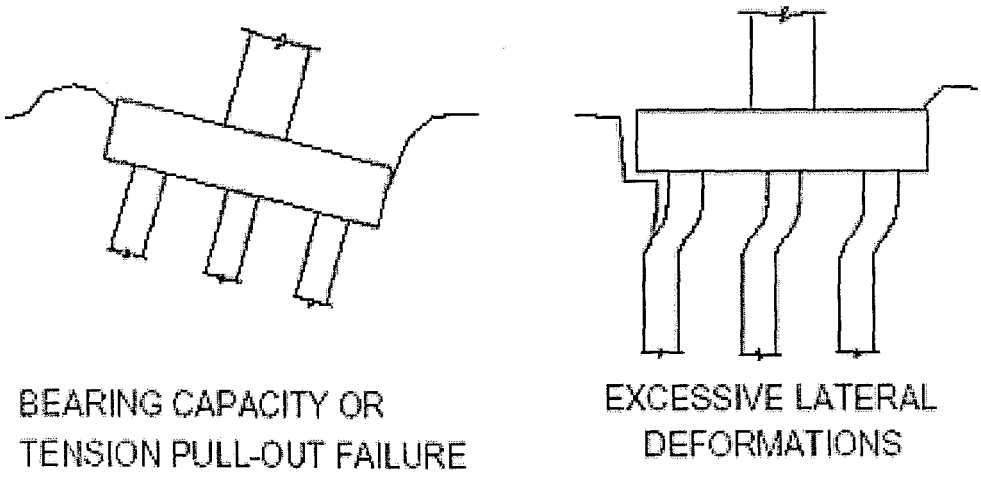

Figure 3-1 Failure Types of Pile Groups Subjected to Seismic Loading

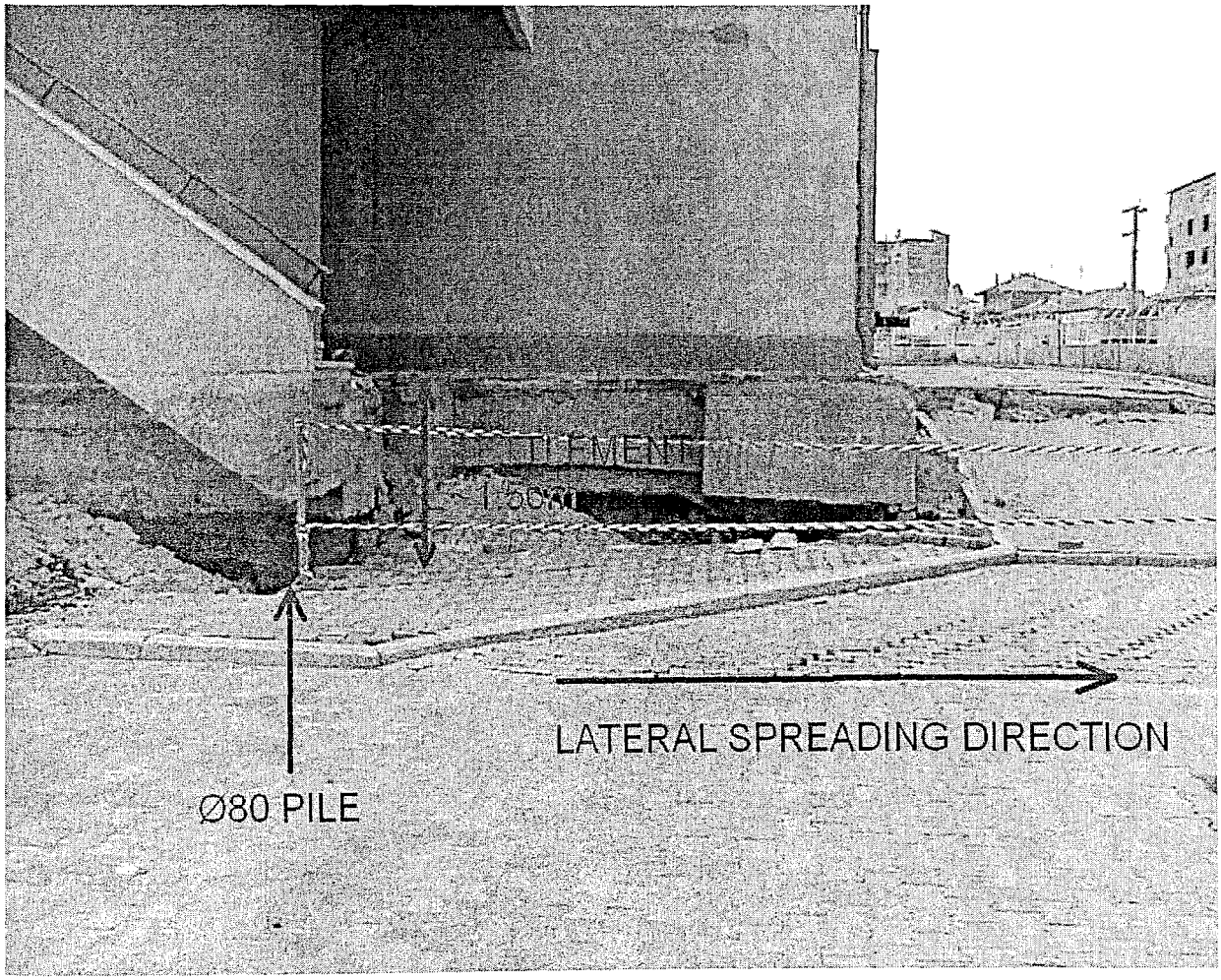

Figure 3-2 Failure of a Pile Group Subjected to Seismic Loading

(Stadium of Adapazari Golcuk, 1999 (NZSEE, 1999))

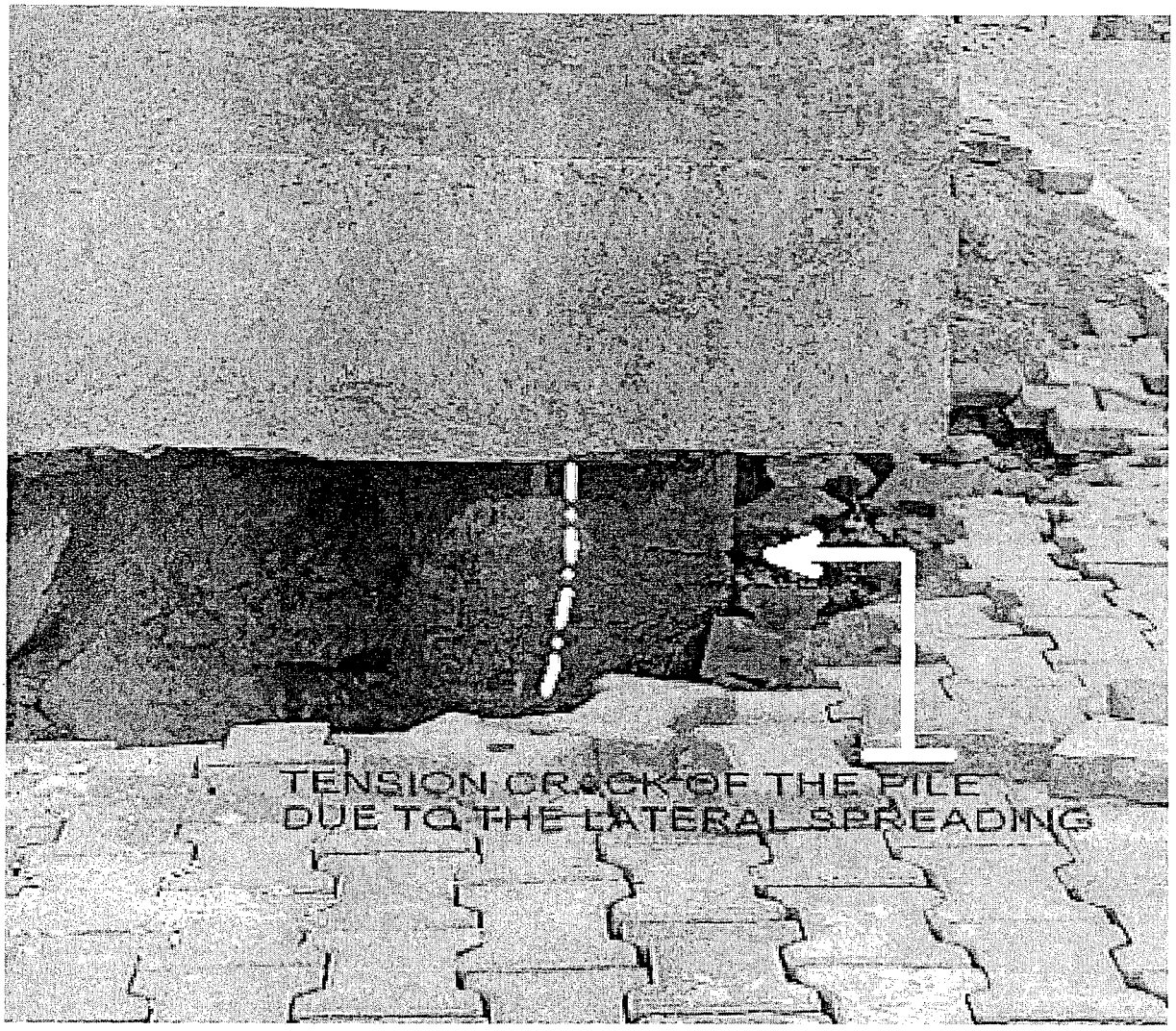

Figure 3-3 Failure of a Pile due to the Excessive Lateral Deformations (NZSEE, 1999)

3.2. Laterally Loaded Piles

As a foundation problem, the analysis of a pile foundation under axial and lateral loading is complicated by the fact that the soil reaction is dependent on the pile movement, on the other hand, is dependent on the soil response. Thus, the problem is a matter of soil-structure interaction. The problem is nonlinear because the soil response is a nonlinear function of pile displacement. To represent the nonlinear response of soil behavior, a discrete model is commonly used for pile and the soil interaction.

The discrete curves of soil response of each depth may not faithfully model the true continuum; however, the curves are firmly based on the results of many full-scale experiments. Research

has shown that the error employing discrete curves is a second-order effect when taking into account the inability of predicting precisely the relevant properties of the soil, especially taking into account the influence of the installation of the piles on soil properties. The discrete model has the merit of allowing engineers to specify various soil properties at each increment along a pile. An example of the specification of p-y curves for various layers of soil is shown in Fig. 3. In contrast to the middle layer which has liquefied, the upper and lower layers consist of soil remain stable. The p-y curves for the middle layer reflect very low resistance, based on the residual strength of the liquefied soil.

If the liquefied soil causes the upper layer become to unstable and to move laterally, a model that may be used to solve for the behavior of the pile is shown in Fig. 4. The dashed line in Fig. 4 shows a possible lateral spreading due to liquefaction. The soils in the upper two layers moving horizontally against the pile create additional lateral forces on the pile. The lateral forces on the pile from the soil may be derived from the reference to the offset p-y curves as illustrated in Fig. 2. The resistance to the lateral displacement of the pile will be derived from the lower layer. The Winkler discrete model can be used in making a solution. In addition to the soil forces, driving and resistance, pile-head forces must be considered.

To include the possible lateral spreading in the design of a pile, the regular computational scheme has to be modified, as represented here. The original differential equation for piles under lateral loading is:

$$EI\,(d^4y/dx^4) + Q\,(d^2y/dx^2) - p + W = 0$$

where;

Q= axial load on the pile

y= the lateral deflection

p= soil reaction per unit length

EI= flexural rigidity

W= distributed load along the length of the pile

In the governing equation for the case where the soil does not move, the soil resistance is represented as p = ky (curves 1 in Fig. 5). If the possible deflection at a depth x below the ground surface is y_1, the soil resistance obtained from the normal p-y curve (curve 1) is p1.

However, if the normal p-y curve offsets an amount y_s to take into account the soil movement, then the actual soil resistance would be p_2 instead of p_1 (curve 2 in Fig. 5).

To account for the change in the soil resistance, the relative displacement between the pile and the soil must be included in the difference equation as

$$EI\,(d^4y/dx^4) + Q\,(d^2y/dx^2) - k\,(y-y_s) + W = 0$$

where,

k= soil modulus

y_s= free-field movement of the soil

The above equation can be solved by the finite difference method. In general, acceptable accuracy can be achieved with the high-speed digital computer and with great efficiency by making use of an available computer code.

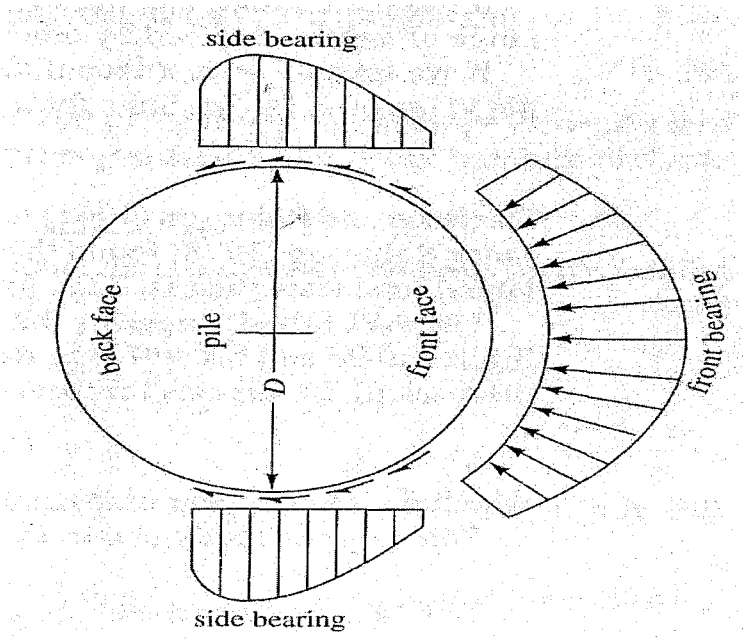

Figure 3-4 Qualitative Front and Side Resistances for a Laterally Loaded Pile

4. CAPACITY ESTIMATIONS

4.1. Description of the Structure

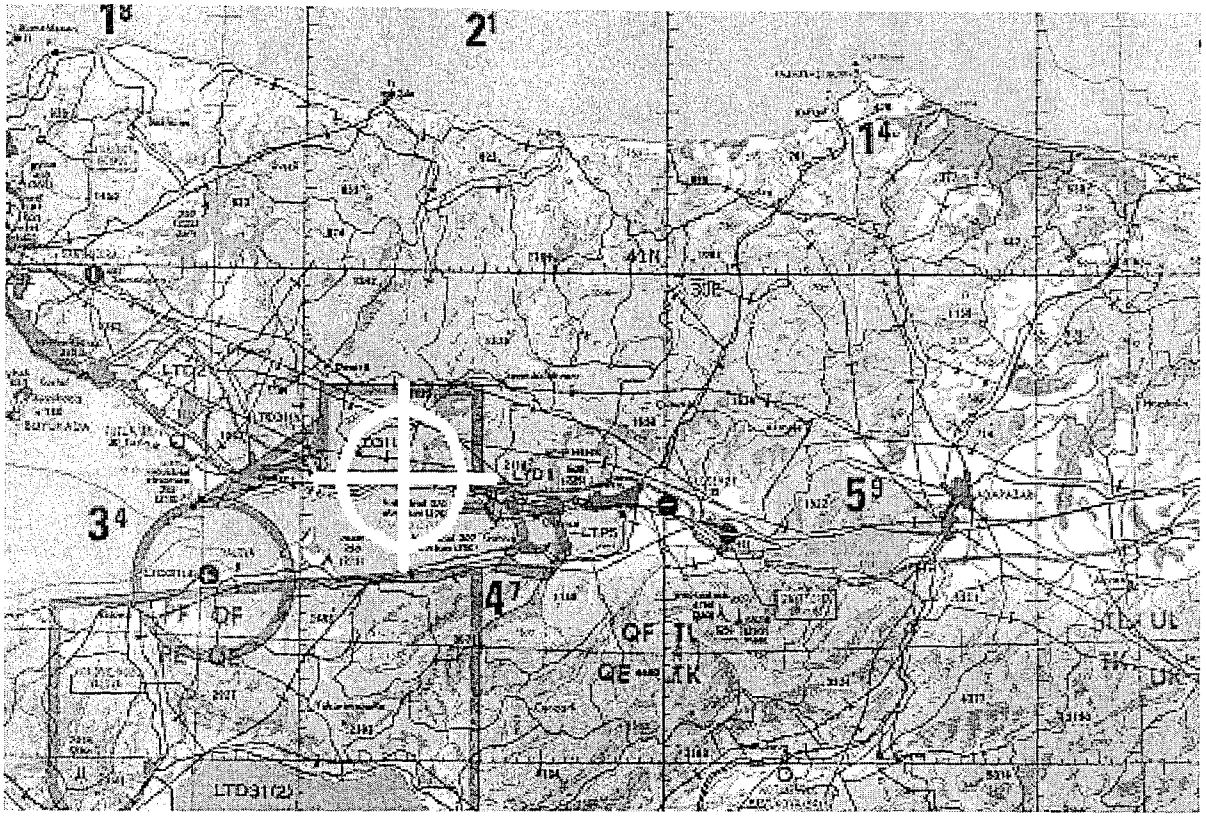

Figure 4-1 Location of the Site in Dilovası

This structure is the association of the two buildings in Diler Iron And Steel Industry Inc. located in Dilovasi. One of these buildings is the electric power transformer building and the other is the cooling water pump facility. These buildings share the same mat foundation as well as the same substructure (the piles). The two superstructures are 2-storeys, 10.0m high and 3 storeys 17.7 m high respectively. The foundation is composed of two rectangles connected to each other. The dimensions are 22.60x10.10 m to 40.80x14.00 m with a thickness of 70 cm. In addition, this 800m^2 mat foundation has no gaps.

The soil underlying the structure is composed of three layers, which are totally 30.30m thick liquefiable medium stiff, brown-gray colored silty and sandy clay (N=14), 1.20m stiff, brown-

gray colored silty clay (N=14) and finally 2.50m green colored overly separated claystone (RQD=10%)

Since the surface layer of the soil is not strong enough to carry such a building, deep foundation, anchored group piles, are used. 77 cast-in-place piles with a diameter of 80 cm are used to transfer the superstructure's gravity load to the claystone layer with the help of the friction resistance of the mid layers. Each pile carries 1063 kN to 1388 kN (their self weights are included). The piles are mostly placed under the columns and structural walls. They have a friction resistance of 923 kN and a point resistance of 418 kN "they are anchored to a 2.5m thick claystone", the computer solution and hand calculations will be shown quite detailed in the following chapters.

Reasons For Selecting This Structure

The main reason for choosing this structure to investigate previously searched topics on has several reasons such as,

1. Its being constructed by the writer's place of work "FEM Construction And Engineering Co.", which provided detailed projects and any additional information about the sub and the superstructure and the properties of the soil the building is based on.
2. Being very close to the NAFL to get most dramatic earthquake analysis results from a probable strong ground motion.
3. Having a simple building, which provides the writer an advantage of searching the characteristics of the soil-structure interaction deeper without any handicaps of the exceptions of the superstructure.

Before modeling the structure, the bearing capacities' of the piles must be investigated deeply and the hand calculation results must be compared with the ones achieved from a computer program SHAFT 1.0, which is released by Prentice Hall, Inc.

4.2. Bearing Capacity of the Piles

(Hand Calculations Compared to SHAFT Program)

In this section the adequate number, depth and the diameter of piles will be calculated by hand, with the means of variable equations from the literature. Firstly the allowable friction, secondly the point load capacities and finally the allowable total load capacities of different diameters of piles will be calculated. The SPT data and laboratory tests' results, which are obtained from the rock samples, will be used for the further calculations. The traditional bearing capacity formulas are associated with site observations and the advices of many experienced geological engineers in this research.

Three test borings have been applied to the site, and the results of these tests differ. Thus, according to the SPT blow-counts data, the weakest test result is accepted for the site (S3). The application places of the borings is shown below:

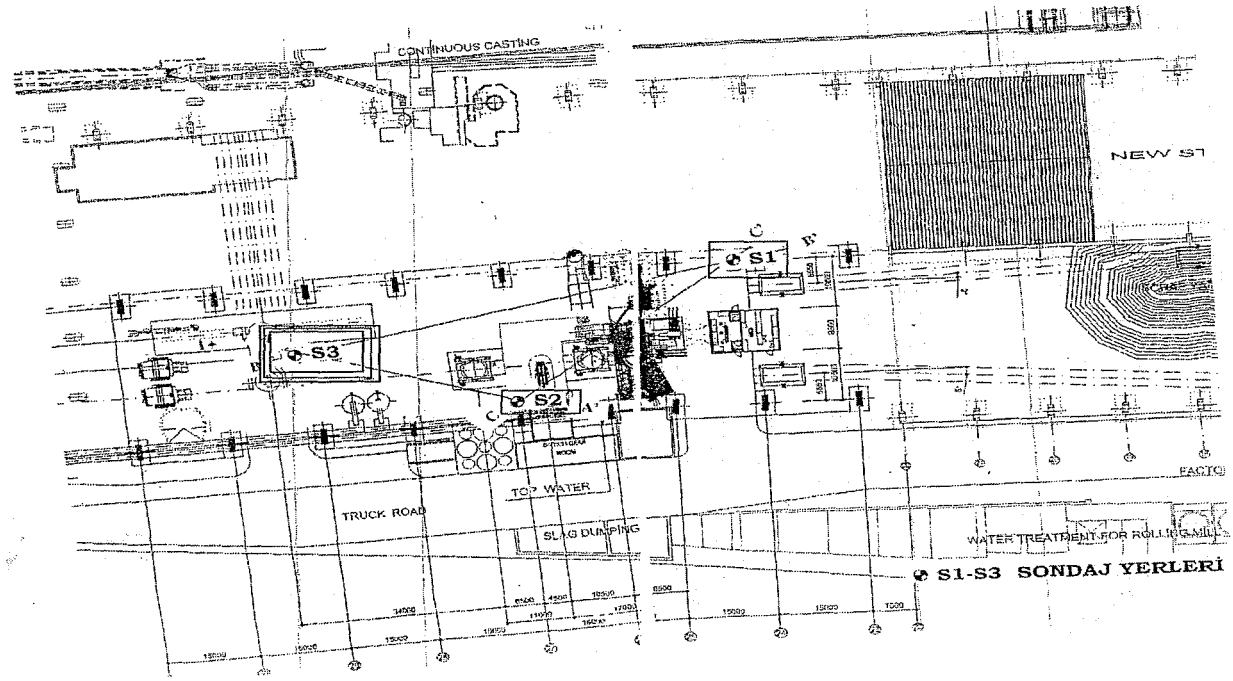

Figure 4-2 The Placements of the Bore Holes at the Site (Alpay, 1998)

There are 31.30m medium stiff, brown-gray colored silty and sandy clay layer and a 1.20m stiff, brown-gray colored silty clay layer and a 2.50m green colored overly separated claystone "the depth of bore is 34.00m". It is considered that a group of cast-in-place piles should be constructed underneath the superstructure down to the rock layer. The profile of the soil is demonstrated below:

--- THE PROFILE OF THE SOIL LAYERS ---

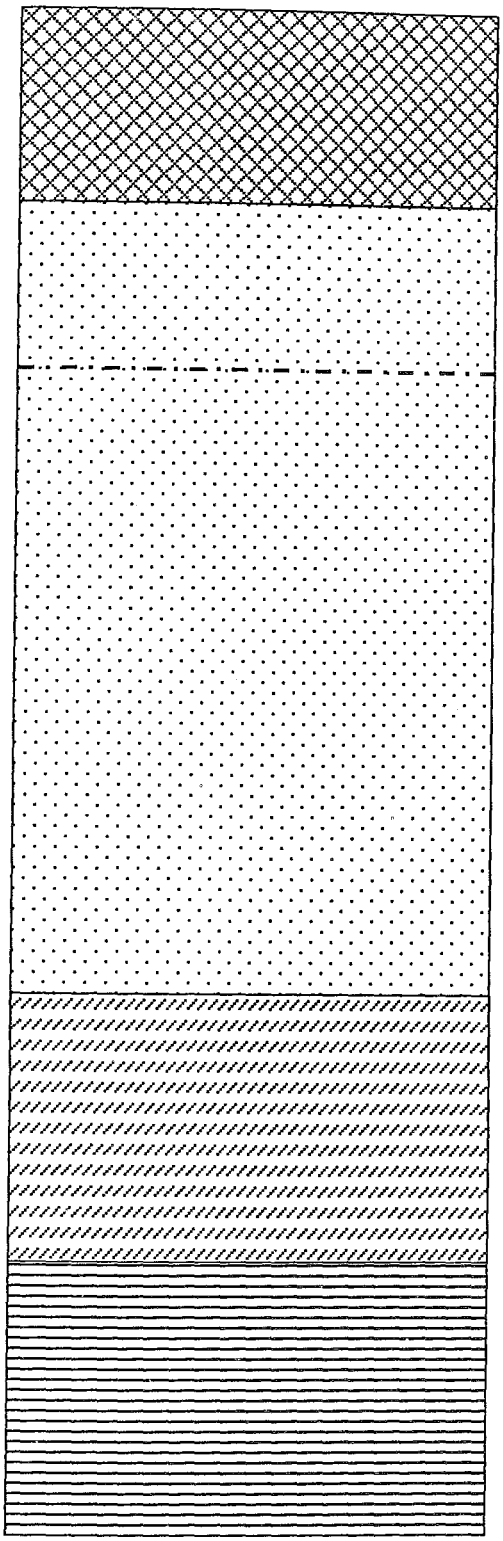

+-0.00m Ground (GWT:–2.25m)

filled soil (clay, sand & iron pieces)

-1.60m

GWT = -2.25m

medium stiff, brown-gray colored silty and sandy clay (N: 14, γ:1.633 – 1.838 gr/cm^3)

-30.30m

stiff, brown-gray colored silty clay (N: 14, γ:1.838 gr/cm^3)

-31.50m

green colored overly separated claystone (RQD: 10%, γ: 1.838 gr/cm^3) "the c and Ø values of this layer will be calculated in the further notes"

-34.00m The end of bore

4.2.1. Standard Penetration Test (SPT)

The Standard Penetration Test, developed around 1927, is currently the most popular and economical means to obtain surface information both on land and offshore. It is estimated that 85 to 90 percent of conventional foundation design is made using the SPT. The test method is standardized as ASTMD 1586 since 1958 with periodic revisions to date. The test consists of the following (Bowles, 1990):

1. Driving the standard split-barrel sampler from a distance of 460 mm into the soil at the bottom of the boring.
2. Counting the number of blows to drive the sampler the last two 150 mm distances (total = 300 mm) to obtain the *N* number.
3. Using a 63.5 kg (140 pounds) driving mass (or hammer) falling "free" from a height of 762 mm (30 inches).

The test is halted if,

1. The blow-counts for 150 mm exceed 50, or 100 for 300 mm.
2. The system sinks the sampler, so no *N* can be counted.

There are 3 standard penetration tests' output data of the soil, which is underlying the structure that is investigated (S1, S2, S3). To compute the *N*, the writer has used the lowest one of the three, which is the boring S3.

The blow counts of the boring S3, measured at the site is just demonstrated below (these blow counts are the uncorrected values, the correction methodology and calculations will be demonstrated in the further notes):

$$N = \frac{2x(6+7+5+7+7+8+10+8+7+6+8+6+7+6+6+6+6+8+8+15)}{20} = 14.7$$

$$\underline{N \approx 14}$$

Boğazici Üniversitesi Kütüphanesi

4.2.2. Correction of *N*

Since there is a wide scatter in blow count *N* in similar soils, it is reasonable to expect that there should be a unique *N* for the soil at some depth. The reasons for the scatter in *N* values are as follows:

1. ***Equipments from different manufacturers.*** A large variety of drilling rigs are in current use; however, the rotary auger with the safety hammer is the most common ones in practice.
2. ***Driving hammer configurations*** seem to have influence on the amount of energy input to the sampler.
3. ***Whether a liner is used inside the split barrel sampler.*** Side friction increases the driving resistance (and surely *N*) and is less without the liner.
4. ***Overburden pressure.*** Soils of the same density will give smaller *N* values if p_o' (effective vertical pressure at a depth) is smaller (as near the ground surface). Oversize boreholes on the order of 150 to 200 mm will also reduce *N* unless a rotary hollow-stem auger is used with the auger left in close contact with the soil in the hole bottom. Degree of cementation may also be significant in giving higher *N* counts in cemented zones that may have little overburden pressure.
5. ***Length of drill rod.*** Above about 10 m does not seem critical; however, for shorter lengths and $N < 30$ it is. This effect was first examined by Gibbs and Holtz and others, who used a computer model to analyze the influence of rod length as well as other factors such as sampler resistance.

Not to mention that, there should be a unique *N* for the soil at some depth to use it in investigating the soil properties. Thus it needs to be corrected and standardized. The standard blow count can be corrected from the measured *N* at the site, as follows:

$N_{Erb}' = N_{55}' = C_N \times N \times \eta_1 \times \eta_2 \times \eta_3 \times \eta_4$

N_{55}' = adjusted N using the subscript for the E_{rb} (standard energy ratio) and the ' to indicate it has been adjusted.

C_N = adjustment for effective overburden pressure p_o' [kPa] computed.

η_i = adjustment factors from (and computed as shown in) Table 4-1

4.2.2.1. E_{rb} (Standard Energy Ratio)

$E_{in} = ½.m.v^2 = ½.W/g.v^2$ *(Theoretical Driving Energy)*

$v = (2gh)^{1/2}$

$E_{in} = ½.W/g.(2gh) = W.h$

W= *weight of the hammer* = 63.5 kg x 9.81 m/s^2

h = *height of the fall* = 762 mm

E_{in} =63.5 x 9.81 x 0.762 = 474.5 *(say, 475J)*

$$E_r = \frac{Actual - hammer - energy - aplliedtosampler, Ea}{Theoretical - Input - Energy, Ein} x100$$

Some of the authors accepted E_r as 70 (E_{rb}) in several recent studies (Riggs, 1986), however some of them use other values such as 60 (Seed & Idriss 1971; Skempton 1986) or 55 (Schmertmann [in Robertson et al. 1983]). In the empirical formulas based on SPT, it is demonstrated that E_{rb} accepted as 70, 60 or 55 as in index of N (*Ex:* N_{70} *or* N_{55}). One can convert his N value to the author's as the following (considering other variables to be constant):

$E_{r1} \, x \, N_1 = E_{r2} \, x \, N_2$

$N_2 = E_{r1} \, x \, N_1 / E_{r2}$

From the equation above, it is obvious that blow counts multiplied by the energy ratio is constant. Thus one can simply convert his N_i value to any other N_j value from that linear relation.

4.2.2.2. C_N (Overburden Pressure Adjustment Factor)

It is known that N increases with the overburden pressure, thus the test gives misleading N values. Since effective overburden pressure affects the SPT, an adjustment factor is needed to get rid of this effect. The adjustment factor can be computed just as the following:

$C_N = (95.76/P_o')^{1/2}$

The given data about the underlying soil layers are defined below:

$\gamma = 1.633\ gr/cm3 = 16.02\ kN/m3$

$\gamma_s = 1.838\ gr/cm3 = 18.03\ kN/m3$

$w = 0.45$

$GWT = 2.25\ m$

$e = 1.22$

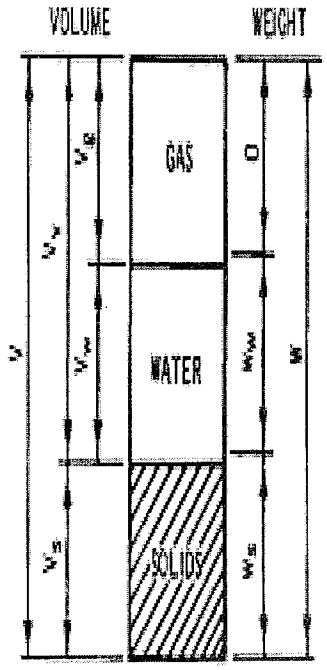

WATER CONTENT	$w = \frac{W_w}{W_s}$
SPECIFIC GRAVITY	$G_s = \frac{W_s}{V_s \gamma_w}$
VOLUME OF SOLIDS	$V_s = \frac{W_s}{G_s \gamma_w}$
VOLUME OF VOIDS	$V_v = V - V_s$
VOID RATIO	$e = \frac{V_v}{V_s} = \frac{n}{1-n}$
POROSITY	$n = \frac{V_v}{V} = \frac{e}{1+e}$
DEGREE OF SATURATION	$S = \frac{V_w}{V_v} = \frac{w G_s}{e}$
UNIT WEIGHT OF WATER (FRESH WATER)	$\gamma_w = \frac{W_w}{V_w} = 62.4$ PCF
DRY UNIT WEIGHT	$\gamma_d = \frac{W_s}{V} = \frac{\gamma_m}{1+w}$
WET UNIT WEIGHT	$\gamma_m = \frac{W}{V}$
SUBMERGED (BOUYANT) UNIT WEIGHT	$\gamma' = \gamma_m - \gamma_w = \frac{G_s - 1}{1+e} \gamma_w$

Figure 4-3 Weight - Volume relationships (U.S. Army Corps of Engineers, 1986)

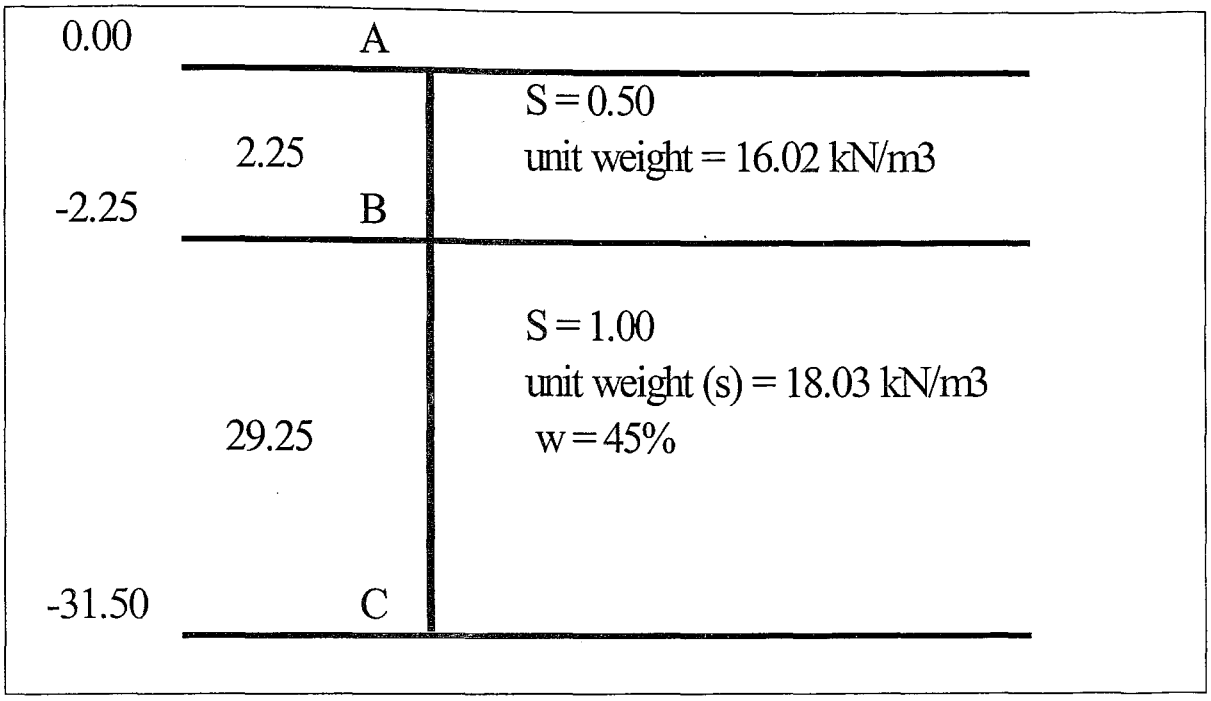

Figure 4-4 The Simplified Profile of the Soil Layers

$w = W_w/W_s = V_v \times 9.81 / (\gamma_s \times 1) = 0.45$

$V_v = e = 1.22$

$\gamma_s = 1.22 \times 9.81 / 0.45 = 26.49\ kN/m3$

$\sigma_A = 0$

$\sigma_B = \gamma \times h = 16.02 \times 2.25 = 36.05\ kN/m^2$

$\sigma_C = \sigma_B + \gamma_s \times h = 36.05 + 18.03 \times 29.25 = 563.43\ kN/m^2$

$U_A = \gamma_w \times h = W_w \times h / V_v = 9.81 \times 1.22 \times (-2.25) / 2 / 1.22 = -11.04\ kN/m^2$

$U_B = 0$

$U_C = U_B + \gamma_w \times h = 0 + 9.81 \times 29.25 = 286.94\ kN/m^2$

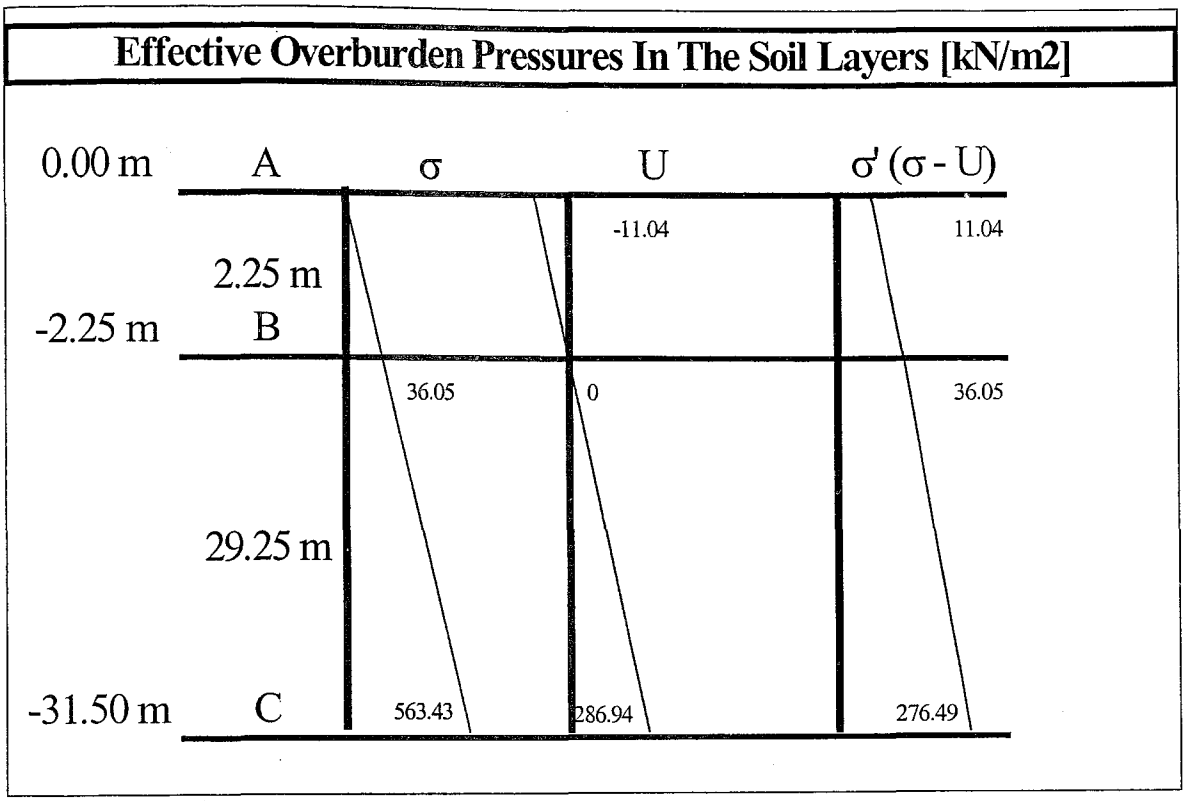

Figure 4-5 Effective Overburden Pressures' Diagram

$$P_o{}'_{avg} = \frac{11.04 + 276.49}{2} = 143.77 kN/m2$$

$$C_N = \left(\frac{95.76}{143.77}\right)^{1/2} = 0.82$$

$C_N = 0.82$

4.2.2.3.SPT Adjustment Factors (η_1, η_2, η_3, η_4)

n_1 Hammer Type Correction

	Avarage Energy Ratio Er				
	Donut		Safety		Remarks
Country	R-P	Trip	R-P	Trip / Auto	
The U.S.	45	-	70-80	80-100	R-P = Rope-pulley or cathead
Japan	67	78	-	-	n1 = Er/Erb = Er/55
U.K.	-	-	50	60	Er = Ea/Ein
China	50	60	-	-	For Turkey Donut: Er = 45
Turkey	45	45	-	-	n1 = Er/55
					n1 = **0.82**

n_2 Rod Length Correction

Length	n_2	Remarks
> 10 m	1.00	
6-10	0.95	*N* is too high when L < 10 m
4-6	0.85	n2 (L=31.50/2=15.75 > 10 m)
0-4	0.75	n2 = **1.00**

n_3 Sampler Correction

	Sampler	n_3	Remarks
	Without Liner	1.00	
With Liner:	Dense sand, clay	0.80	*N* is too high with liner
	Loose sand	0.90	n3 (with liner, clay) = **0.80**

n_4 Borehole Diameter Correction

Hole Diameter	n_4	Remarks
60-120 mm	1.00	Base Value; *N* is too when
150 mm	1.05	there is an oversize borehole
200 mm	1.15	n4 (Ø = 76 -89 mm) = **1.00**

Table 4-1 SPT Adjustment Factors η_i

After the calculation of E_{rb}, C_N and η_1, η_2, η_3, η_4, finally the adjusted *N'* can be computed just as the following:

$$N_{Erb}' = N_{55}' = C_N \times N \times \eta_1 \times \eta_2 \times \eta_3 \times \eta_4$$

$$N_{55}' = 0.82 \times 14 \times 0.82 \times 1.00 \times 0.80 \times 1.00 = 7.53 \quad say,$$

$$\underline{N_{55}' = 7}$$

Since the corrected N is computed, bearing capacity of the piles can be calculated from the empirical formulas that needs N' in the following chapters. In addition, the efficiency of the group piles is 100%, because all of the piles are anchored to the rock layer.

4.3. Skin Resistance "Q_s"

Since the absence of cohesion c value, the simplified equation $c = 4.5N \sim 6N$ (Bowles, 1990) will be used. Let us say $c = 5N$ for being conservative. Thus, firstly the average N value must be found.

$N' = 7$

$c = 5N'$

$c = 5 \times 7$

$c = 35\ kN/m^2$

The equation $q_s = \alpha \times c$ will be used to find skin resistance in such a cohesive soil. The α value can be computed as the following;

$\alpha = 1$	*for*	$c =< 45\ kN/m^2$	*(for cast-in-place piles)*
$\alpha = 0.30$	*for*	$c > 45\ kN/m^2$	*(for cast-in-place piles)*

(Alpay, 1998)

The reason for using the α factor is that, while constructing a cast-in-place pile in a cohesionless media such as sand, is that the soil around the pile flows towards the pile and confines it quickly, so one can take the efficiency of skin friction as 100%. But during a cast-in-place pile construction in a cohesive soil (such as clay), since drilling machine shears (cuts) the soil material, it takes time for soil to confine the pile, so the α factor is used to lower the skin resistance.

Since the c value in the example is lower than 45 kN/m^2

$(c = 35\ kN/m^2 =< 45\ kN/m^2)$

α can be taken as 1. Then the equation becomes,

$q_s = \alpha \times c$

$q_s = 1 \times 35$

$q_s = 35\ kN/m^2$ *(found as 32 – 49 kN/m^2 in laboratory tests)*

$As = \Pi \times D \times L$

$As = \Pi \times 1.00 \times 31.50$

$As = 98.96\ m^2$ *(for Ø100 pile)*

$As = \Pi \times D \times L$

$As = \Pi \times 0.80 \times 31.50$

$As = 79.16\ m^2$ *(for Ø80 pile)*

$Qs = q_s \times As$

$Qs = 35 \times 98.96$

$Qs = 3464\ kN$ *(for Ø100 pile)*

$Qs = 35 \times 79.16$

$Qs = 2770\ kN$ *(for Ø80 pile)*

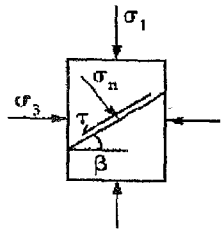

$|\tau| = \tau_0 + \mu\sigma_n$

τ_0 = cohesion μ = coeff. of friction

$|\tau| = \frac{1}{2}(\sigma_1 - \sigma_3)\sin 2\beta$

$\sigma_n = \frac{1}{2}(\sigma_1 + \sigma_3) + \frac{1}{2}(\sigma_1 - \sigma_3)\cos 2\beta$

The equation for $|\tau|$ and σ_n are the equations of a circle in (σ, τ) space:

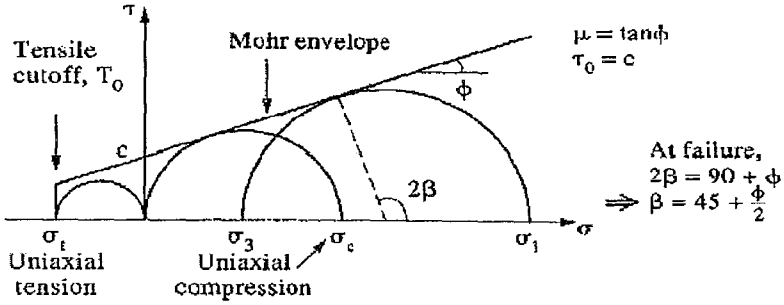

Figure 4-6 Mohr – Coulomb Failure Criterion

4.4. Point Capacity "Q_p"

First of all to solve this bearing capacity problem, the terms of Terzaghi's equation of bearing capacity, must be calculated. Since the soil underneath the pile is rock, the problem must be considered as a *bearing capacity of a foundation on rock.*

According to Stagg and Zienkiewicz (1968), the developers of Terzaghi's equations, the bearing capacity factors for sound rock are approximately alike the following;

$$N_q = \tan^6(45^o + \emptyset/2) \quad N_c = 5\tan^4(45^o + \emptyset/2) \qquad N_\gamma = N_q + 1$$

Since the absence of laboratory tests applied on the rock sample at the depth of 34.00m, the uniaxial "unconfined" compressive strength ranges of rocks will be used that are listed **Table: 2**, by means of the observations of the people who had worked on the site. Then, these values will be used to predict the cohesion *c* by means of the diagram below.

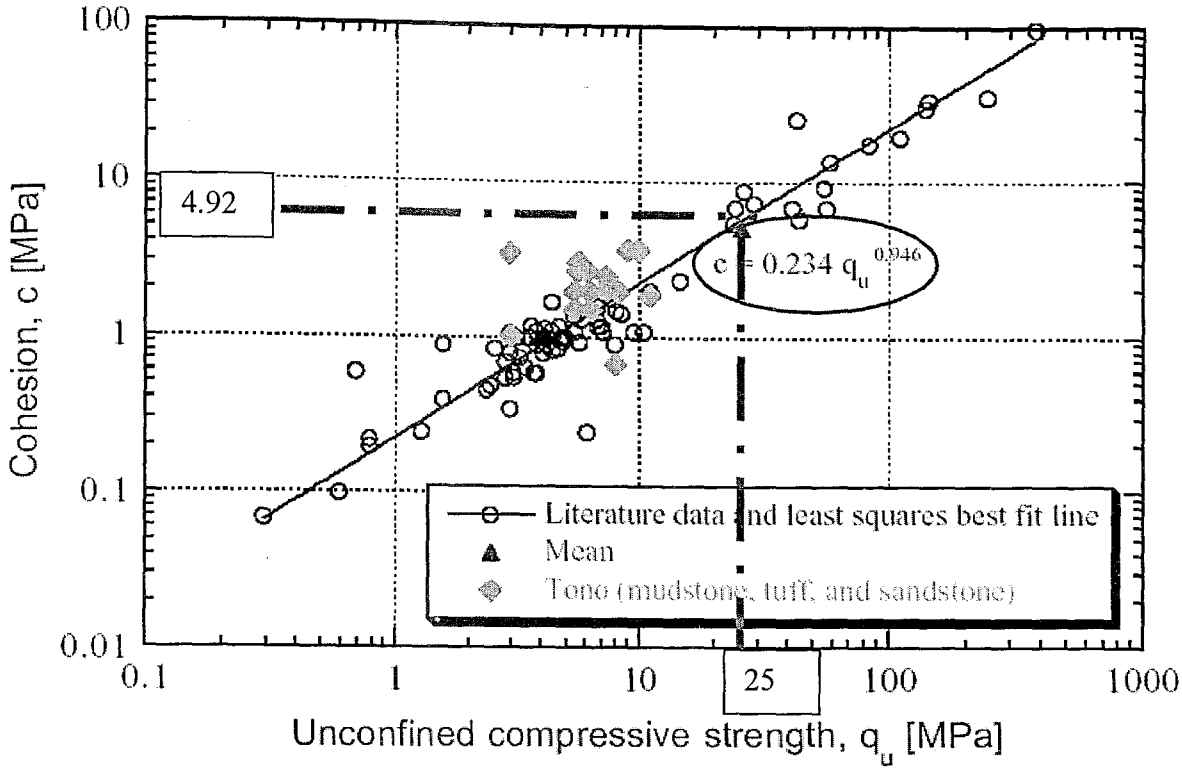

Figure 4-7 Relationship between q_u and c (soft rock system) (JNCDI, 1999)

From the above diagram it is seen that one can find the average cohesion of a soft rock if the q_u range of the material is known. Since it is a rock mechanism that is worked out, one cannot use the conventional cohesion equation $c = q_u /2$, thus the equation shown in the figure above, $c = 0.234q_u^{0.946}$ must be used instead. If one finds 25 MPa for the unconfined compression strength of this overly separated claystone from the figure above, then the c becomes,

$c = 0.234q_u^{0.946}$

$c = 0.234 \times 25^{0.946}$

$c = 4.92$ *"can be rounded to"*

$c = 4$ MPa *"it is reasonably conservative, cohesion may be overly so"*

From many experiments and observations it is also known that the cohesion of rocks mostly ranges from 3.5 MPa to 17 MPa, thus $c = 4$ MPa is a reasonably conservative assumption.

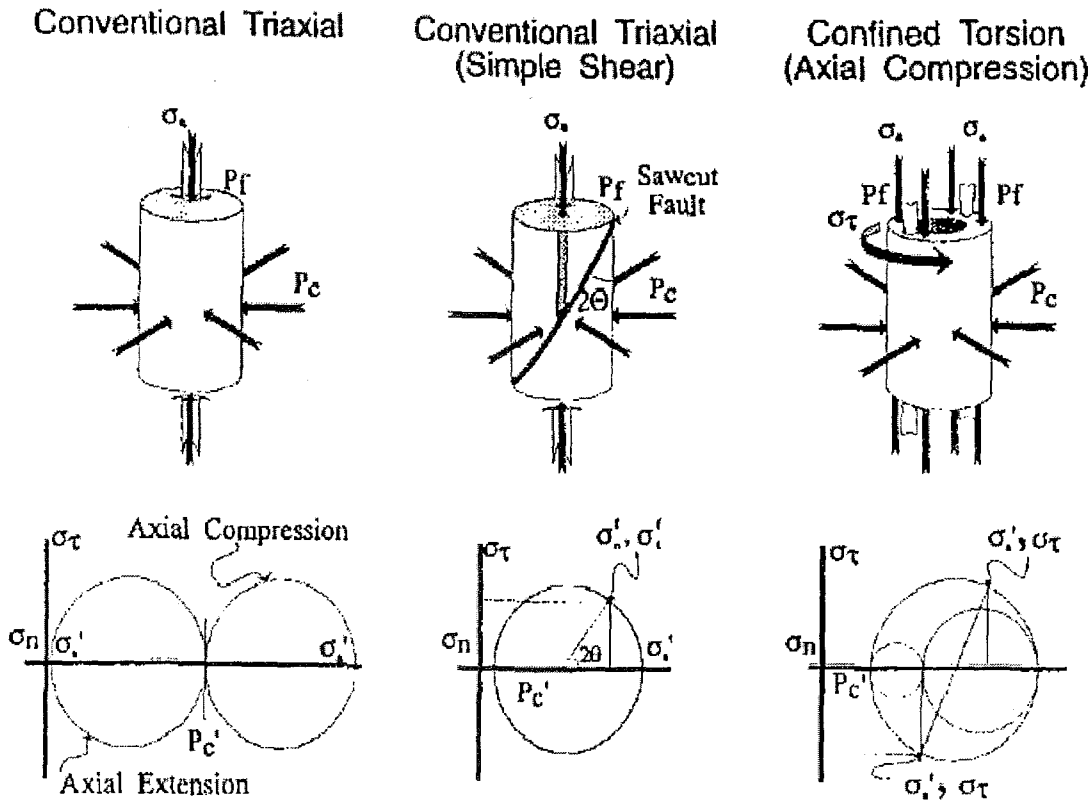

Figure 4-8 Tests of Conventional Triaxial, Simple Shear and Confined Torsion

Term	Uniaxial Compressive Strength (MPa)	Point Load Index (MPa)	Schmidt Hardness (Type L - hammer)	Field Estimate of Strength	Examples*
R5 Extremely Strong	>250	>10	50-60	Rock material only chipped under repeated hammer blows	fresh basalt, chert, diabase, gneiss, granite, quatzite
R4 Very Strong	100-250	4-10	40-50	Requires many blows of a geological hammer to break intact rock specimens	Amphibolite, sandstone, basalt, gabbro, gneiss, granodiorite, limestone, marble rhyolite, tuff
R3 Strong	50-100	2-4	30-40	Hand held specimens broken by a single blow of a geological hammer	Limestone, marble, phyllite, sandstone, schist, shale
R2 Medium Strong	**25-50**	**1-2**	**15-30**	**Firm blow with geological pick indents rock to 5mm, knife just scrapes surface**	**Claystone, coal, concrete, schist, shale, siltstone**
R1 Weak	5-25	**	<15	Knife cuts material but too hard to shape into triaxial specimens	chalk, rocksalt, potash
R0 Very Weak	1-5	**		Material crumbles under firm blows of geological pick, can be scraped with knife	highly weathered or altered rock
Extremely Weak	0.25-1	**		Indented by thumbnail	clay gouge

Table 4-2 Physical Strengths of Rocks (Lang & Lang)

** All rock types exhibit a broad range of uniaxial strengths, which reflect the heterogeneity in composition and anisotropy in structure. Strong rocks are characterized by well-interlocked crystal fabric and few voids*

***Rocks with a uniaxial compressive strength below 25 MPa are likely to yield highly ambiguous results under point load testing.*

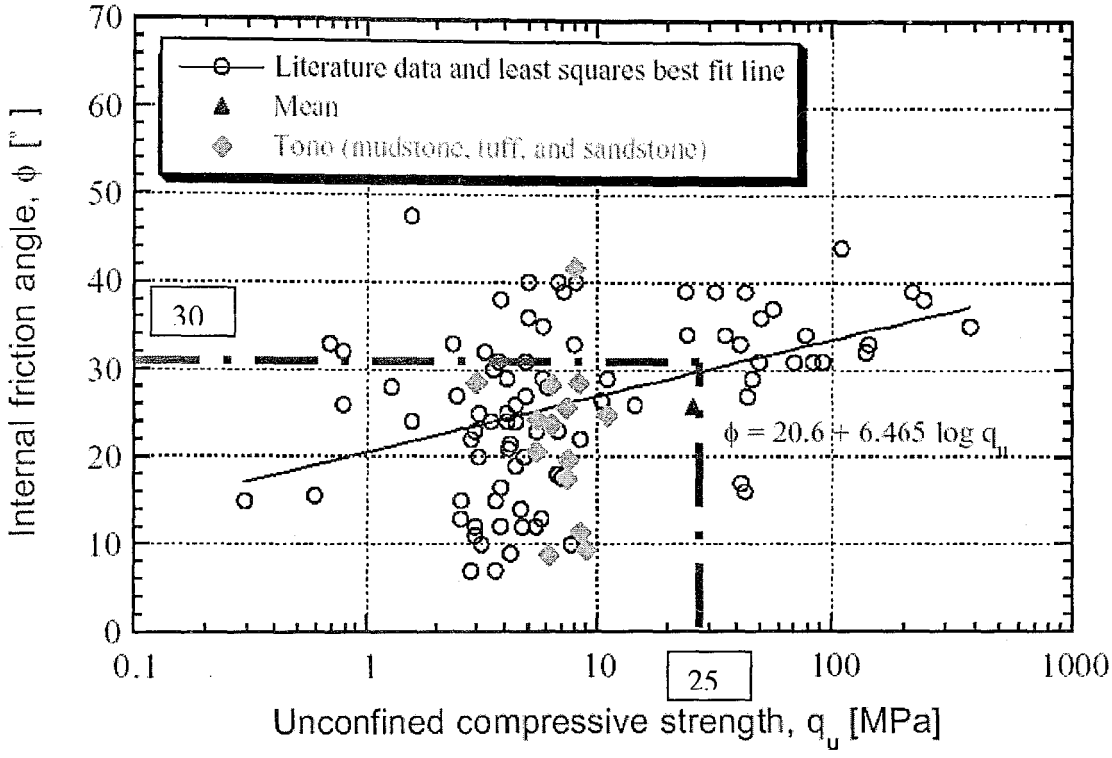

Figure 4-9 Relationship between Ø and q_u (soft rock system) (JNCDI, 1999)

Now it is available to calculate the internal friction angle of the claystone, which has an unconfined compressive strength of 25 MPa.

$$Ø = 20.6 + 6.465 \log q_u$$

$$Ø = 20.6 + 6.465 \log 25$$

$$Ø = 29.64^o \ldots\ldots \text{say, } \underline{Ø = 30^o}$$

Then the calculation of the bearing capacity of claystone is illustrated with the equation below;

$$q_{ult} = cN_c s_c + qN_q + 0.5\gamma BN_\gamma s_\gamma \qquad \textit{(Terzaghi)}$$

For		strip	round	square
s_c	=	1.0	1.3	1.3
s_γ	=	1.0	0.6	0.8

Table 4-3 Coefficients for Different Shapes of Foundations

The traditional calculation method of N_c ,N_q and N_γ terms differs for rock just like shown below;

$N_q = tan^6 (45^o + Ø/2)$ $N_c = 5\ tan^4 (45^o + Ø/2)$ $N_\gamma = N_q + 1$

$q_u = 25\ MPa$
$c = 4\ MPa$
$Ø = 30^o$
$RQD = 10\%$

Table 4-4 Properties of the Rock Layer

$N_q = tan^6 (45^o + 30^o/2)$

$\underline{N_q = 27}$

$N_c = 5\ tan^4 (45^o + 30^o/2)$

$\underline{N_c = 45}$

$N_\gamma = 27 + 1$

$\underline{N_\gamma = 28}$

$q_{ult} = cN_cs_c + qN_q + 0.5\gamma BN_\gamma s_\gamma$

$q_{ult} = 4 \times 45 \times 1.3 + 34E+3 \times 1.736E-5 \times 27 + 0.5 \times 1.736E-5 \times 1E+3 \times 28 \times 0.6$

$q_{ult} = 234.00 + 15.94 + 0.15$ *if the results are rounded,*

$q_{ult} = 234 + 16 + 0$

$\underline{q_{ult} = 250\ MPa}$

Now the reduction factor RQD* can be used from **Table: 5** below,

Rock description	R.Q.D
Excellent	>0.90
Good	0.75-0.90
Fair	0.50-0.75
Poor	0.25-0.50
Very poor	<0.25

Table 4-5 RQD Values (Bowles, 1990)

$q_{ult}' = q_{ult}\,(RQD)^2$

$q_{ult}' = 250(0.10)^2$ *"RQD varies about 10–25% for very poor rocks as claystone"*

$q_{ult}' \cong 2.5\ MPa < f_c'\ (25\ MPa)$ **O.K.** ✓

The ultimate point bearing capacity Q_p of the pile can be calculated as;

$Q_p = 2500 \times \Pi \times 1.00^2 / 4 \cong 1963\ kN$ *"for Ø100"*

$Q_p = 2500 \times \Pi \times 0.80^2 / 4 \cong 1256\ kN$ *"for Ø80"*

**RQD can be explained briefly as the following; rock quality designation (RQD) is an indexer measure of the quality of a rock mass [Stagg & Zienkiewicz (1968)] used by many engineers. RQD is computed from recovered core sample as;*

$$RQD = \frac{\sum Lengths - of - intact - pieces - of - core > 100mm}{Length - of - core - advance}$$

For example, a core advance of 1500 mm produced a sample length of 1310 mm consisting of dust, gravel and intact pieces of rock. The sum of length of pieces 100 mm or larger (pieces vary from gravel to 280 mm) in length is 890 mm. Then the RQD = 890 / 1500 = 0.59

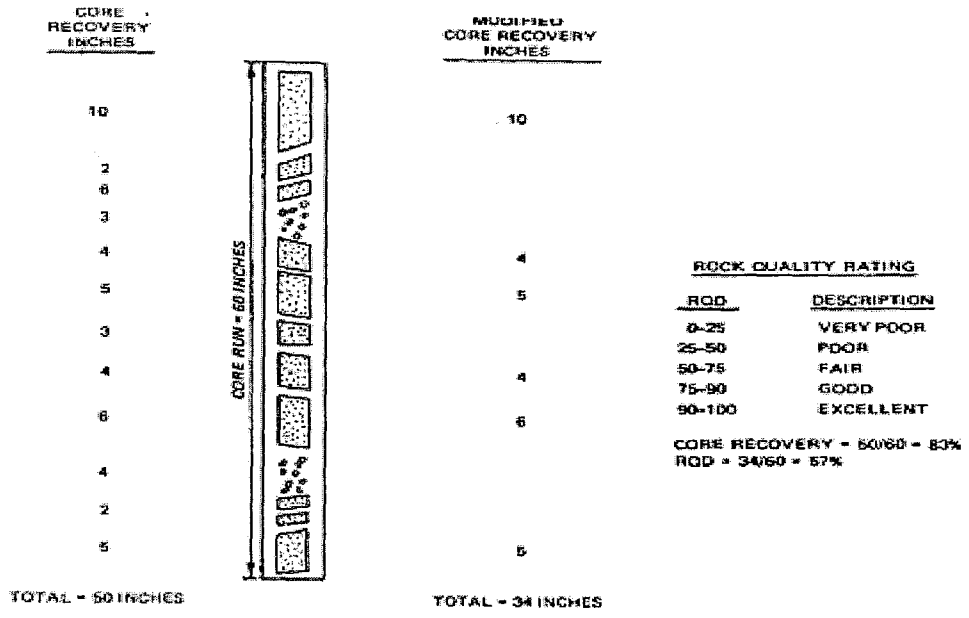

Figure 4-10 Illustration of RQD Sampling (U.S. Army Corps of Engineers, 1986)

After all of the calculations above, the final results of the skin resistance and end bearing capacities of the piles are found as the following, with comparison to computer program *Shaft* results.

Results Comparison Table [kN]		Handmade Solutions		CPU Program *Shaft*
Ø100	Qs=	3464	+6%	3262
	Qp=	1963	+39%	1414
Ø80	Qs=	2770	-1%	2807
	Qp=	1256	+39%	905

Table 4-6 Comparison of Hand Calculations To Shaft Outputs

The final allowable vertical load capacities of Ø80 piles are found as,

$$Q_a = (Q_s + Q_p) / FS = 2770/3 + 1256/3 = 923 + 419$$

$$\underline{Q_a = 1342 \text{ kN}}$$

4.4.1. Comparison of Hard and Soft Rock Mechanism

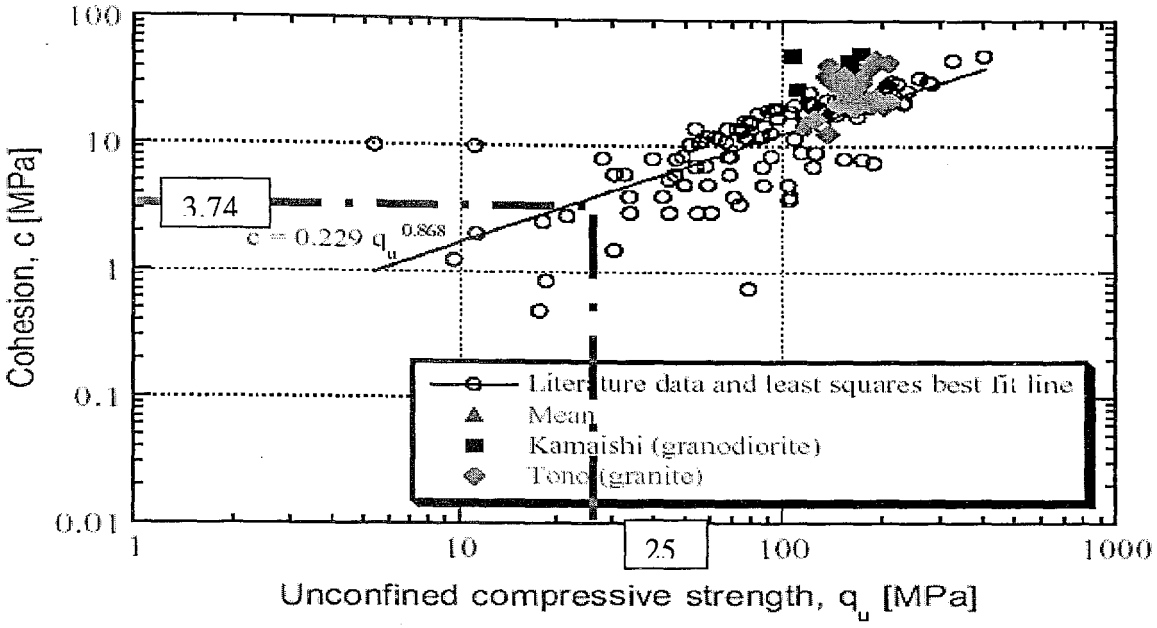

Figure 4-11 Relationship between q_u & c for Hard Rock Mechanism (JNCDI, 1999)

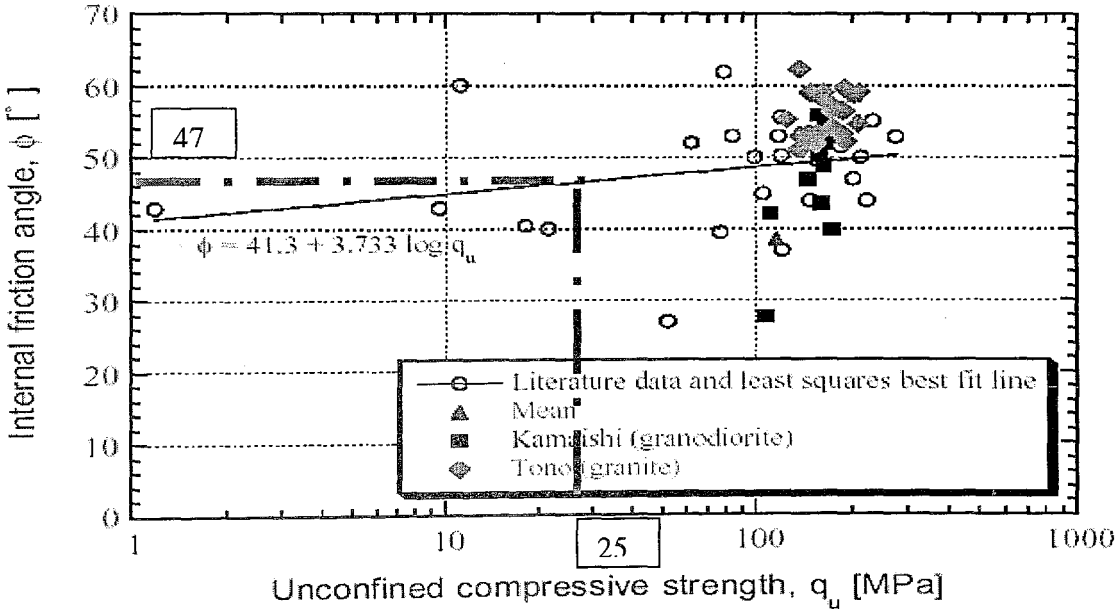

Figure 4-12 Relationship between q_u & Ø for Hard Rock Mechanism (JNCDI, 1999)

**Cohesion c decreases from 4.92 to 3.74 MPa and internal friction angle Ø increases from 30° to 47° for hard rock mechanism.*

If the system were accepted as a hard rock mechanism, then the values c and Ø would become 3.74 MPa and 47° respectively. Thus the point bearing capacity for Ø80 pile would be just as the following;

$N_q = tan^6 (45^o + Ø/2) N_c = 5\ tan^4 (45^o + Ø/2)$ $N_\gamma = N_q + 1$

q_u = 25 MPa
c = 3 MPa
Ø = 47°
RQD = 10%

Table 4-7 Properties of Rock Layer

$N_q = tan^6 (45^o + 47^o/2)$

$N_q = 267$

$N_c = 5\ tan^4 (45^o + 47^o/2)$

$N_c = 207$

$N_\gamma = 267 + 1$

$N_\gamma = 268$

$q_{ult} = cN_c s_c + qN_q + 0.5\gamma BN_\gamma s_\gamma$

$q_{ult} = 3 \times 207 \times 1.3 + 34E+3 \times 1.736E-5 \times 267 + 0.5 \times 1.736E-5 \times 8E+2 \times 268 \times 0.6$

$q_{ult} = 807.30 + 157.59 + 1.12$ *"if the results are rounded",*

$q_{ult} = 807 + 158 + 1$

$\underline{q_{ult} = 966\ MPa}$ *"original result was 250 MPa, the change is +**286%**"*

$q_{ult}' = q_{ult} (RQD)^2$

$q_{ult}' = 966(0.10)^2$ *"RQD varies about 10–25% for very poor rocks as claystone"*

$\underline{q_{ult}' \cong 9.66\ MPa} < f_c'\ (25\ MPa)$ ***O.K.*** ✓

The ultimate point bearing capacity Q_p of the pile can be calculated as;

$Q_p = 9660 \times \Pi \times 0.80^2 / 4 \cong \underline{4855\ kN}$ *"the original one was 1256 kN"*

The final allowable vertical load capacities of Ø80 piles are found as,

$Q_a = (Q_s + Q_p) / F.S. = (2770 + 4855) / 3$

$$\mathbf{Q_a = 2541\ kN}$$

The original Q_a was 1342 kN so the increment is,

2541-1342= 1199 kN (89%)

Thus, it is obvious that an increment of 17° in Ø (even though a decrease of 1000 kPa in cohesion) changes the results dramatically (89%). So, the engineer must be sure of the kind and the physical properties of the rock material to avoid a fatal mistake in bearing capacity calculations.

5. MODELING

The Projects of the Structure

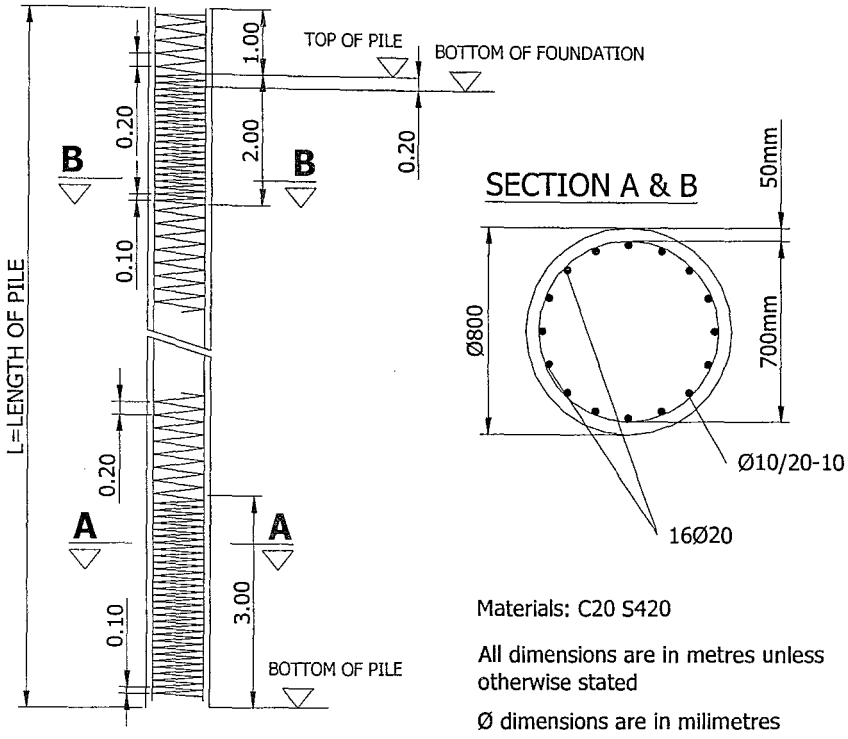

Figure 5-1Reinforcement Details of the Piles

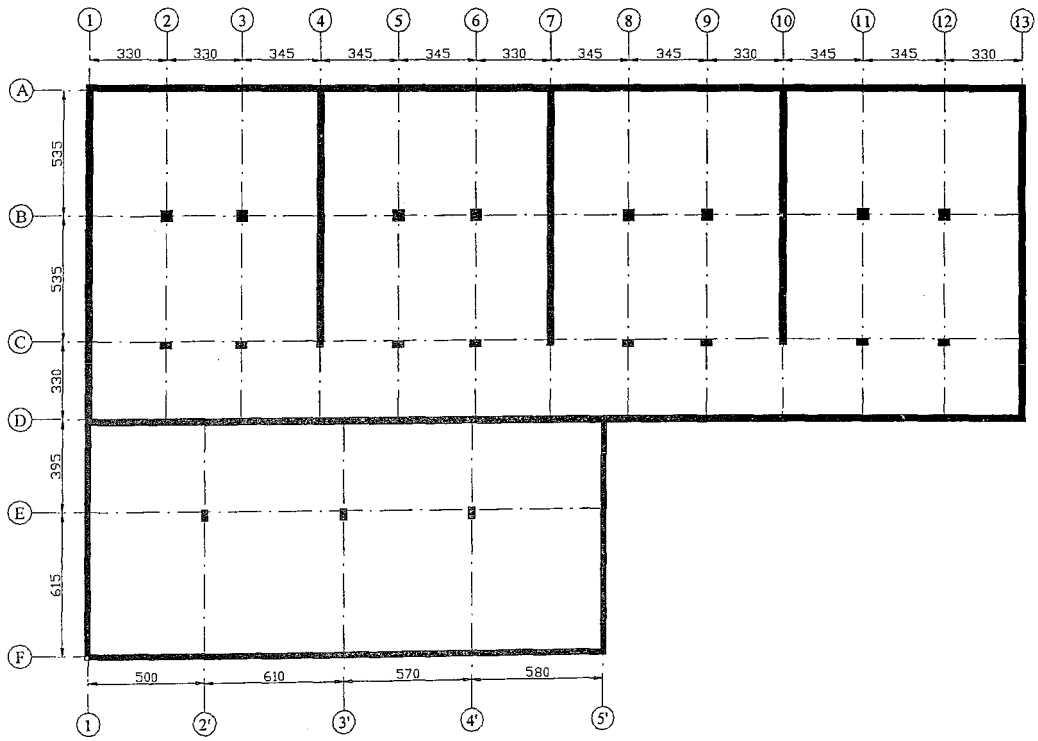

Figure 5-2 Plan View of the Basement

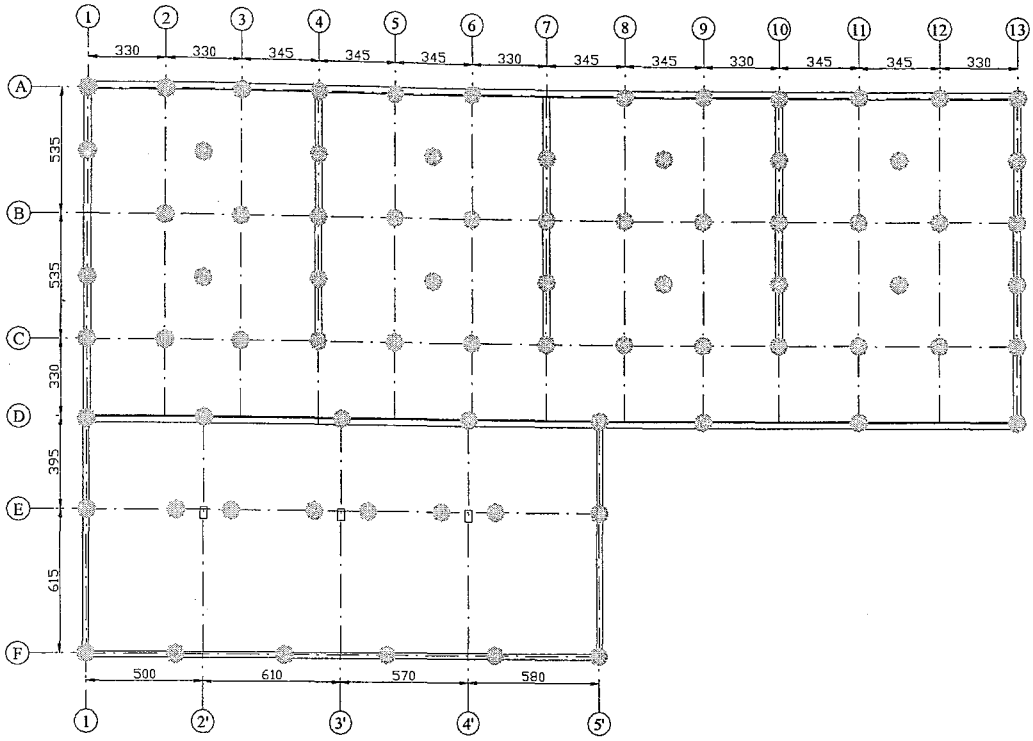

Figure 5-3 Plan View of the Pile Applications

5.1. Analysis of the Pile Materials

C25 (BS25) concrete and S420 (BCIIIa) steel are used in the cast-in-place group piles as well as in the superstructure. Both of the materials will be investigated thoroughly in the following, one by one.

Mander model is accepted for defining the unconfined concrete. 28 day strength = 25.00 MPa, E = 30,000 MPa (TS500), M = 2.5 ton/m^3 and W = 25 kN/m^3 are some of the main properties of the unconfined concrete. It is supposed to crush at 0.004m/m and spall at 0.005m/m.

Strain hardening steel model is used to define the steel. Its properties are, E = 210,000 MPa, yields at f_y = 420 MPa and ϵ = 0.002 and fails at ϵ = 0.12. It follows the same path during compression. 16 / Ø20 has been used for reinforcing the concrete.

There is a lot to write about the confined concrete but since it will be explained later, making an overview on this can provide a general knowledge, before getting to the analysis. All parts of the piles are confined with Ø10 S420 steel in a distance of s = 20 cm, not to mention that,

confinement bars are at shorter distances at the ends to supply more ductility and strength to (s=10 cm). As a result, the compression strength of the concrete is increased from 25.00 to 28.62 MPa at the middle and to 30.99 MPa at the confinement zones.

5.1.1. Unconfined Concrete Model

The properties of the unconfined concrete is as follows:

28-Day compressive strength:	*25 MPa*
Tension strength:	*0 MPa*
Post-crushing strength:	*0 MPa*
Crushing strain:	*0.004*
Spalling strain:	*0.005*
Elastic modulus:	*30,000 MPa*

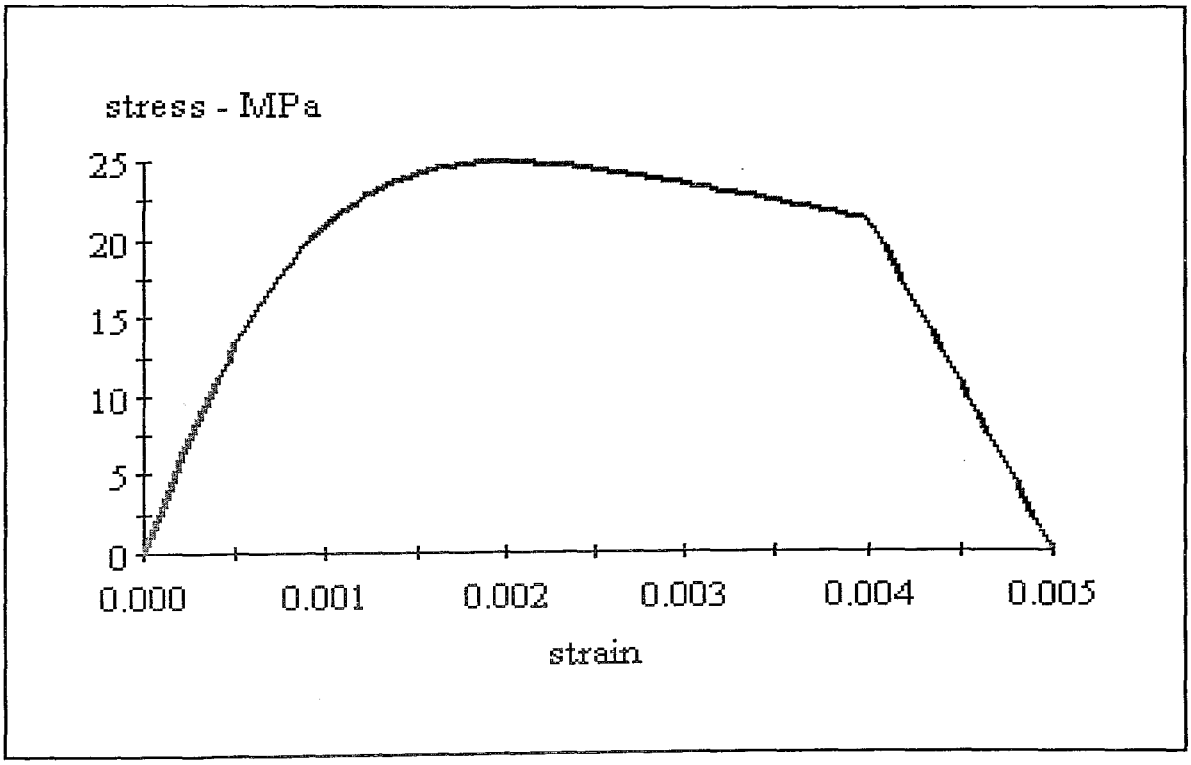

Figure 5-4 The Stress – Strain Diagram of the Unconfined Concrete

Model Details:

For Strain - $\varepsilon < 2 \cdot \varepsilon_t$	$fc = 0$
For Strain - $\varepsilon < 0$	$fc = \varepsilon \cdot Ec$
For Strain - $\varepsilon < \varepsilon_{cu}$	$fc = \frac{f'_c \cdot x \cdot r}{r - 1 + x^r}$
For Strain - $\varepsilon < \varepsilon_{sp}$	$fc = f_{cu} + (f_{cp} - f_{cu}) \cdot \frac{(\varepsilon - \varepsilon_{cu})}{(\varepsilon_{sp} - \varepsilon_{cu})}$

$$x = \frac{\varepsilon}{\varepsilon_{cc}}$$

$$r = \frac{Ec}{Ec - E_{sec}}$$

$$E_{sec} = \frac{f'_c}{\varepsilon_{cc}}$$

ε = Concrete Strain

fc = Concrete Stress

Ec = Elastic Modulus

E_{sec} = Secant Modulus

ε_t = Tension Strain Capacity

ε_{cu} = Ultimate Concrete Strain

ε_{cc} = Strain at Peak Stress = .002

ε_{sp} = Spalling Strain

f'_c = 28 Day Compressive Strength

f_{cu} = Stress at ε_{cu}

f_{cp} = Post Spalling Strength

5.1.2. Steel Model

The properties of the steel concrete is as follows:

Yield stress: *420 MPa*

Fracture stress: *550 MPa*

Yield strain: *0.002*

Hardening strain: *0.002*

Failure strain: *0.12*

Elastic modulus: *210,000 MPa*

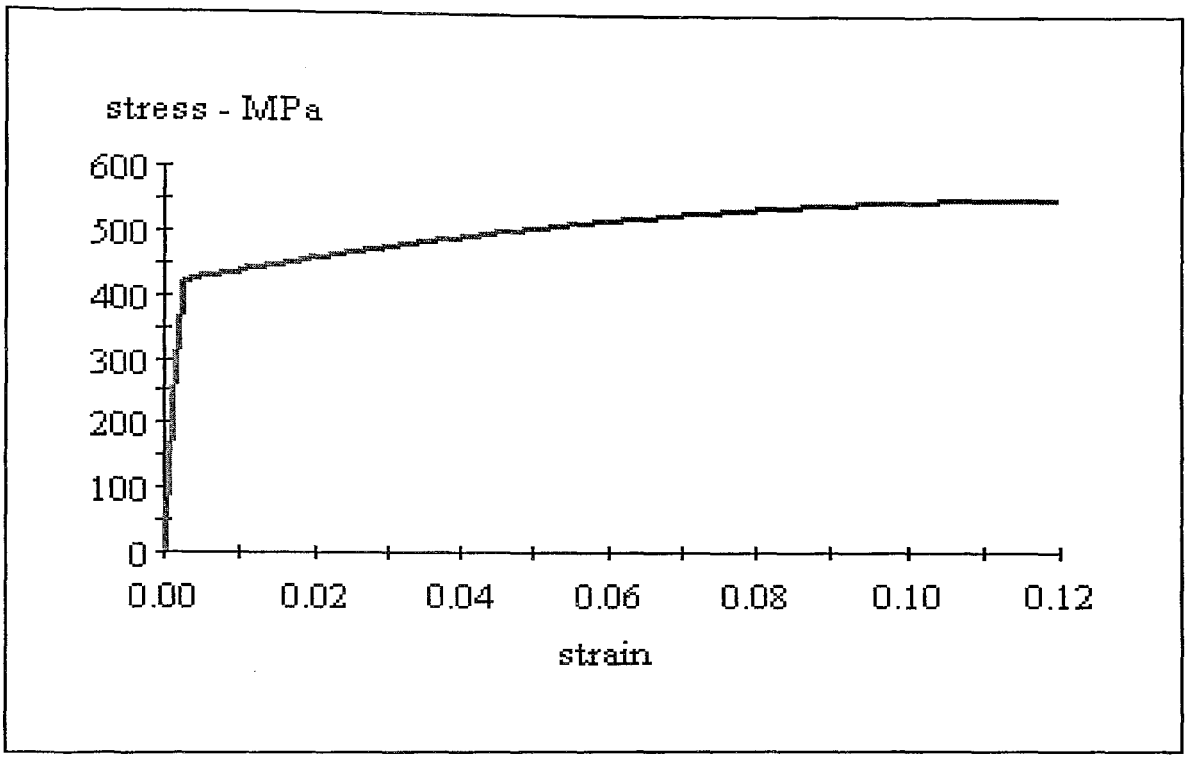

Figure 5-5 The Stress – Strain Diagram of the Steel

Model Details:

For Strain - $\varepsilon < \varepsilon_y$ $fs = E \cdot \varepsilon$

For Strain - $\varepsilon < \varepsilon_{sh}$ $fs = f_y$

For Strain - $\varepsilon < \varepsilon_{su}$ $fs = f_u - (f_u - f_y) \cdot \left(\frac{\varepsilon_{su} - \varepsilon}{\varepsilon_{su} - \varepsilon_{sh}} \right)^2$

ε = Steel Strain

fs = Steel Stress

f_y = Yield Stress

f_u = Fracture Stress

ε_y = Yield Strain

ε_{sh} = Strain at Strain Hardening

ε_{su} = Failure Strain

E = Elastic Modulus

5.1.3. Confined Concrete Model (Confinement Zones)

The properties of the confined concrete is as follows:

28-Day compressive strength: *25 MPa*
Confined concrete strength: *30.99 MPa*
Tension strength: *0 MPa*
Post-crushing strength: *0 MPa*
Strain at peak stress: *0.004396*
Crushing strain: *0.001422*
Elastic modulus: *30,000 MPa*

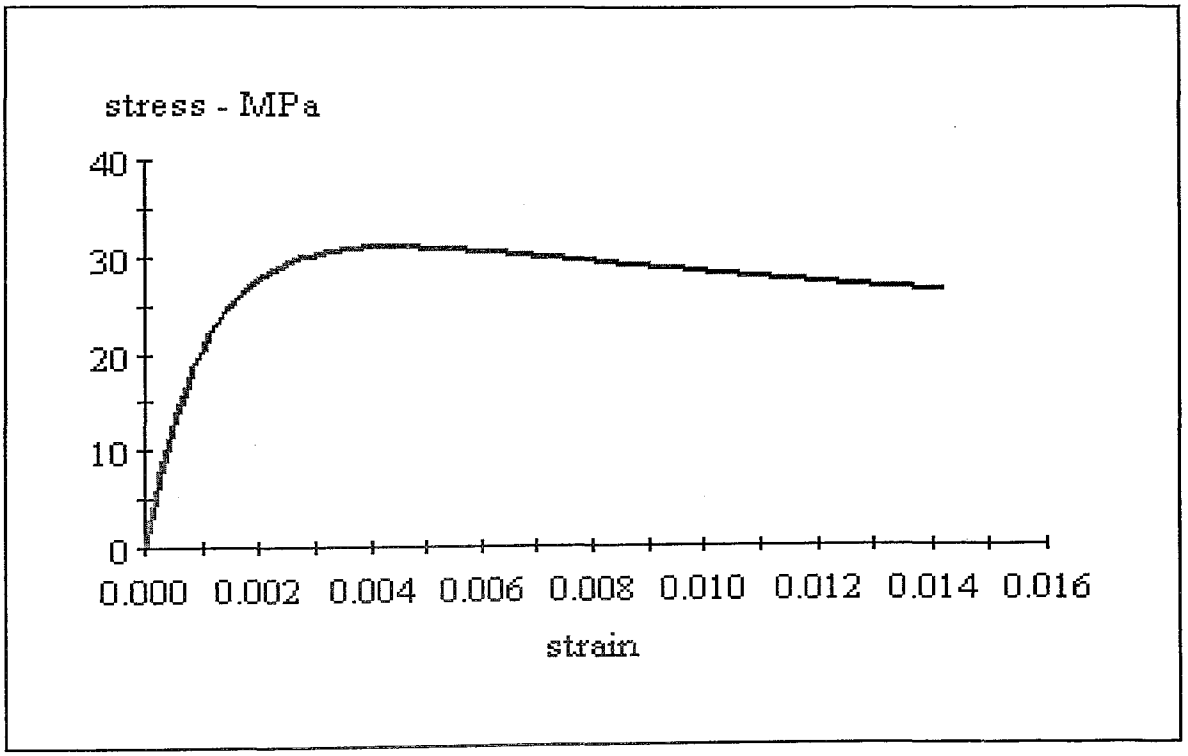

Figure 5-6 The Stress – Strain Diagram of the Confined Concrete (Confinement Zone)

Model Details:

For Strain - $\varepsilon < 2 \cdot \varepsilon_t$	$fc = 0$
For Strain - $\varepsilon < 0$	$fc = \varepsilon \cdot Ec$
For Strain - $\varepsilon < \varepsilon_{cu}$	$fc = \frac{f'_{cc} \cdot x \cdot r}{r - 1 + x^r}$

$$x = \frac{\varepsilon}{\varepsilon_{cc}}$$

$$\varepsilon_{cc} = .002 \cdot \left[1 + 5 \cdot \left(\frac{f'_{cc}}{f'_c} - 1\right)\right]$$

$$r = \frac{Ec}{Ec - E_{sec}}$$

$$E_{sec} = \frac{f'_{cc}}{\varepsilon_{cc}}$$

ε = Concrete Strain

fc = Concrete Stress

Ec = Elastic Modulus

ε_t = Tension Strain Capacity

ε_{cu} = Ultimate Concrete Strain

ε_{cc} = Strain at Peak Stress

f'_c = 28 Day Compressive Strength

f'_{cc} = Confined Concrete Strength

5.1.4. Confined Concrete Model (Mid Regions)

The properties of the confined concrete is as follows:

28-Day compressive strength:	*25 MPa*
Confined concrete strength:	*30.99 MPa*
Tension strength:	*0 MPa*
Post-crushing strength:	*0 MPa*
Strain at peak stress:	*0.004396*
Crushing strain:	*0.001422*
Elastic modulus:	*30,000 MPa*

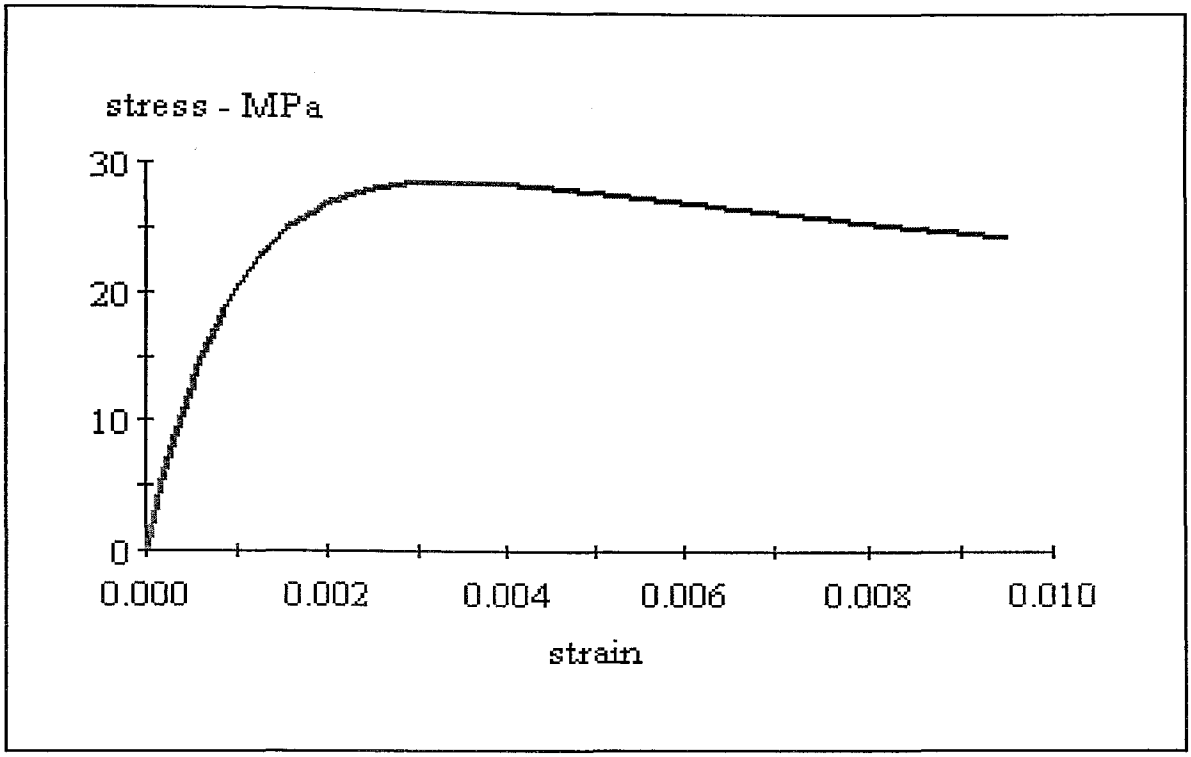

Figure 5-7 The Stress – Strain Diagram of the Confined Concrete (Mid Region)

5.2. Estimating the Piles' Capacities

The capacities of the reinforced concrete pile columns are calculated by means of the XTRACT computer program. They are loaded with the actual normal loads due to the G and Q, not to mention that their skin friction is subtracted from N. Since the skin resistance increases with the depth, normal loads (N) decrease from the top to the bottom end.

As mentioned above, N varies for different depths, thus the moment bearing capacities also differ from section to section. For the sake of accuracy piles are divided into 12 parts to calculate the moment and shear capacities for 12 different N values change due to increasing skin resistance and their self-weights. In addition, they are also divided for changes of soil layers, because the restrain conditions differ in those layers.

In addition, the 77 piles' N values also differ from each other. The most precise way to measure the piles' moment and shear capacities is, to use an average N value that will be quite conservative. The computation of this average/optimal N value is as the following:

$N = N_{avg} + N_{stdev}$

N = *optimal normal force*

N_{avg} = *average of the all 77 piles' Normal loads, of the same depth*

N_{stdev} = *standard deviation of the N values that computed*

The average, standard derivations and the optimal normal loads of the piles' sections, is shown in the following figure and table:

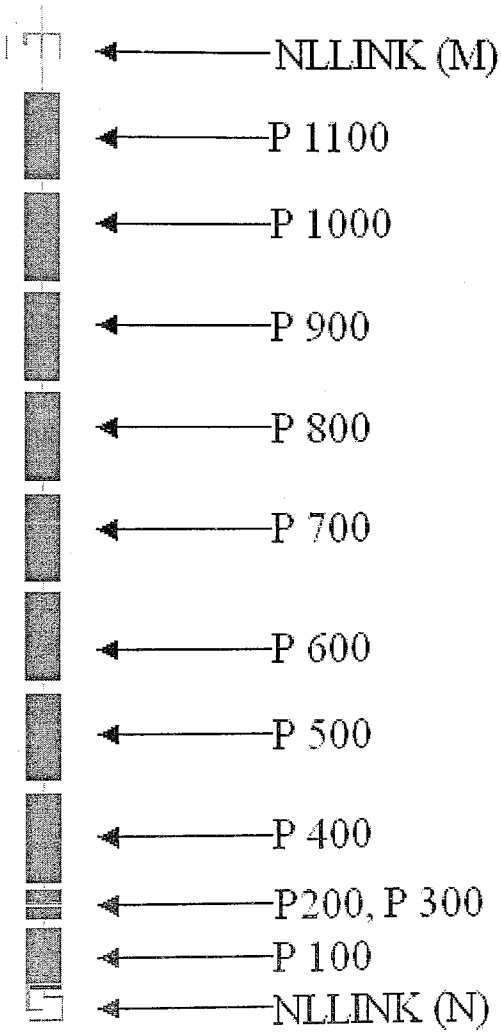

Figure 5-8 Demonstration of Pile's Sections and IDs

P 100	-34,00-36,50	*Depth [m]*
AVARAGE	-306,89	*Nstdev [kN]*
STDEV	39,47	*Navg [kN]*
AV-STAD	**-346**	*Navg-Nstdev[kN]*

P 200	-33,40-34,00
AVARAGE	-287,42
STDEV	37,44
AV-STAD	**-325**

P 300	-32,80-33,40
AVARAGE	-304,88
STDEV	37,44
AV-STAD	**-342**

P 400	-29,355-32,80
AVARAGE	-338,46
STDEV	41,31
AV-STAD	**-380**

P 500	-25,91-29,355
AVARAGE	-396,17
STDEV	41,31
AV-STAD	**-437**

P 600	-22,46-25,91
AVARAGE	-453,85
STDEV	41,32
AV-STAD	**-495**

P 700	-19,01-22,46
AVARAGE	-511,49
STDEV	41,32
AV-STAD	**-553**

P 800	-15,565-19,01
AVARAGE	-569,17
STDEV	41,31
AV-STAD	**-610**

P 900	-12,12-15,565
AVARAGE	-626,88
STDEV	41,31
AV-STAD	**-668**

P 1000	-8,67-12,12
AVARAGE	-684,56
STDEV	41,32
AV-STAD	**-726**

P 1100	-5,22-8,67
AVARAGE	-742,20
STDEV	41,32
AV-STAD	**-784**

NLLINK	-2,50-5,22
AVARAGE	-834,12
STDEV	37,36
AV-STAD	**-871**

Table 5-1 $N_{avg} - N_{stadev}$ [g+q] of the Piles at All Sections

Moment capacities of the piles are computed by the XTRACT program, as follows:

Firstly, the program calculates the ultimate, spalling, hardening, crushing and failing stresses and the corresponding strain values of the materials, with the consideration of their confinements.

Then it gives a specific N load, which is determined by the user, and begins to move the N load step by step, in x-x or y-y direction that desired. While the moment increases with this movement, the program reports the conditions of every three material "confined/unconfined concrete and steel" in each increment. For instance, if the steel in the compression zone yields it loads the compression concrete more.

After a several increments, it stops the analysis if one of the confined concrete or steel exceeds the failing strain after the cover concrete spalls. Then it reports the final moment and curvature values.

It bilinearizes the M-Kappa diagram if desired, and gives the EI effective and Yield EI effective to be used in further modeling.

5.2.1. Flexural Capacity for Different N Values

It is obvious that, M-Kappa and P-M interaction diagrams do not differ dramatically for a 400 kN (325 kN to 784 kN) increment of N for such a huge section. Thus, changing frame section properties only in the bottom and the uppermost section is adequate, for the sake of simplicity.

Furthermore, P-M interaction diagrams will be used to examine the piles' performances under spectral, time-history and lateral spreading analysis.

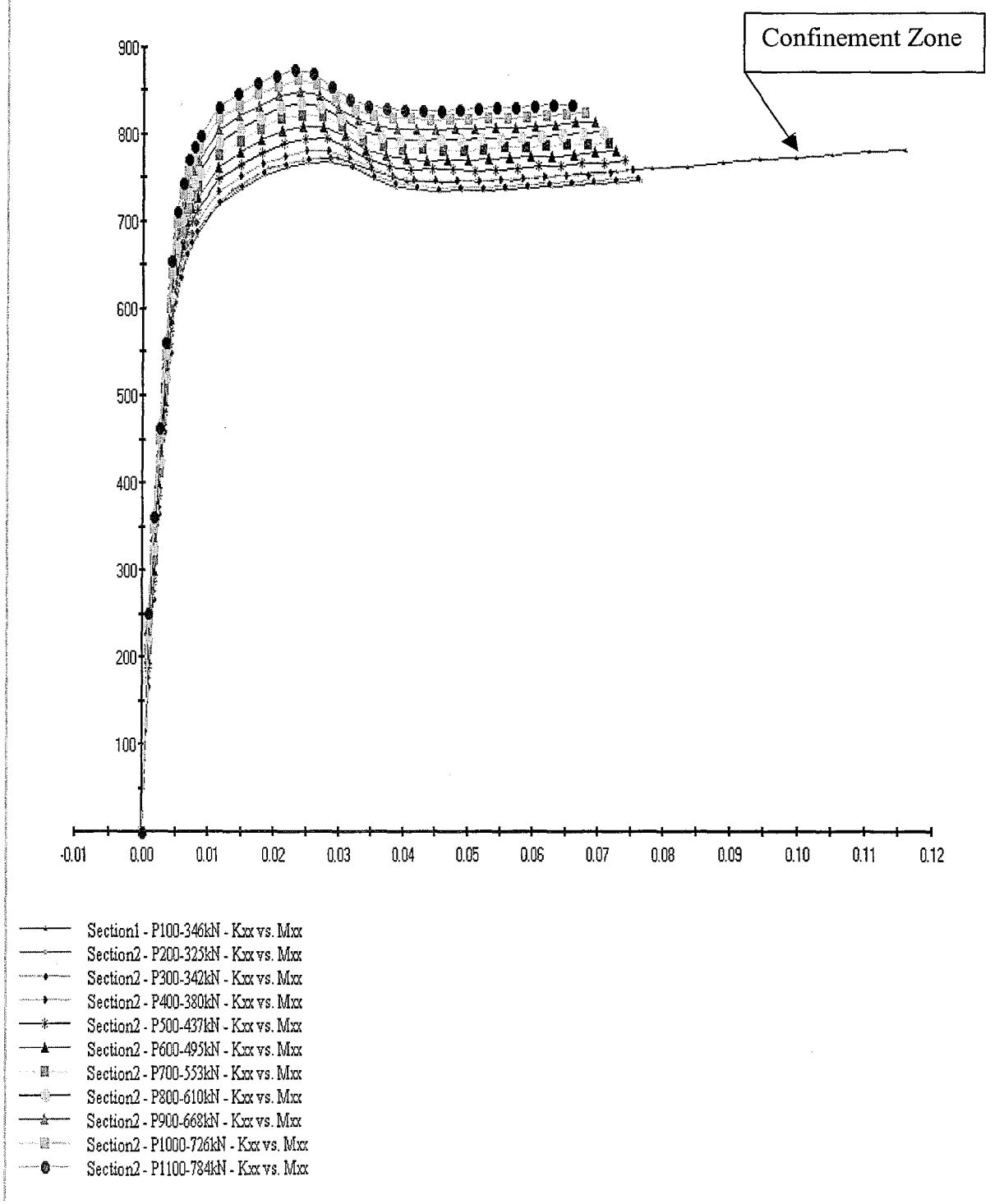

Figure 5-9 M – Kappa Diagrams for Different N Values

As seen in the figure, all of the pile sections' M–Kappa interactions do not differ, except the ones at the confinement zones. Thus, one M-K diagram will be used for all the middle sections.

5.2.1.1. Flexural Capacity of Confinement Zones

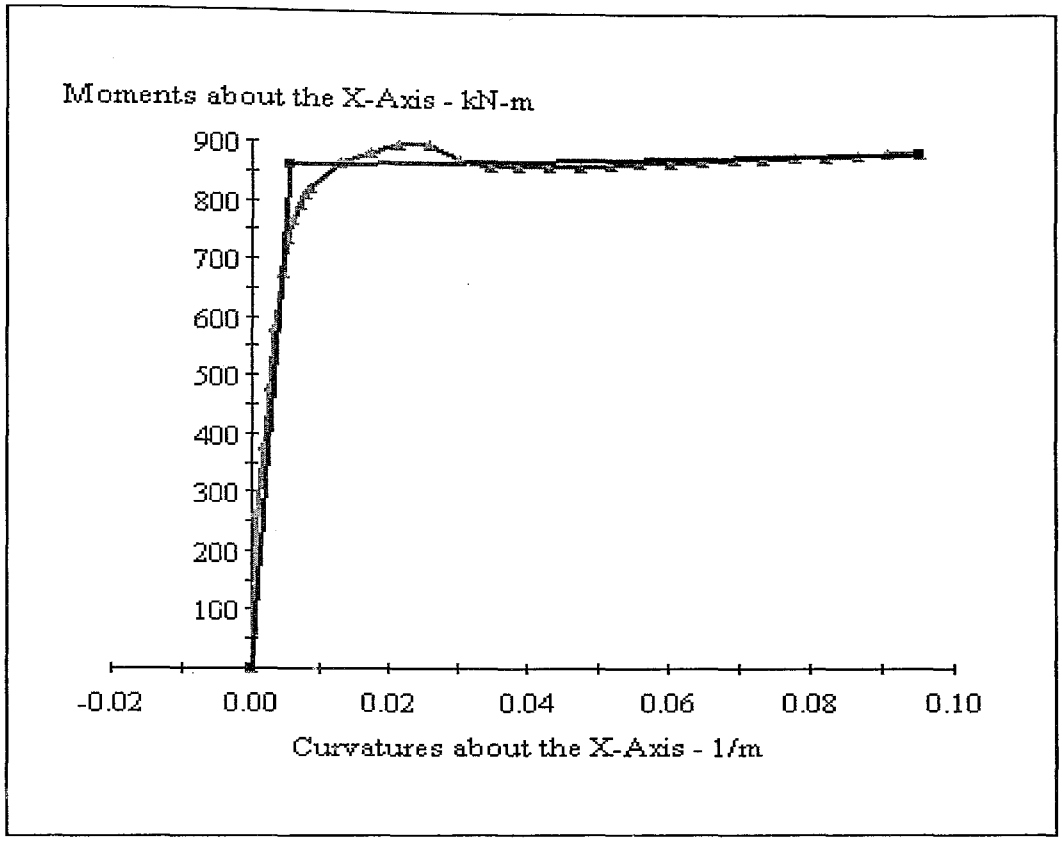

Figure 5-10 M-Kappa Diagram of the Confinement Zone

Failing Material:	Not Available
Failure Strain:	-------
Curvature at Initial Load:	-,1571E-19 1/m
Curvature at First Yield:	4,231E-3 1/m
Ultimate Curvature:	95,21E-3 1/m
Moment at First Yield:	674,2 kN-m
Ultimate Moment:	885,5 kN-m
Centroid Strain at Yield:	,6039E-3 Tension
Centroid Strain at Ultimate:	18,35E-3 Tension
N.A. at First Yield:	14,27 cm
N.A. at Ultimate:	19,28 cm
Energy per Length:	80,69 kN
Effective Yield Curvature:	5,394E-3 1/m
Effective Yield Moment:	859,7 kN-m
Over Strength Factor:	1,030
EI Effective:	1,59E+8 N-m^2
Yield EI Effective:	287,2E+3 N-m^2
Curvature Ductility:	17,65

5.2.1.2. Flexural Capacity of Middle Region

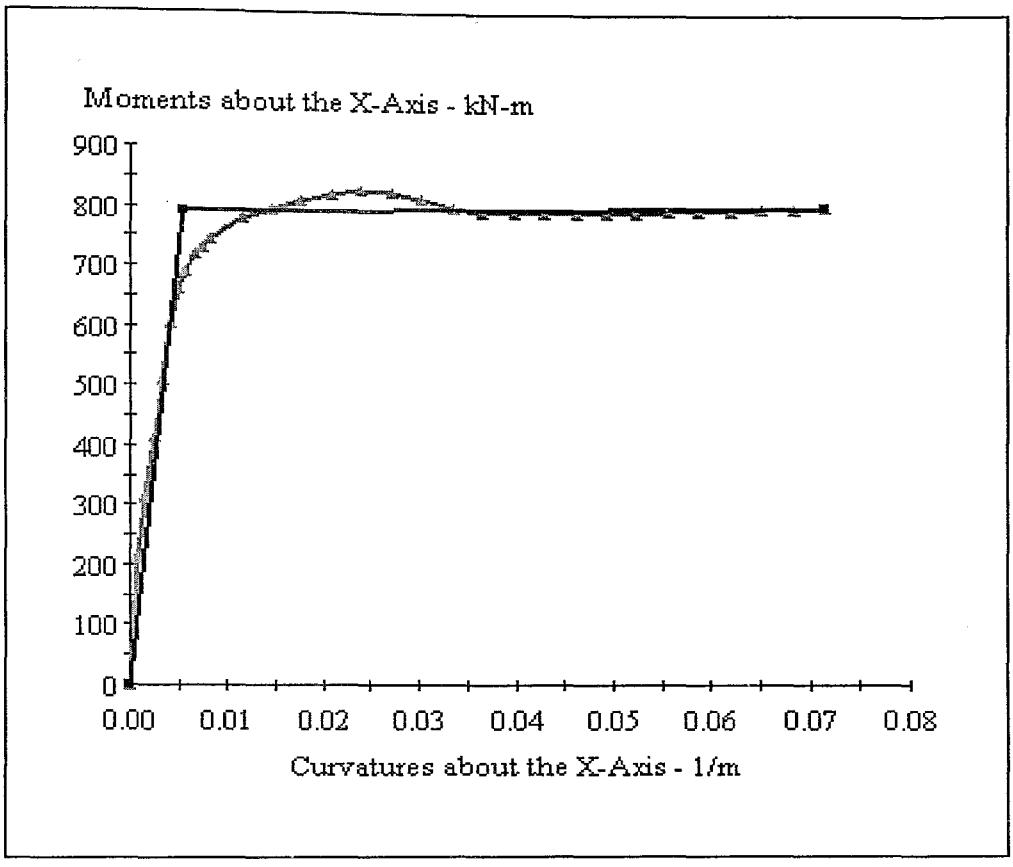

Figure 5-11 M-Kappa Diagram of the Middle Region

Failing Material:	Not Available
Failure Strain:	-------
Curvature at Initial Load:	,2023E-20 1/m
Curvature at First Yield:	4,070E-3 1/m
Ultimate Curvature:	71,41E-3 1/m
Moment at First Yield:	602,2 kN-m
Ultimate Moment:	800,5 kN-m
Centroid Strain at Yield:	,6569E-3 Tensior
Centroid Strain at Ultimate:	14,86E-3 Tensior
N.A. at First Yield:	16,14 cm
N.A. at Ultimate:	20,81 cm
Energy per Length:	54,74 kN
Effective Yield Curvature:	5,357E-3 1/m
Effective Yield Moment:	792,6 kN-m
Over Strength Factor:	1,010
EI Effective:	1,48E+8 N-m^2
Yield EI Effective:	119,0E+3 N-m^2
Curvature Ductility:	13,33

5.2.2. P-M Interactions

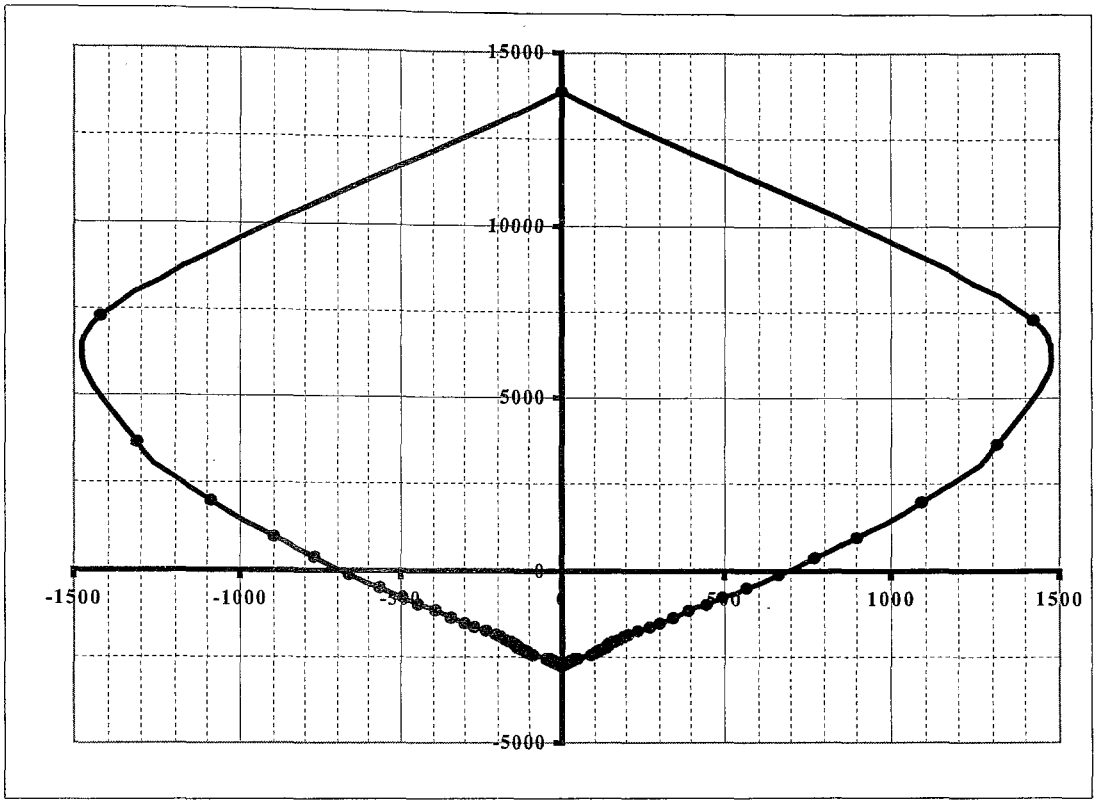

Figure 5-12 P-M Interaction Curve of the Confinement Zones

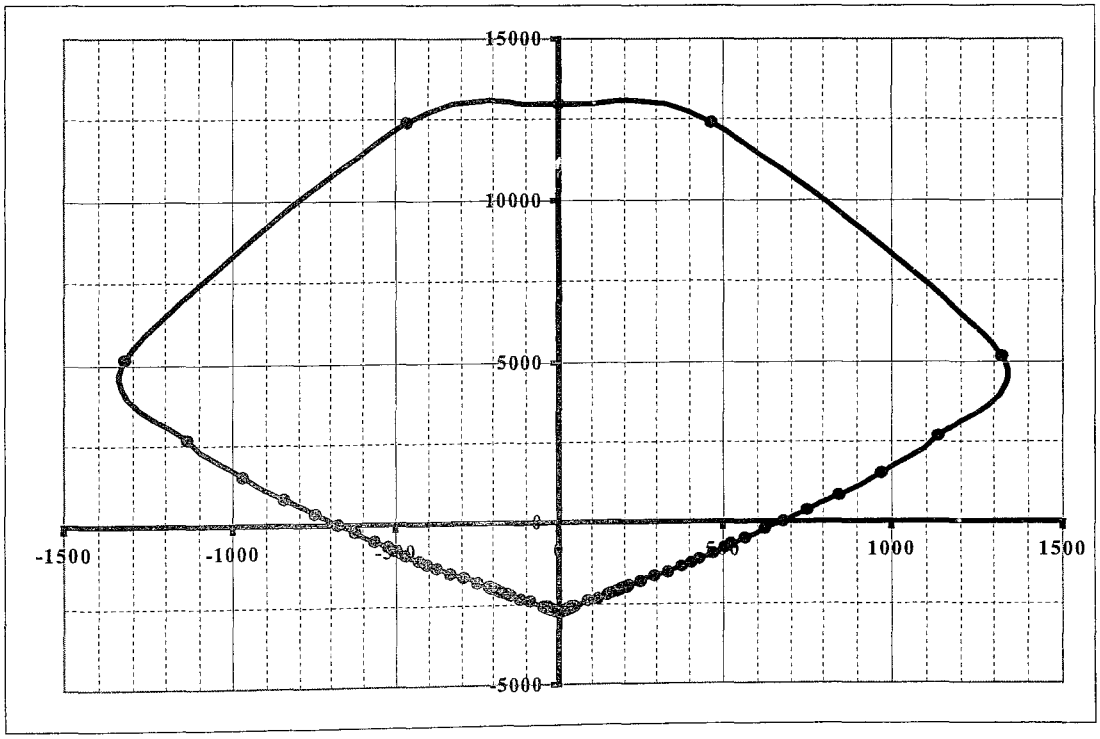

Figure 5-13 P-M Interaction Curve of the Middle Sections

5.2.3. Shear Capacity

The formulation by Priestley (1996) has been used to estimate the shear capacity of the pier columns. The proposed method by Priestley provides significantly improved correlation with experimental results. The column shear capacity is given as;

$$V_n = V_c + V_p + V_s$$

V_c: *concrete component of shear capacity*

V_p: *contribution of the axial load in the column*

V_s: *contribution of the transverse reinforcement*

- The concrete contribution of the column is given as:

$$V_c = k * \sqrt{fc'} * A_e$$

k: factor to account for member ductility. For this analysis, the factor is related to curvature ductility

$$= \left\{ \begin{array}{lll} 0.29 & for & \mu \leq 3 \\ 0.43 - 0.048\mu & for & 3 < \mu \leq 7 \\ 0.15 - 7.3 * 10^{-3}\mu & for & 7 < \mu \leq 15 \\ 0.042 & for & \mu > 13 \end{array} \right\} \text{ for uniaxial ductilty}$$

μ: *Curvature ductility*

fc': *Compressive strength of concrete*

A_e: *Effective shear area (0.8 x A_{gross})*

When the coefficients of the Vc equation are computed for the model:

$\mu = 17.65$, *thus* $k = 0.042$

$A_e = 0.8 \times 0.50 = 0.4\ m^2$

$f_c' = 25{,}000\ kN/m^2$

$V_c = k * \sqrt{fc'} * A_e$

$V_c = 0.042 \times 25{,}000^{0.5} \times 0.4$

$\underline{V_c = 2.66\ kN}$

- Axial load contribution to the shear capacity that is explained above is given as:

$$V_p = \frac{D - c}{2 * a} * P$$

D: *Overall section depth*

c : *Depth of the flexural compression zone*

a : *L for single bending, L/2 for double bending.*

L : *Height of the column*

P : *Axial load in member*

For the model the above variables are as follows:

$D = 0.80\ m$

$c = 0.1928\ m$

$a = 34 / 2 = 17\ m$

$L = 34\ m$

$P = 871\ kN$

$$V_p = \frac{D - c}{2 * a} * P$$

$V_p = (0.80 - 0.1928) / (2 \times 17m) \times 871$

$\underline{V_p = 106.30\ kN}$

- The contribution of the transverse reinforcement is given as:

$$V_s = \frac{A_s * f_y * D'}{s} * \cot(\phi)$$

D': *Distance between transverse reinforcement*

f_y: *Yield stress of transverse reinforcement*

ϕ: *Angle of inclined cracking*

A_s: *Area of transverse reinforcement*

S: *Spacing of transverse reinforcement layer*

For the model the above variables are as follows:

$D' = 0.70\ m$

$f_{yh} = 420{,}000\ kN/m^2$

$\emptyset = 30^o$

$A_s = 2 \times \Pi \times 0.01^2 / 4 = 1.57E\text{-}4\ m^2$

$S = 0.10\ m$

$V_s = (1.57E\text{-}4 \times 420{,}000 \times 0.70) / 0.10 \times \cot(30^o)$

$\underline{V_s = 799.48\ kN}$

And the total shear capacity is the following:

$V = V_c + V_p + V_s$

$V = 2.66 + 106.30 + 799.48$

$$\underline{\boldsymbol{V = 908\ kN}}$$

5.2.4. Modification Factors

Since the assumption is that the hinging will occur on at the top of the piles, the nllink elements will be installed to only the edge region to provide the non-linear behavior. Essentially the structural elements of the main building also may yield but they are assumed as if they will not. Thus the writer had the advantage of investigating the soil and substructure deeper without the exceptions of the superstructure.

With the help of XTRACT program's outputs of M-Kappa interactions, the modified moment of inertias of the pile sections will be computed as follows:

EI_{eff} =1.48E+5 kN/m^2 "M_n/Kappa$_n$ P 700"

E_c = 30,000,000 [kPa]

$I_{Ø80}$ = 2.034E-2 [m^4]

$E_cI_{Ø80}$ = 610,200

$$Modification\ Factor = \frac{EI_{eff}}{E_c I_{Ø80}} = \frac{1.48E+5}{610{,}200} = \underline{0.243}$$

5.3. Modeling the Superstructure in SAP2000 Program

Firstly the superstructure modeled in SAP2000 computer program. The model is composed of 1079 joints, 283 frames (columns and beams) and 1031 shells (structural walls, mat foundation and slabs). The complete model is composed of 2080 joints, 1130 frames, 1131 shells, 154 non-linear link elements and 1848 springs. The shells are divided to 2 by 2m to get the most precise results. Also the frames are connected to these shells to maintain the synchronism during cyclic movements.

The total mass of the structure is 10,479 tons, where 3551 tons of it comes from the super and 6927 tons from the substructure (Mat foundation is added to the sub. Mat foundation' s mass is ~3637 tons when Mq is added).

5.3.1. Views of the Model

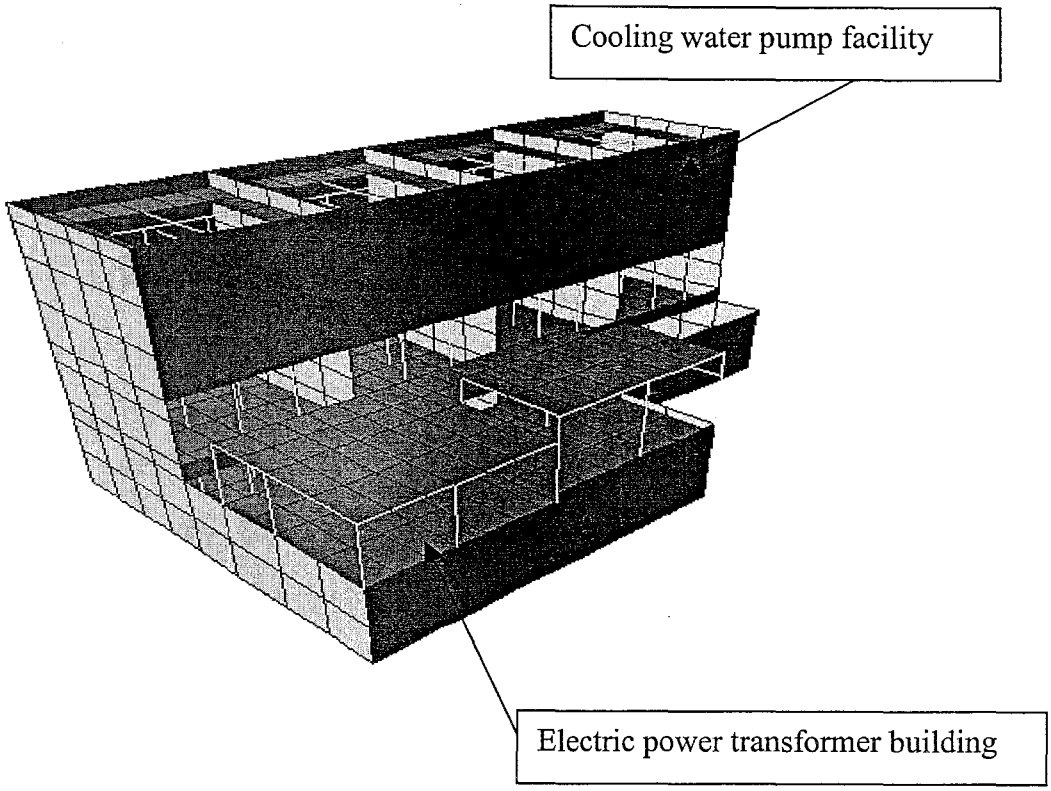

Figure 5-14 3-D View of the SAP2000 Model

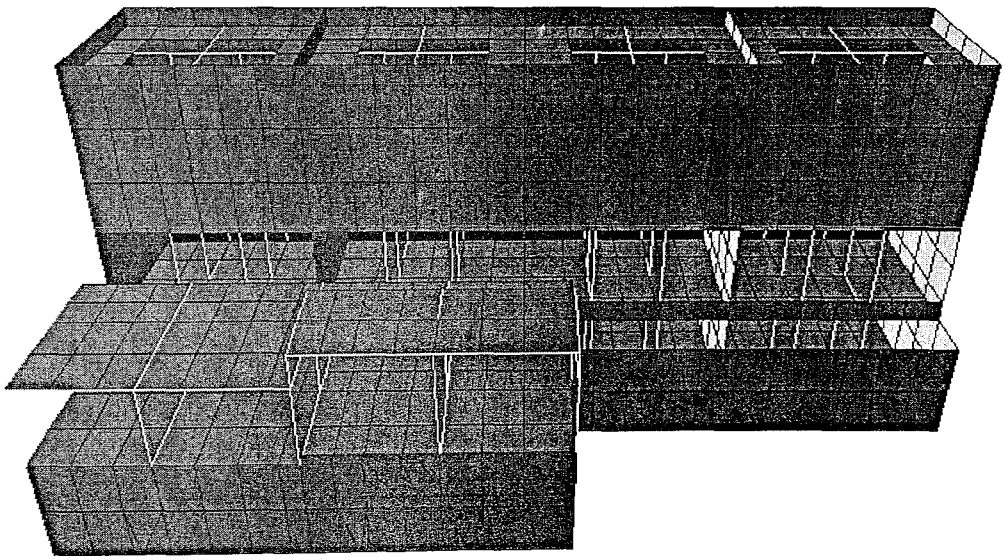

Figure 5-15 X-Z Direction View

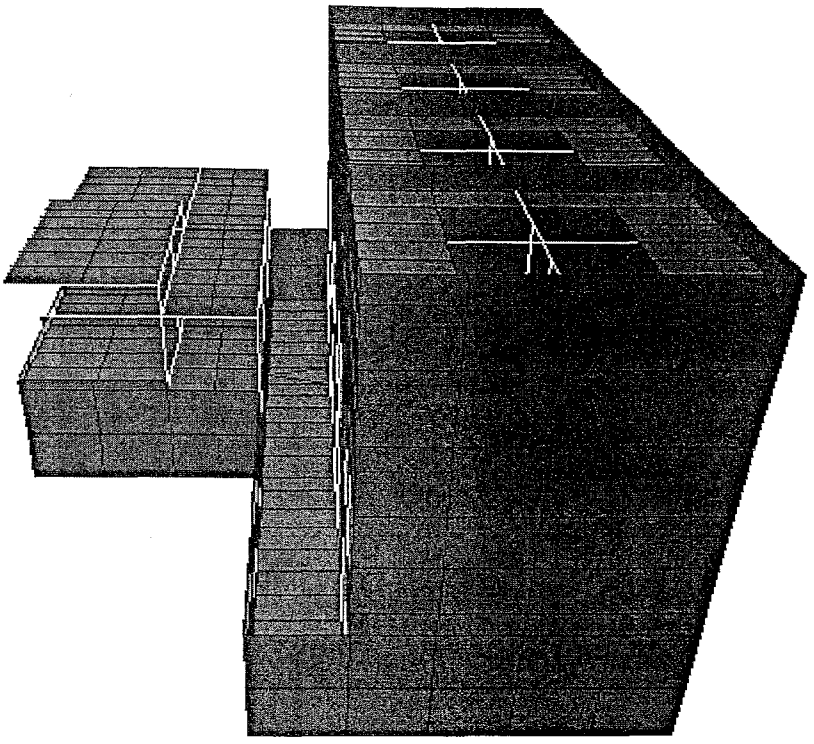

Figure 5-16 Y-Z Direction View

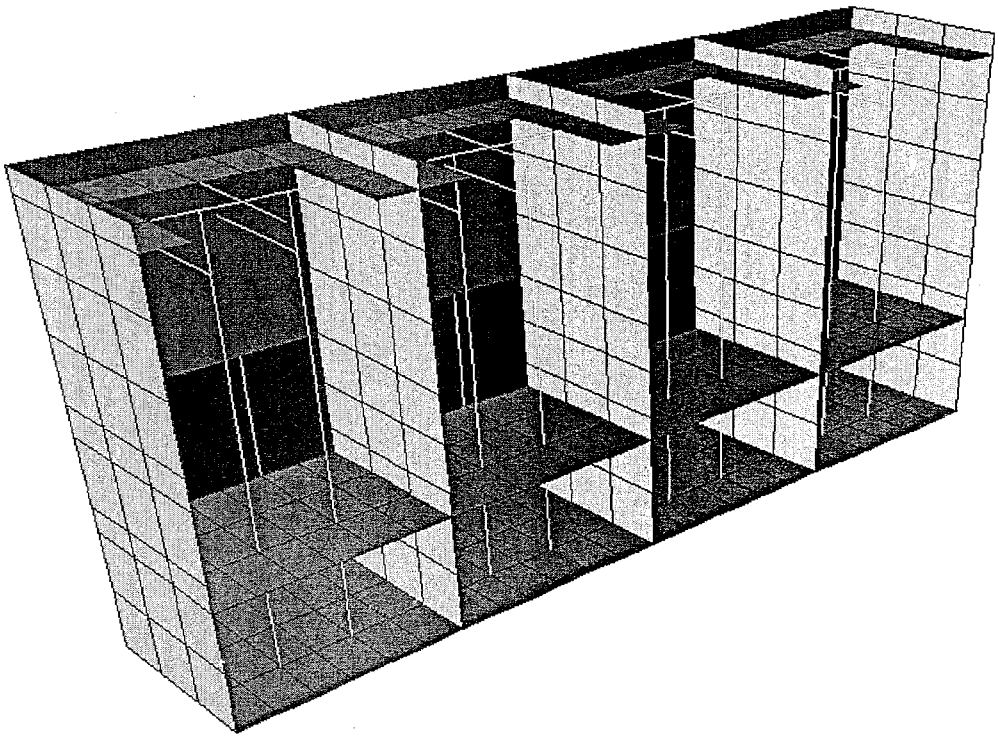

Figure 5-17 3-D Cross-Section of the Cooling Water Pump Facility

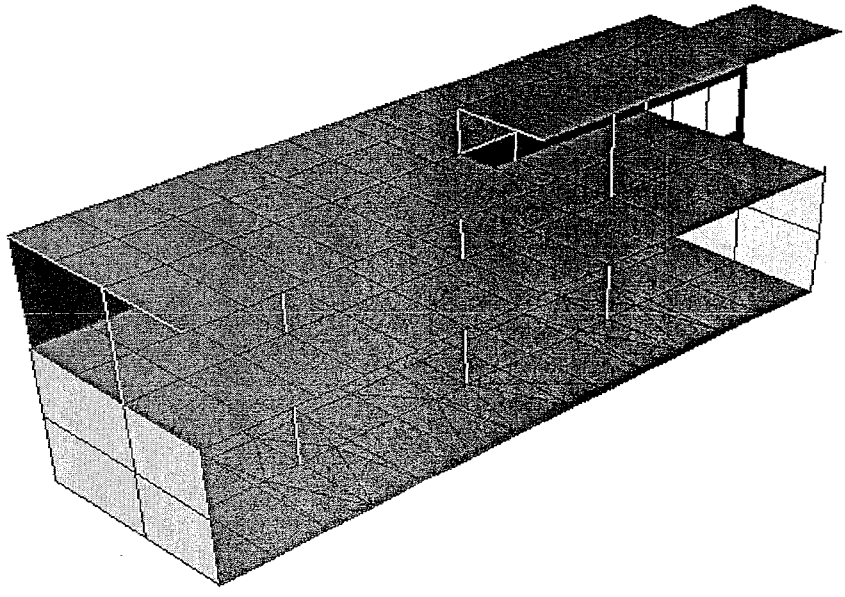

Figure 5-18 3-D Cross-Section of the Electric Power Transformer Building

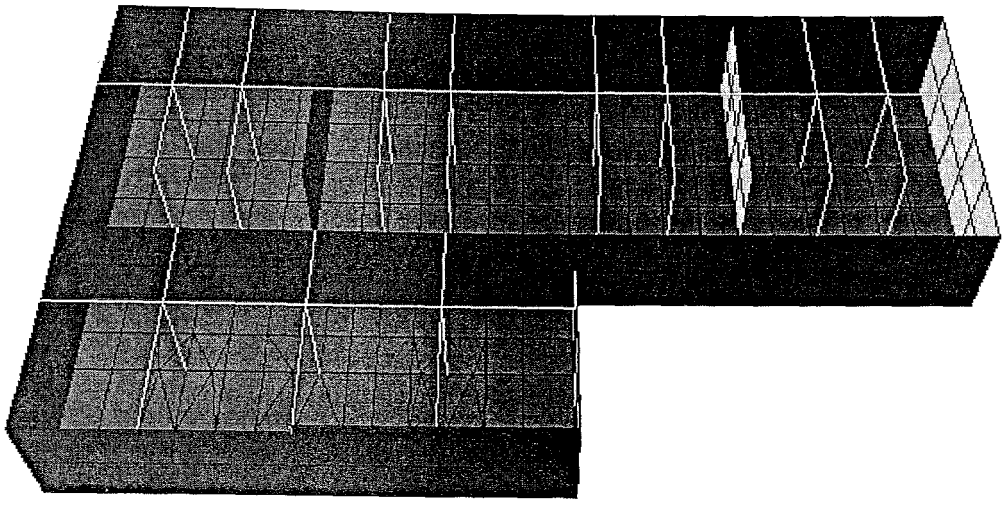

Figure 5-19 X-Z Cross-Section (the 1st Storey and the Mat Foundation)

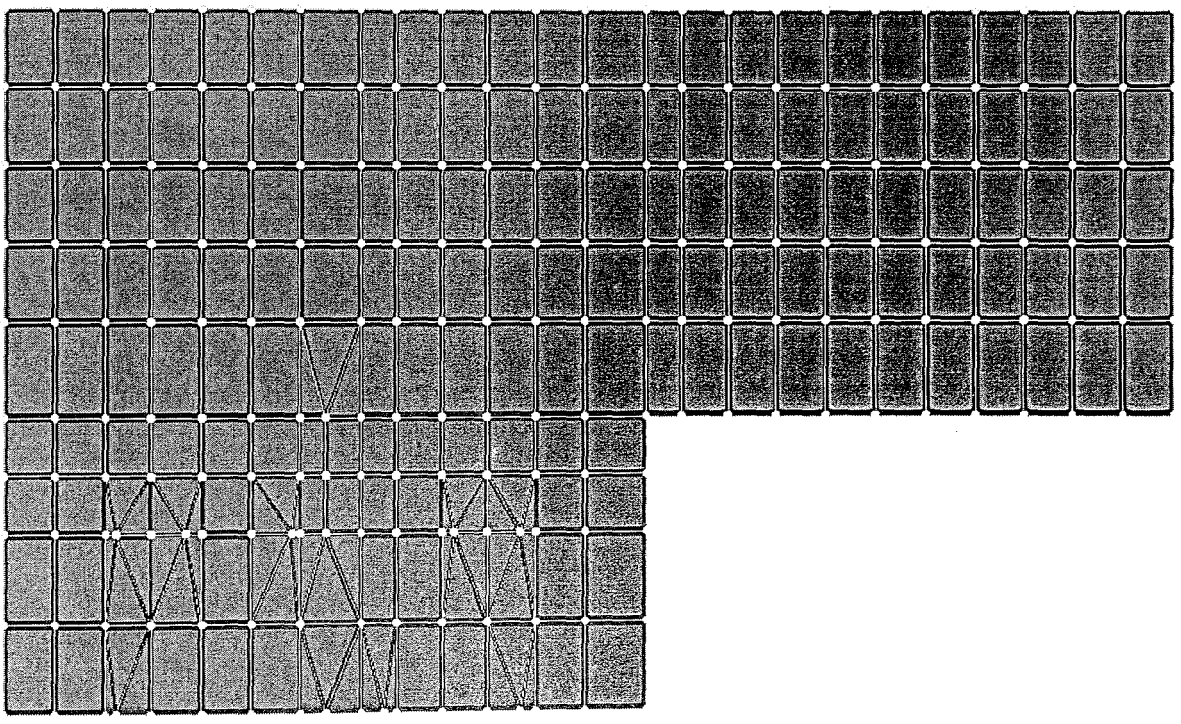

Figure 5-20 X-Y View of the Mat Foundation

5.3.2. Determination of Live/Dead-Load and Mass

Since the live load of the building is composed of cranes, gigantic motor pumps and other massive materials, Q is taken as 10 kN/m^2 as an observational engineering judgment. It is applied directly to the slabs

The computation of the live load's mass is just as above,

Purpose of Occupancy of Building	n
Depot, warehouse, etc.	0.80
School, dormitory, sport facility, cinema, theatre, concert hall, carpark, restaurant, shop, etc.	0.60
Residence, office, hotel, hospital, etc.	0.30

Table 5-2 Live Load Participation Factor (n) (TSC-98, P.18)

$n = 0.8$

$Q = 10\ kN/m^2$

$Q' = 10 * 0.8 = 8\ kN/m^2$

$Mq_{unit\text{-}area} = 8 / 9.81 = 0.815\ ton/m^2$

To add its mass to the slab concrete's mass,

$Mq_{unit\text{-}area} = 8 / 9.81 = 0.815\ ton/m^2$ *"for h = 0.20m slab"*

If it were h = 1.00 m then,

$Mq'/unit\text{-}volume = 0.815 / 0.20 = 4.08\ ton/m^3$

$M(total)_{unit\text{-}volume} = 4.08 + 2.50 = 6.58 \cong 6.5\ ton/m^3$

Total masses of the structure is as follows:

Superstructure: *3551 tons*

Mat foundation: *3637 tons*

Substructure: *3290 ton*

TOTAL MASS: *10479 ton*

5.4. Modeling the Substructure

As a foundation problem, the modeling of the substructure and the soil must be considered together, because the piles act together with the surrounding soil. To overcome this problem the piles divided into 12 parts and joined to the soil, which is modeled using springs. The 12 parts of the piles are modeled different from each other according to their strengths and ductilities.

The piles are modeled as Ø80 cm circular, reinforced concrete frames. Non-linear link elements added to the top of the piles to measure moment and shear forces during time-history analysis, which will be analyzed in the further chapters. Since the piles are not anchored to a strong type rock, it is judged that the bedrock releases a considerable amount of bending moment. To overcome this problem, instead of restraining bottom of the piles to M_{x-x} or M_{y-y}, the rigidity of the anchor is modeled using springs.

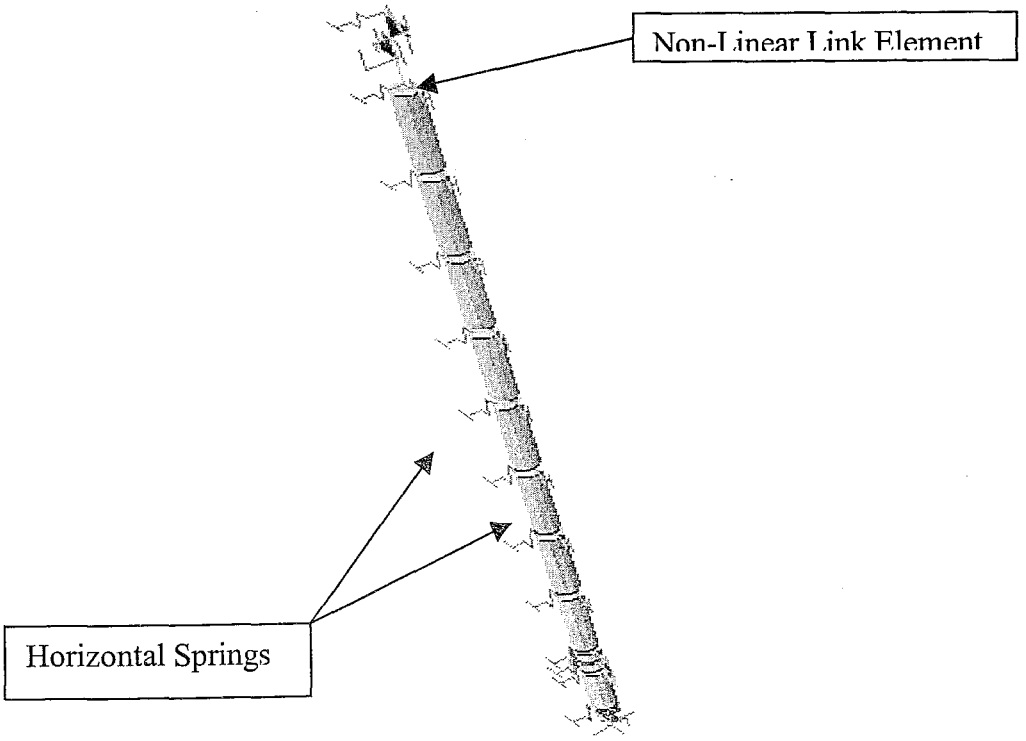

Figure 5-21 Demonstration of a Pile With Springs

5.4.1. Shear & Bending Moment Hinges

In this section non-linear link elements are used to model the hinges, which might occur at the top of the piles, where they are connected to the mat foundation and probably will get the maximum bending moment and shear force.

In addition, since there will be no hinging at the middle of any piles, it is not necessary to assign a nllink element at those sections.

5.4.1.1. Determination of the Hinge Length

Before determining the properties of the nllink elements', the hinging length of the piles must be computed. To calculate this length the following equation is used:

$$l_p = 0.08l + 0.022 \times f_{ye} \times d_{bl} \geq 0.044 \times f_{ye} \times d_{bl}$$ *(Priestly, 2000, P.308)*

where,

l_p : *hinge length [m]*
l : *buckling length of the frame (pile) [m]*
f_{ye} :*yield stress of the reinforcement material [MPa]*
d_{bl} : *diameter of the longitudinal reinforcement [mm]*

when the variables are written, the equation becomes:

$$l_p = 0.08l + 0.022 \times f_{ye} \times d_{bl} \geq 0.044 \times f_{ye} \times d_{bl}$$
$$l_p = 0.08 \times 34 + 0.022 \times 420 \times 0.80 \geq 0.022 \times 420 \times 0.80$$
$$l_p = 2.72 \geq 0.37$$

since the right side of the equation cannot exceed the left side, the length is accepted as:

$$\underline{l_p = 2.72 \text{ m}}$$

5.4.1.2. Hinge Capacities

To add the hinges to the base model of the substructure, the non-linear moment-curvature and shear-deflection properties are needed. The outputs of the XTRACT program are used while determining the initial and post stiffness of the nllink elements. The calculations of the nllink elements' bending moment and shear stifnesses, by means of the outputs are as the following:

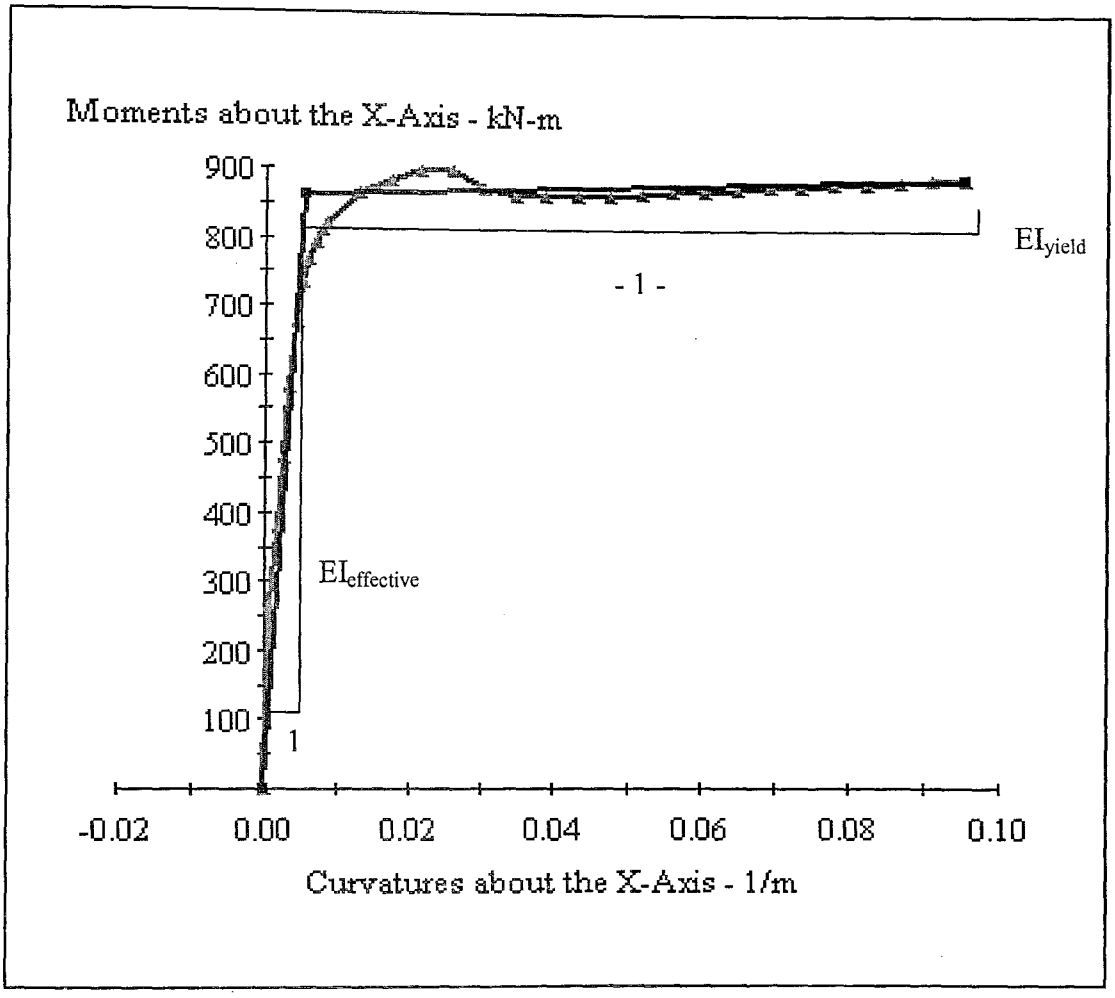

Figure 5-22 M- Kappa diagram of the hinge (P(g) = 871 kN)

$EI_{effective} = 1.59E+5\ kNm^2$
$EI_{yield} = 2.87E+2\ kNm^2$
$L\ (hinge\ length) = 2.72\ m$

Table 5-3 The Outputs of the XTRACT Computer Program

The bending moment coefficients are:

$R_{stiffness}$ *(Bending moment stiffness)* $= 12\ EI_{eff} / L_p$

$R_{stiffness} = 12 \times 1.59E+5 / 2.72 =$ *58456 kNm [1/rad]*

$R_{strength}$ *(effective yield moment)*= *860 kNm*

$$R_\alpha \text{ (post-yield stiffness ratio)} = \frac{EI_{yield}}{EI_{effective}}$$

$$R_\alpha = \frac{2.87E+2}{1.59E+5} = 1.8E\text{-}3$$

And the shear-force coefficients are:

$U_{stiffness}$ *(Shear stiffness)* $= 12\ EI_{eff} / L_p^3$

$U_{stiffness} = 12 \times 1.59E+5 / 2.72^3 =$ *94814 kN/m*

$U_{strength}$ *(effective yield moment / (L / 2))* $= 860 / (2.72 / 2) =$ *632 kN*

$(l_p = L/2)$

$$U_\alpha \text{ (post-yield stiffness ratio)} = \frac{EI_{yield}}{EI_{effective}}$$

$$U_\alpha = \frac{2.87E+2}{1.59E+5} = 1.8E\text{-}3$$

The bending moment and shear stiffness of the pile are same in both X-X and Y-Y directions because the piles' sections are symmetrical in both directions.

5.4.2. Distribution of Pile Friction Forces

Friction part of the pile (31.50 m) is divided into 11 parts considering the change of soil property from layer to layer and pile stiffness. $q_s = 35$ kN/m^2 is used which was calculated as explained in the 4th chapter and this value is multiplied with the area of every section to compute the every upward force that is applied to the pile by the soil.

	Depths	Mid Points	Lengths	Force / m (Fs/m)	TOTAL UPWARD FORCES (Fs)
	[m]	[m]	[m]	[kN/m]	[kN]
	-2,50				
		-4,45			
Qs	-5,22		4,45	29,32	130
		-6,95			
Qs	-8,67		3,45	29,32	101
		-10,40			
Qs	-12,12		3,45	29,32	101
		-13,84			
Qs	-15,57		3,45	29,32	101
		-17,29			
Qs	-19,01		3,45	29,32	101
		-20,74			
Qs	-22,46		3,45	29,32	101
		-24,19			
Qs	-25,91		3,45	29,32	101
		-27,63			
Qs	-29,36		3,45	29,32	101
		-31,08			
Qs	-32,80		2,02	29,32	59
		-33,10			
Qs	-33,40		0,90	29,32	25
		-33,70			
	-34,00				
			31,50		**923**

Qs(ult) =	2770	[kN]	*Ultimate skin friction (Chapter 4)*
Qs(a) =	923	[kN]	*Allowable skin friction (Chapter 4)*
qs:	35	[kN/m2]	*Skin fric. / Unit area (Chapter 4)*
As / m (pi*D*L):	2,51	[m2/m]	*Surface area / Unit length*
Fs / m:	29,32	[kN/m]	*Skin fric. / Unit length*

Table 5-4 Distribution of Pile Friction Forces

5.4.3. Modeling the Soil

5.4.3.1. Modeling the Normal Force Hinge

In this section, point resistance of the piles will be modeled as a normal force hinge to allow firstly the skin resistance to grasp the pile and release the exceeding *P* to the pile point. If the point resistance were entered as a simple force in the opposite direction of the gravity, the model would be unable to illustrate the acting of the pile during an earthquake. Not to mention that, it would be impossible to observe the vertical displacements as well, because the piles would give the same upward resistance to the vertical loads coming from the superstructure.

Thus the skin resistance modeled as distributed upward forces applied to the pile, and only the exceeding normal force ($P > Q_s$) reaches to the bottom. A simple demonstration of the normal load hinge is below:

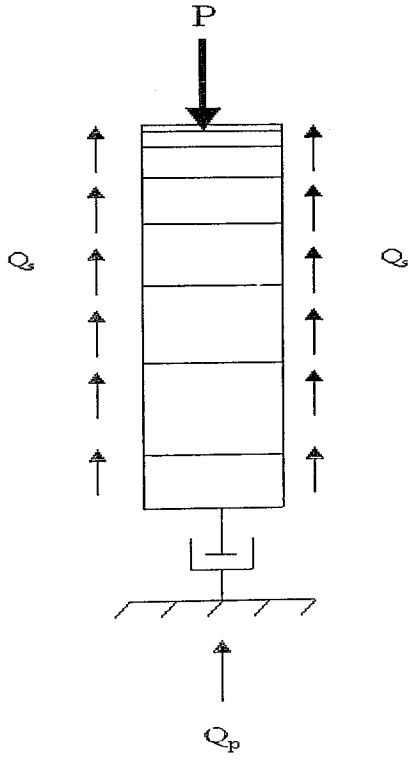

Figure 5-23 Illustration of Vertical Deformation of a Pile and Normal Force Hinge

($Q_s / \Delta L > W_{pile} / \Delta L$)

5.4.3.2. Determination of the Settlement of Pile Points

To determine the settlement of pile points, firstly modulus of elasticity of the rock layer must be found. It is E = 3E+6 kPa for claystones (Bowles, P.278). From the previous calculations in chapter 4.4., the Qp is found to be 419 kN. If this value is converted to pressure:

$$\sigma = Q_p / A_p = 419 / (\pi.0.80^2 / 4) = 834\ kN/m^2$$

σ (P/A) [kN/m2]	0	834
ε (σ/E) [−]	0	2,78E-04

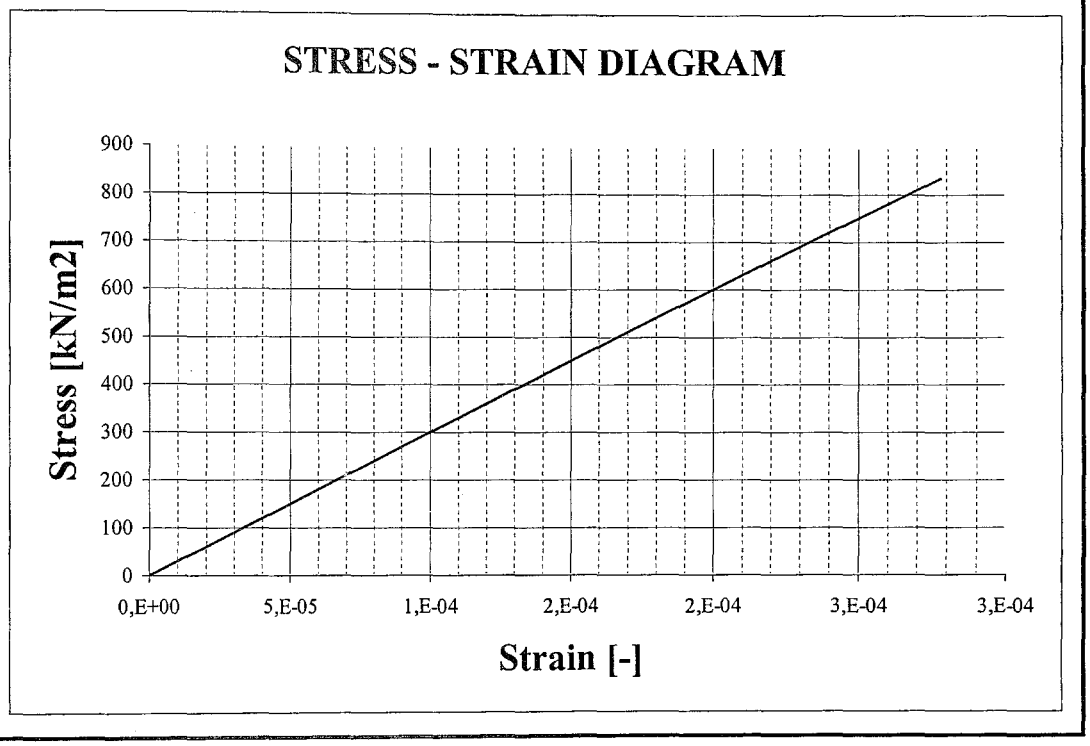

Table 5-5 Stress – Strain Diagram of the Claystone

Once ε is found to be 2.78E-4, then the point settlement can be found from the following equation:

$$\varepsilon = \Delta h / h$$

$$2.78E{-}4 = \Delta h / 34 \rightarrow \Delta h_{max} = 9.452E{-}3\ m \approx 9.5\ mm$$

Now the coefficients of the normal force hinge can be computed as follows:

$$U_{stiffness} = N_{nominal} / \Delta h_{nominal} = 419 / 9.5E{-}3 = \underline{44105\ kN/m}$$

$$U_{strength} = N_{nominal} = \underline{419\ kN}$$

U_α = can be taken as = 1E-8 "to prevent the pile-point to take Normal load, after a 9.5 mm deflection"

5.4.3.3. Lateral Subgrade Modulus & Springs

The subgrade modulus of the soil layers, which are given from the in-situ tests are as follows:

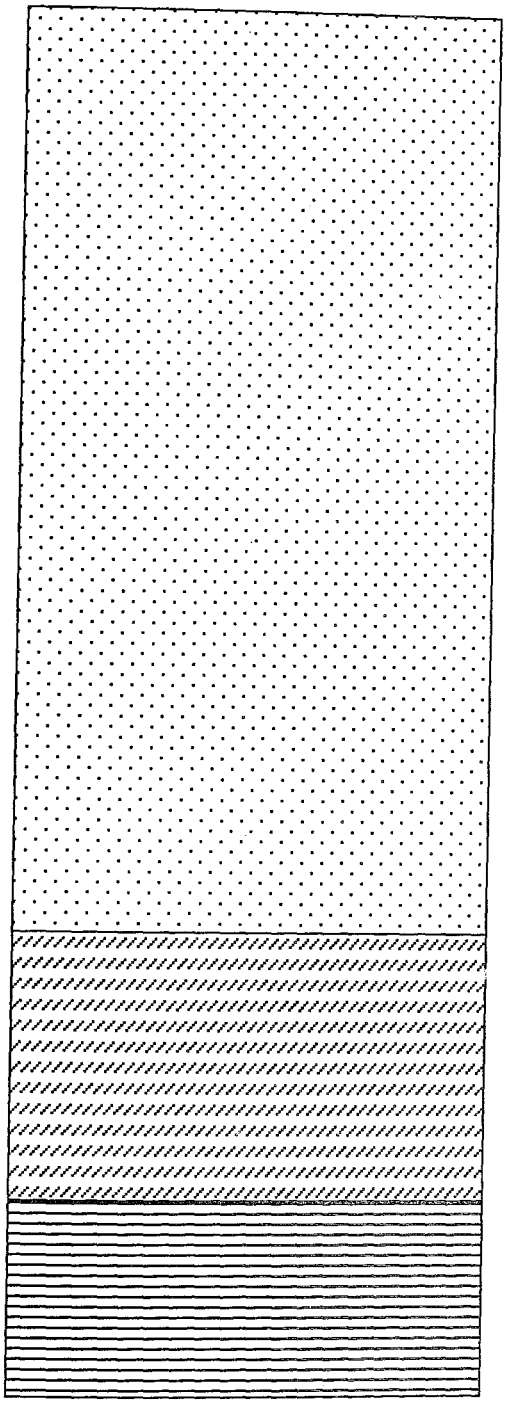

For the comparison, the average k_s values of the soil layers are as the following:

Soil	ks, [MN/m3]
Dense sandy gravel	220-400
Medium dense coarse sand	157-300
Medium sand	110-280
Fine or silty, fine sand	80-200
Stiff clay (wet)	60-220
Stiff clay (saturated)	30-110
Medium clay (wet)	39-140
Medium clay (saturated)	10-80
Soft clay	2-40

Table 5-6 Range of Lateral Subgrade Modulus, k_s (Bowles, 1990, P.941)

As seen in the table above, the subgrade modulus of medium stiff and stiff clay is in the range of 10000 to 80000, which means 10000 kN/m3 is a quite conservative value to accept. The same case is for the claystone, for which k_s is measured as 40000 kN/m3 in the in-situ tests is in the range of 30000 ~ 110000 kN/m3 and above.

Now, the spring coefficients resisting to the piles can be calculated as the following:

$$k = A \times k_s$$

where;

k = *spring coefficient*

A = *cross-section area of the pile*

k_s = *subgrade modulus of the soil*

then, the spring coefficients for the three layers, from top to bottom, become as follows:

A1 = 0.80 (cross-sectional width) x 3.45 (unit frame length) = 2.76 m^2

A2 = 0.80 (cross-sectional width) x 1.20 (unit frame length) = 0.96 m^2

A3 = 0.80 (cross-sectional width) x 2.50 (unit frame length) = 2.00 m^2

k1 = 2.76 x 10000 = 27600 kN/m

k2 = 0.96 x 20000 = 19200 kN/m

k3 = 2.00 x 40000 = 80000 kN/m

5.4.3.4. Views of the Substructure Model

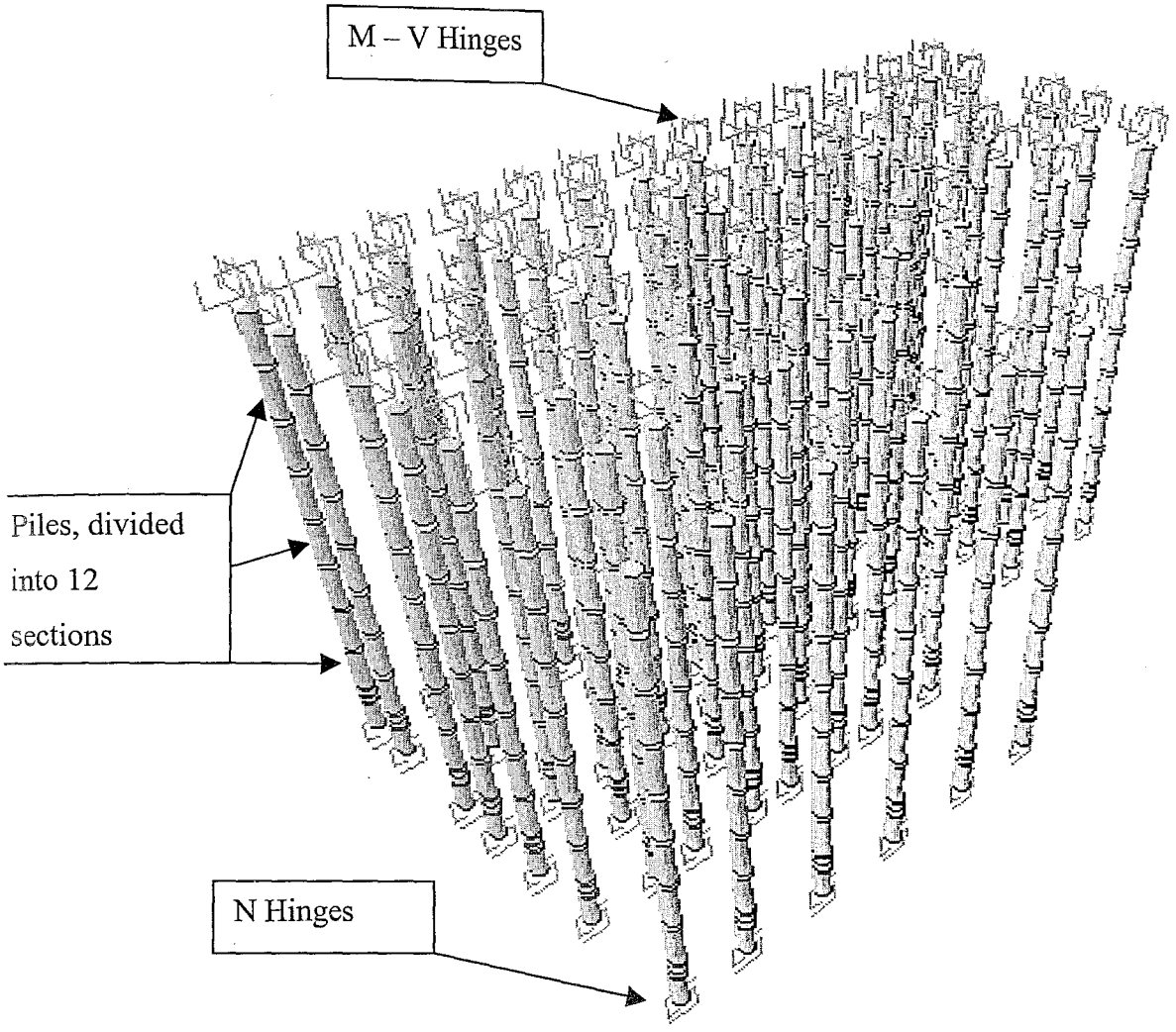

Figure 5-24 3-D View of the Substructure (77 x 12)

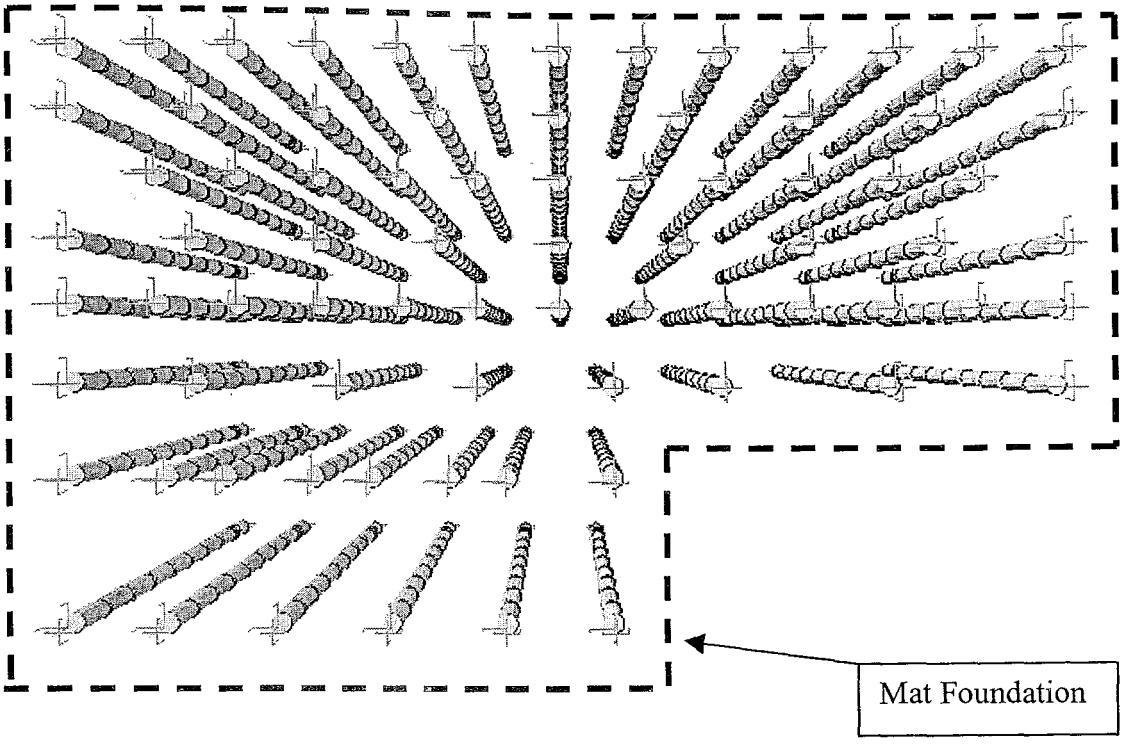

Figure 5-25 X-Y View of the Piles

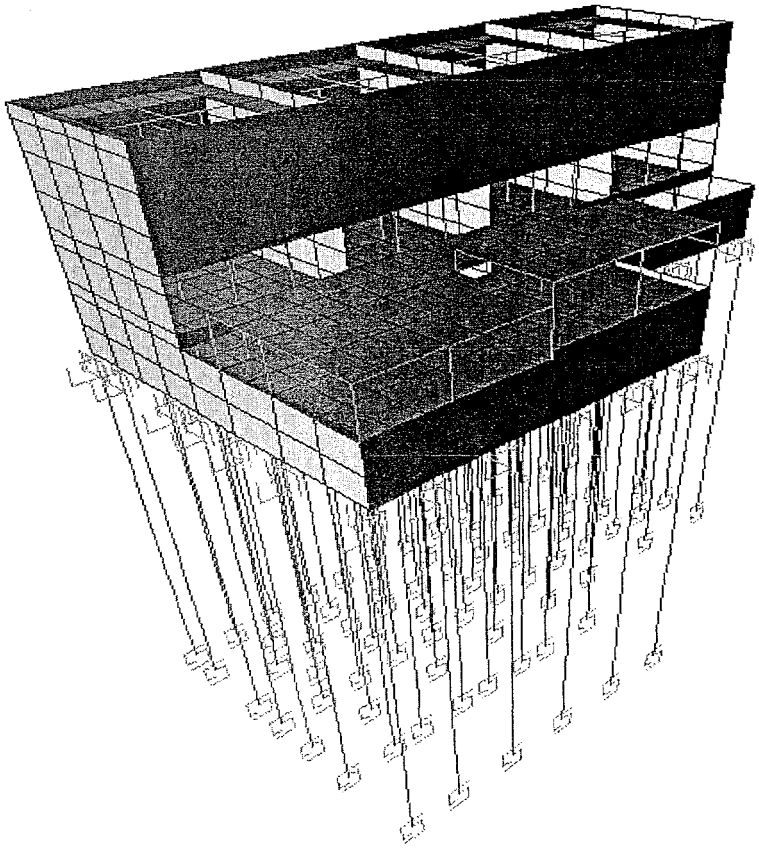

Figure 5-26 The 3-D View of the Entire Structure

5.5. Liquefaction Possibility of the Site

Evaluating the liquefaction potential of the site must be achieved before making the liquefaction-induced lateral spreading analysis. Thus, the writer applies the conditions of the site to some reasonable empirical assumptions, which are mostly based on SPT blow-counts, that were mentioned in chapter 2.

For evaluating the liquefaction potential of the site, the following procedure will be followed:

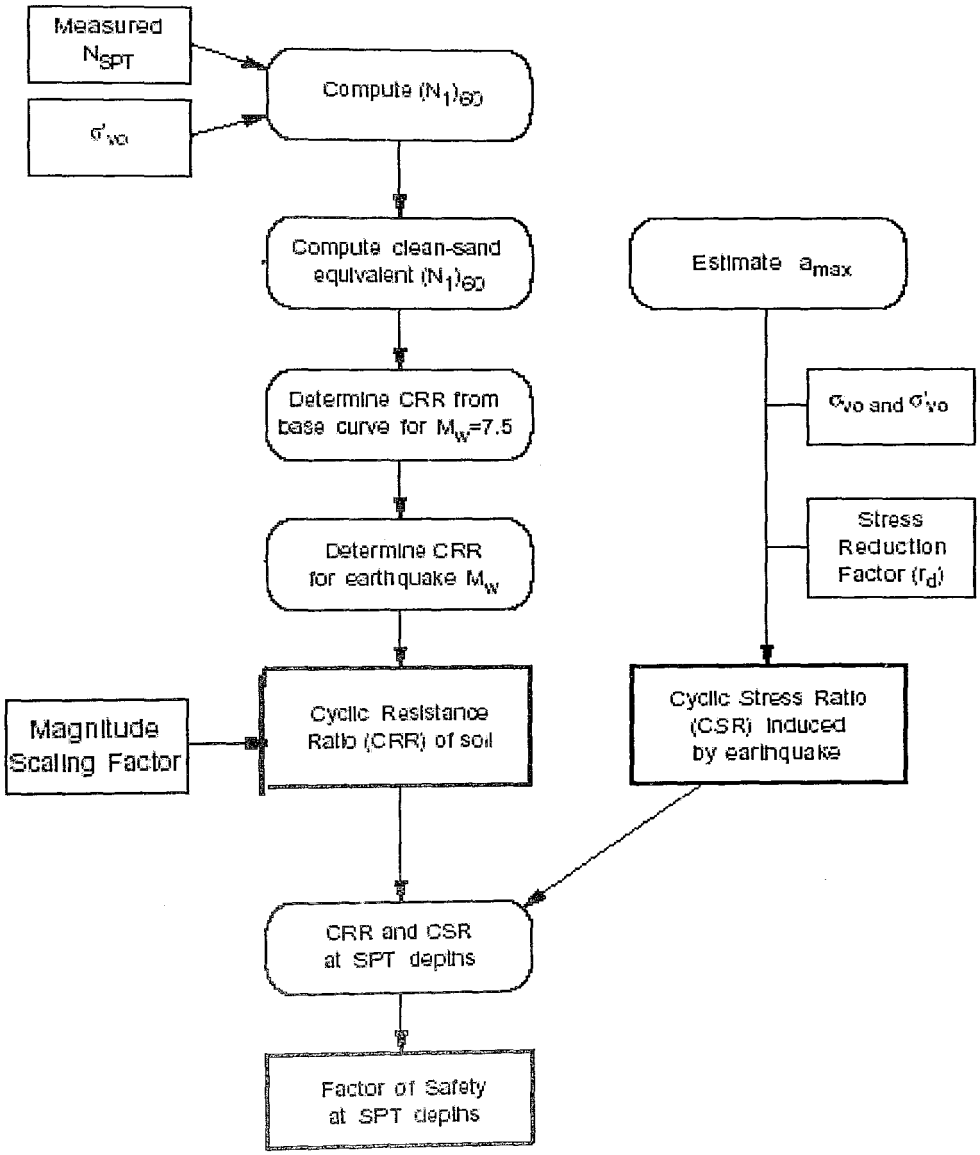

Table 5-7 The Flowchart for Evaluating the Liquefaction Potential of a Site Based on SPT

5.5.1. Determination of CRR for $M_w = 7.5$

The first step in the liquefaction analysis procedure is to find the Cyclic Resistance Ratio for the soil based on the corrected clean sand equivalent. This is done by an empirical equation based on the liquefaction catalog (Seed & Idriss (1983-1985)) for a magnitude of 7.5 earthquake (Modified by Robertson and Fear (1996)). This equation provides a good approximation for soils where $N_{60}' < 30$ (the worked site's soil's N is smaller than 7). The average SPT blow-counts is given as $N=14$ from the geological outputs. Then, the corrected SPT was calculated as $N_{55}'=7$ in Chapter 4. As also mentioned in the same chapter, there is a linear relation between these corrected N values, which provides the engineer a quite simple way to convert the corrected N values of a site. The conversion equation is below:

$$E_{r1} \, x \, N_1 = E_{r2} \, x \, N_2$$

$$N_2 = E_{r1} \, x \, N_1 / E_{r2}$$

$$N_{60}' = 55 \, x \, N_{55}' / 60$$

$$N_{60}' = 55 \, x \, 7 / 60$$

$$N_{60}' = 6.42$$

$$\underline{N_{60}' = 6}$$

Once the effective overburden pressure in the liquefaction depth for N_{55}' is calculated there is no need to consider it again. Since the N_{60}' value is known, now the CRR can be computed from the equation below:

$$100 \, x \, CRR_{M=7.5} = \frac{95}{34 - (N1)60} + \frac{(N1)60}{1.3} - \frac{1}{2}$$

$$CRR = CRR_{M=7.5} \, x \, MSF \qquad \textit{(Magnitude Scaling Factor)}$$

$$100 \, x \, CRR_{M=7.5} = \frac{95}{34-6} + \frac{6}{1.3} - \frac{1}{2}$$

$$\underline{CRR_{M=7.5} = 0.08}$$

Since the M_w that is assumed for the region is 7.5, there is no need to scale the magnitude.

5.5.2. Determination of CSR for $M_w = 7.5$

Once the liquefaction resistance is known at a certain depth, the average Cyclic Shear Stress Ratio generated by an earthquake must be estimated as indicated on the right side of the flow chart. The representative horizontal shear stress is computed with a simplified equation suggested by Seed and Idriss (1971) and expressed in terms of the Cyclic Stress Ratio (CSR) given by Seed & Idriss (1983; 1985)

$$CSR = 0.65 \times a_{max}/g \times \sigma_{vo}/\sigma_{vo}' \times r_d$$

$$r_d = 1.0 + 1.6 \times 10^{-6} (z^4 - 42z^3 + 105z^2 - 4200z^1)$$

Where,

r_d: *Stress reduction factor*

σ_{vo}: *Total vertical overburden stress [563.43 kN/m^2]*

σ_{vo}': *Effective vertical overburden stress [276.49 kN/m^2]*

a_{max}: *PGA of a probable earthquake [0.71g =6.97 m/s^2]*

z: *Depth of the soil layer from the ground surface [31.50 m]*

$$r_d = 1.0 + 1.6 \times 10^{-6} (z^4 - 42z^3 + 105z^2 - 4200z^1)$$

$$r_d = 1.0 + 1.6 \times 10^{-6} (31.50^4 - 42x31.50^3 + 105x31.50^2 - 4200x31.50)$$

$$\underline{r_d = 0.43}$$

$$CSR = 0.65 \times a_{max}/g \times \sigma_{vo}/\sigma_{vo}' \times r_d$$

$$CSR = 0.65 \times 6.97/9.81 \times 563.43/276.49 \times 0.43$$

$$\underline{\boldsymbol{CSR = 0.40}}$$

5.5.3. Factor of Safety for Liquefaction for $M_w = 7.5$

If the computed Cyclic Resistance Ratio (CRR) is less than or equal to Cyclic Stress Ratio (CSR) generated by the earthquake, liquefaction is assumed for that location. The factor of

safety against liquefaction is defined with the equation below (Ishihara (1993); Seed and Harder (1990)).

$$FS_{liq} = \frac{CRR}{CSR}$$

$$FS_{liq} = \frac{0.08}{0.40} = 0.20$$

$FS_{liq} = 0.20 << 1.00$ "Liquefaction is INEVITABLE"

5.5.4. Comparison of Liquefaction Potential

The liquefaction possibility of the site is evaluated based on Seed and Idriss's CSR and CRR procedure. Now the results can be checked/compared by the graphical data of Seed and Idriss as well as other geotechnical engineers' assumption methods of liquefaction potential evaluation, which were stated in Chapter 2.

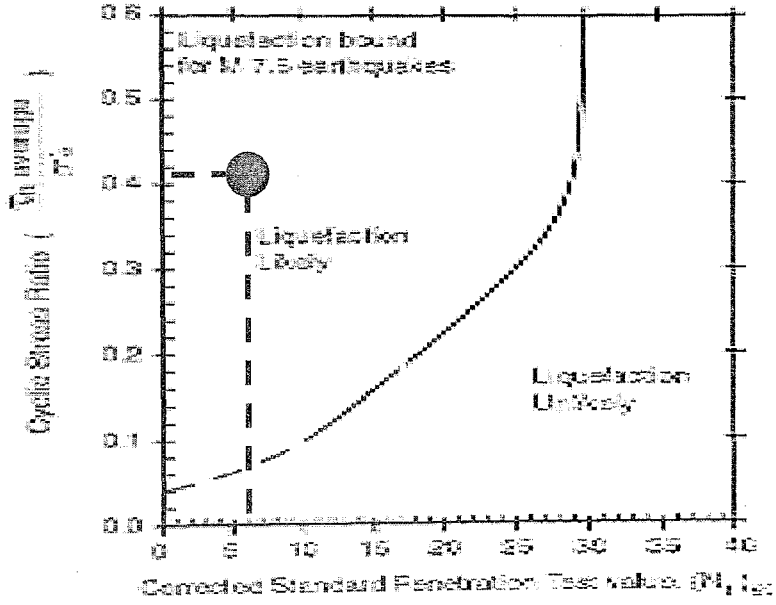

Figure 5-27 Liquefaction Pot. Anly. According to the Empirical Evaluation Method of Seed

($M_w = 7.5$, $N_{60}' = 6$, CSR = 0.40)

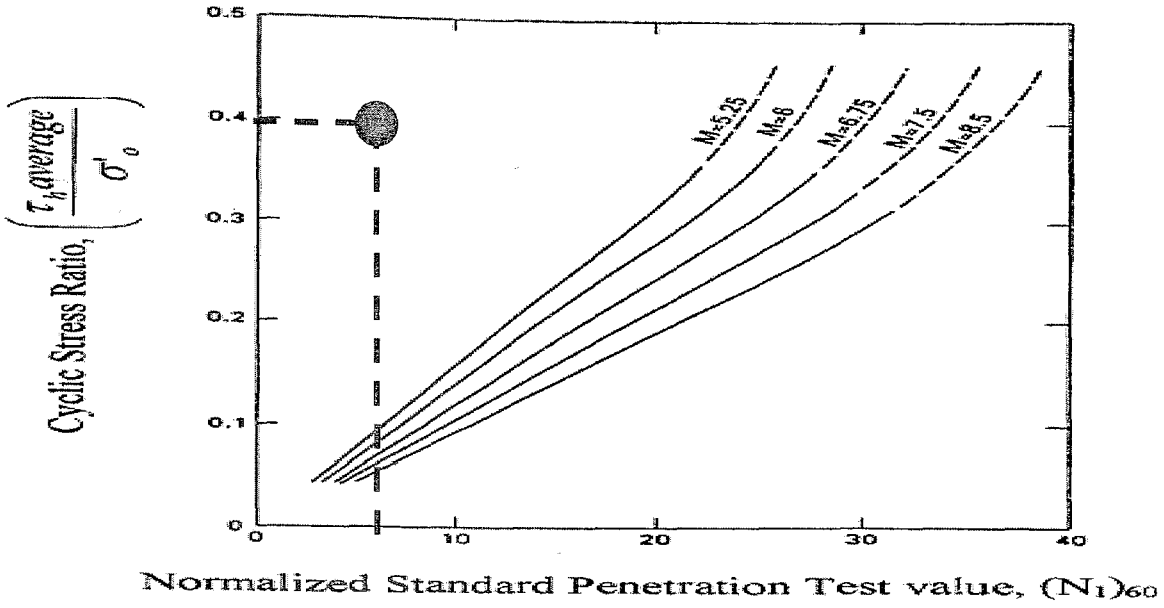

Figure 5-28 Seed & Idriss (1983-1985) Curves for CSR & Various Values of M_w

(N_{60}'= 6, CSR = 0.40)

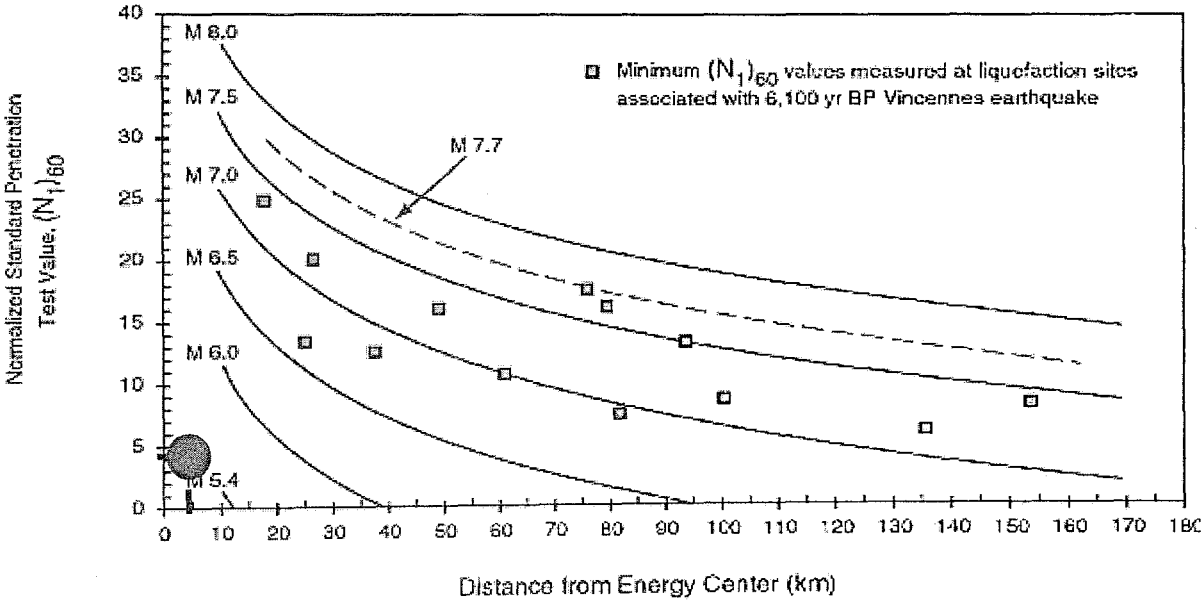

Figure 5-29 Minimum Field-Measured Values of Normalized SPT N_{60} as a Function of R

(R = 4.83 km, N_{60}'= 6)

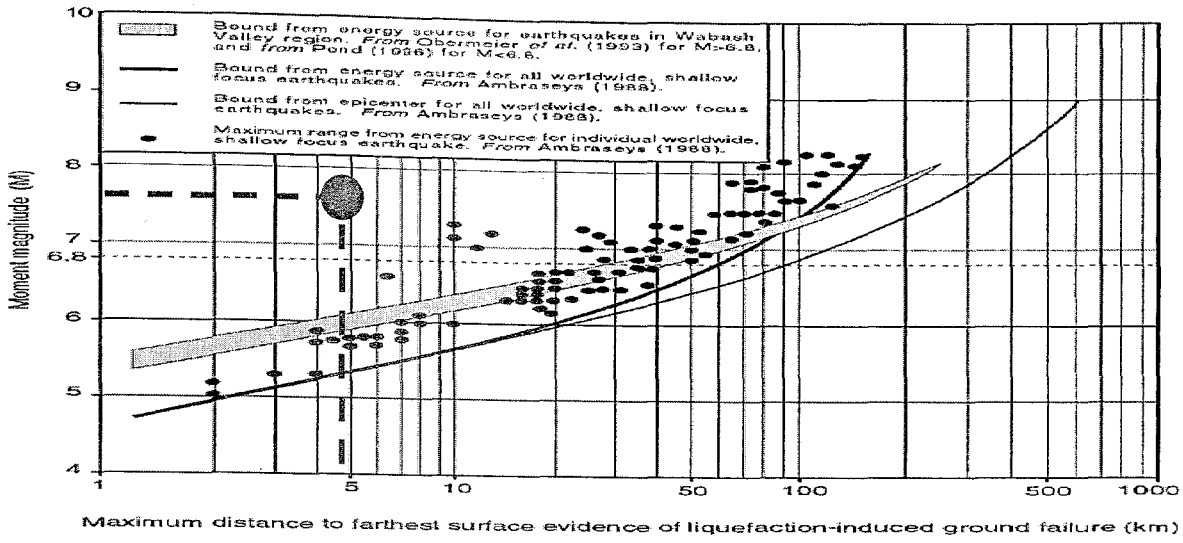

Figure 5-30 Obermeier's M_w vs. R of Liquefaction Effects (Near-Field Regions R<50 Km)

(R = 4.83 km, M_w = 7.5)

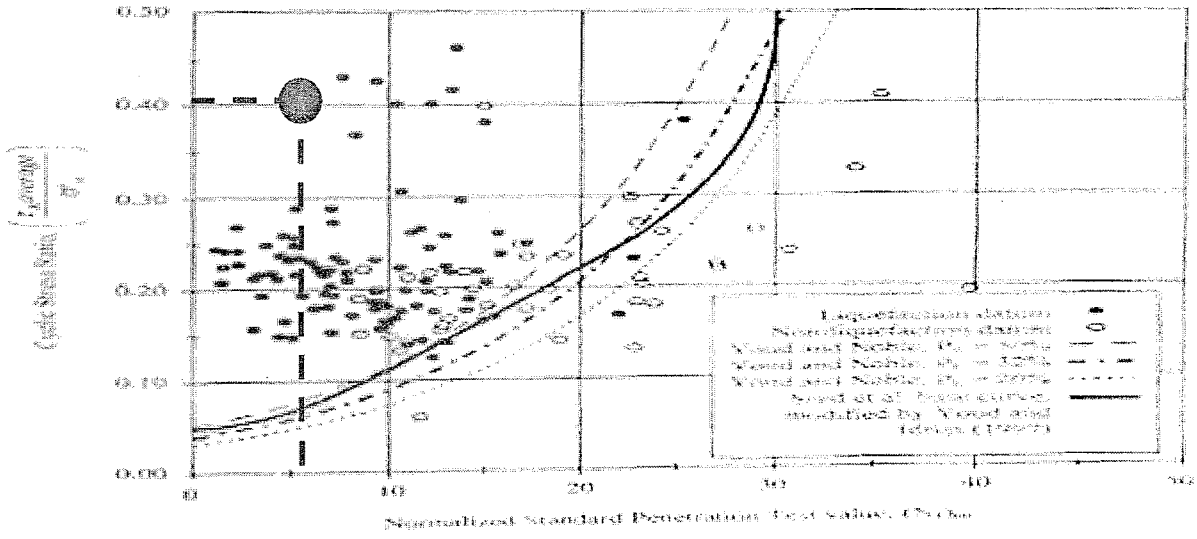

Figure 5-31 Probabilistic Liquefaction Resistance Curves for N_{60}' vs. CSR for Various P_L

(Youd & Idriss)

(CSR = 0.40, N_{60}'= 6)

Also as seen in the comparisons, the liquefaction is inevitable for that site even if the M_w of the probable earthquake is much less than 7.5. Thus extra precautions must be considered against liquefaction.

6. ANALYSIS

6.1. Lateral Spreading Analysis

As previously mentioned, lateral spreading is a result of the action of gravity-induced shear stress, which in excess of the residual shear strength of the liquefied soil. In this section, the lateral force on the pile group due to the lateral displacement will be computed by means of empirical formulas.

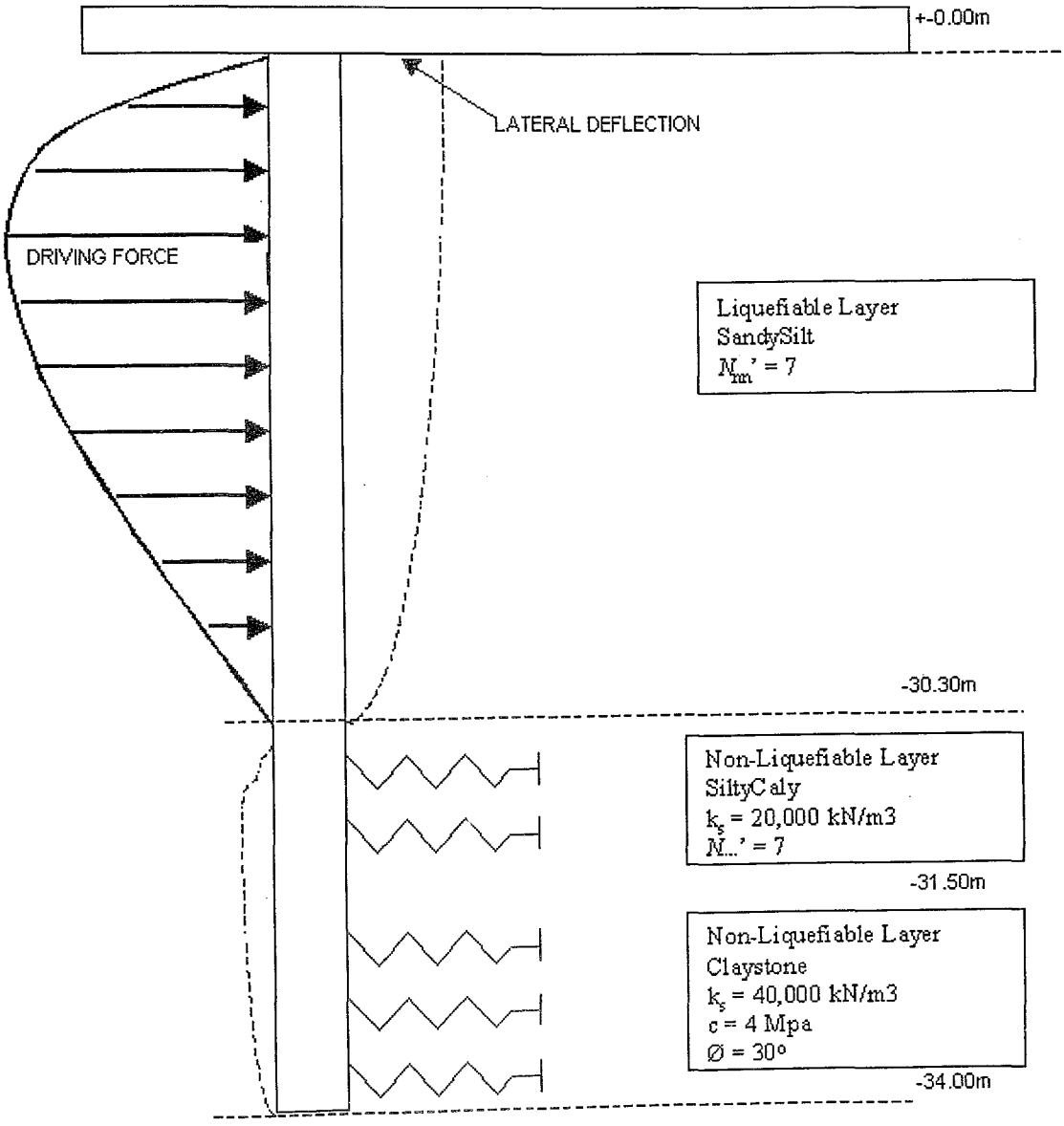

Figure 6-1 Schematic Illustration of the Lateral Spreading Model

6.1.1. Estimation of Lateral Displacement

There are many evaluation methods to predict the lateral displacement of the liquefiable soil layer after ground shaking. In geotechnical earthquake engineering practice, liquefaction-induced ground deformations are usually estimated using three different types of empirical models, which predict separately. (1) The occurrence of liquefaction (Seed & Idriss, 1983-1985), (2) The ground settlement (Ishihara, 1993), and (3) The lateral ground deformation (Hamada et al., 1986; Pease and O'Rourke, 1993; Youd and Perkins, 1987; and Barlett and Youd, 1995). There are four basic models for assessing liquefaction-induced lateral displacement:

- Youd and Perkins (1987), LSI Model
- Barlett and Youd (1992), MLR Model
- Rauch (1997)
- Hamada et al. (1986)

6.1.1.1. Youd and Perkins (1987), LSI Model

The LSI model has similarities to attenuation curves for peak ground acceleration. It relates the amplitude of horizontal ground deformation to distance from seismic energy source and moment magnitude as follows:

$$log\ LSI = -3.49 - 1.86\ log\ R + 0.98\ M_w$$

Where,

LSI: *general maximum amplitude of ground failure displacement [inch]*

R: *horizontal distance to seismic energy source [km]*

M_w: *earthquake moment magnitude*

If the variables of the site are applied to the formula,

$log\ LSI = -3.49 - 1.86\ log\ 4.83 + 0.98\ x\ 7.5$

$log\ LSI = -3.49 - 1.27 + 7.35$

$log\ LSI = 2.59$

$LSI = 389"$

$\underline{LSI = 9.96\ m}$

The comparison between the measured displacements and those calculated using the LSI equation, for all the entries in the Bartlett and Youd (1992) database.

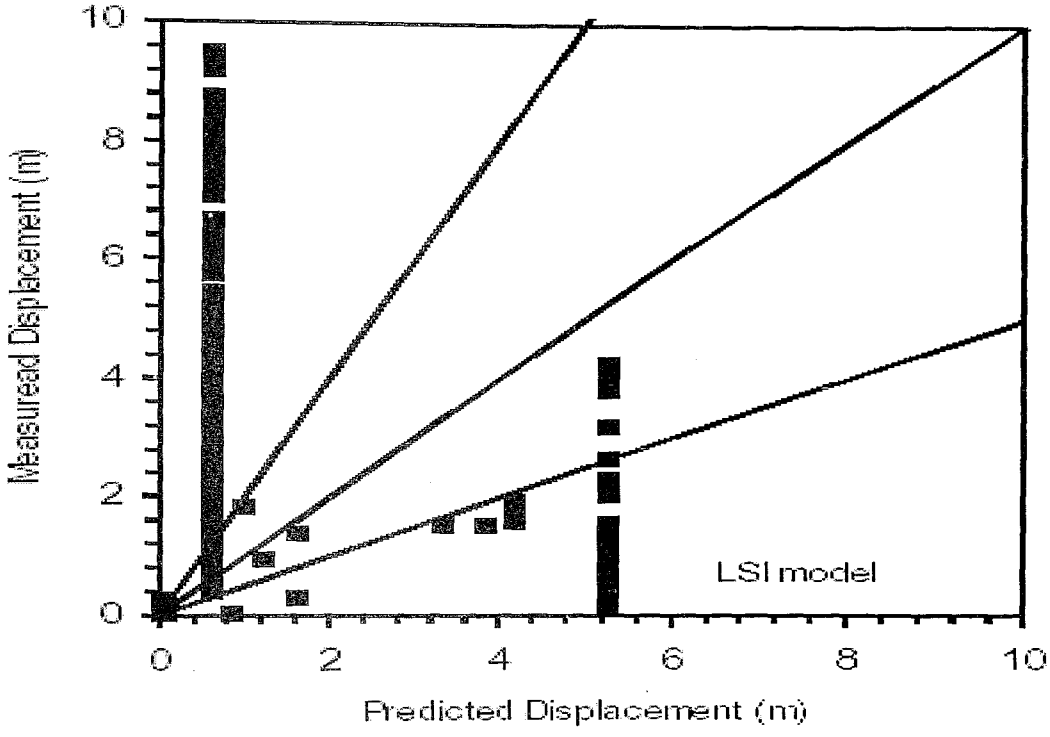

Figure 6-2 LSI Model

Measured Versus Predicted Liquefaction-Induced Lateral Displacement
(Data Points from Bartlett and Youd (1992) Database)

The points should fall on the line with a 1:1 slope for a perfect prediction, and on the lines with 1:0.5 and 1:2 slope when the prediction is half or twice the measured value, respectively. As shown in the figure, there is a poor agreement between measured and calculated displacements, which implies that the distance R and magnitude M_w are not sufficient for predicting liquefaction-induced displacement especially when the distance R gets very close or too far away from the epicenter.

6.1.1.2. Barlett and Youd (1992), MLR Model

Bartlett and Youd, who are the developers of Multiple Linear Regression, devised two separate models: one for ground slope of infinite extent, and the other one for free face:

Ground slope:

$$\log (D+0.01) = -15.787+1.178\ M_w-0.927\ \log R\ -0.013\ R + 0.429\ \log S + 0.348\ \log T_{15} + 4.527\ \log(100-F_{15})-0.922\ D50_{15}$$

Free face

$$\log (D+0.01) = -16.366+1.178\ M_w-0.927\ \log R\ -0.013\ R + 0.657\ \log W + 0.348\ \log T_{15} + 4.527\ \log(100-F_{15})-0.922\ D50_{15}$$

Where,

D: *horizontal displacement [m]*

M_w: *moment magnitude*

R: *nearest horizontal distance to seismic energy source or fault rupture [km]*

S: *slope of ground surface [%]*

W: *free face ratio [%]*

T_{15}: *thickness of saturated cohesionless soils (excluding depth >20 and >15% clay content) with $N1_{60}$<15 [m]*

F_{15}: *average fine content (% finer than 75 [μm]*

$D50_{15}$:average D_{50} grain size in T_{15} [mm]

If the equation for ground slope is used for the model, the equation becomes as follows:

$$\log (D+0.01) = -15.787 + 1.178\ M_w - 0.927\ \log R - 0.013\ R + 0.429\ \log S + 0.348\ \log T_{15} + 4.527\ \log(100-F_{15}) - 0.922\ D50_{15}$$

log (D+0.01) = -15.787+1.178 x 7.5 - 0.927 log4.83 - 0.013 x 4.83 + 0.429 log4.1 + 0.348 log 30.3 + 4.527 log(100 - 50) - 0.922 0.10

log (D+0.01) = -15.79+8.84 – 0.63 – 0.06 + 0.26 + 0.52 + 7.69 - 0.09

log (D+0.01) = 0.74

D = 5.49 m

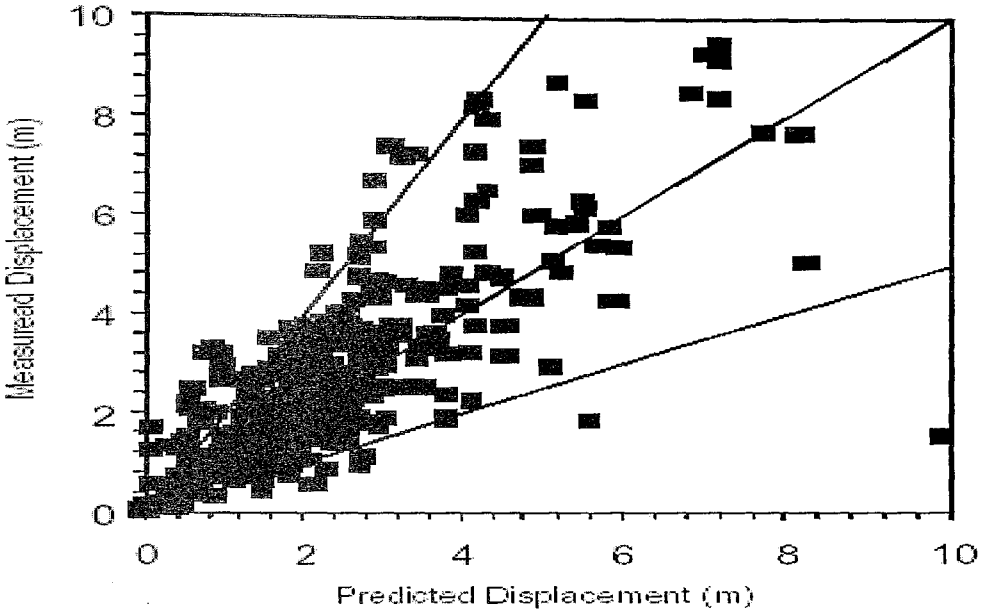

Figure 6-3 MLR Model

The Comparison between Predicted and the Measured Liquefaction-Induced Lateral Displacement

As shown in the figure, most of the model predictions are scattered within the lines with 1:0.5 and 1:2 slope, while they should fall close to the line with a 1:1 slope for a perfect prediction.

6.1.1.3. Rauch (1997) Model

Rauch (1997) considered liquefaction-induced ground deformation as slides of finite area, instead of individual displacement vectors. He applied multiple-linear-regression methods to these liquefaction-induced slides.

$$D = (D_R - 2.21)^2 + 0.149$$

Where,

$D_R = (613\ M_w - 13.9\ R_f - 2420\ A_{max} - 11.4\ T_d)/1000\ [m]$

D: *average horizontal displacement [m]*

R_f: *shortest horizontal distance to fault rupture[km]*

M_w: *moment magnitude*

A_{max}: *peak horizontal acceleration at ground surface [g]*

T_d: *duration of strong earthquake motions (>0.05g) [s]*

If the data of the site is applied to the formula,

$D_R = (613 \times 7.5 - 13.9 \times 4.83 - 2420 \times 0.71 - 11.4 \times 50) / 1000$

$D_R = (4597.50 - 67.14 - 1718.20 - 570.00) / 1000$

$D_R = 2.24\ m$

$D = (2.24 - 2.21)^2 + 0.149$

$D = 0.15\ m$

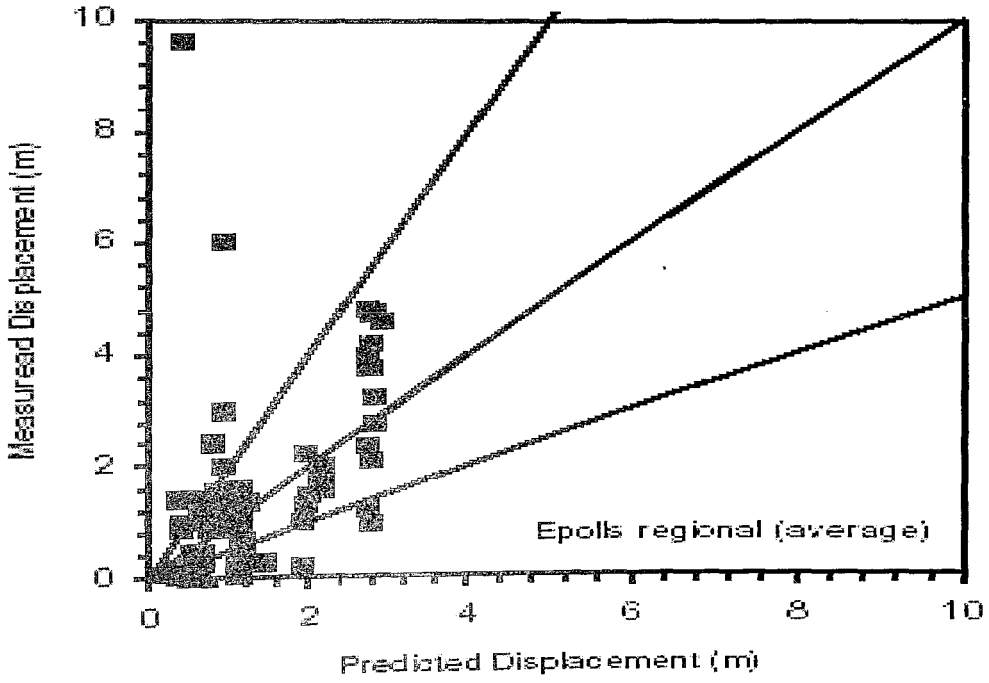

Figure 6-4 Rauch Model

The Comparison between Predicted and the Measured Liquefaction-Induced Lateral Displacement. As shown in the figure, there is a poor agreement between measured and predicted.

6.1.1.4. Hamada et al. (1986) Model

Hamada et al (1986) predict the amplitude of horizontal ground deformation only in terms of slope and thickness of liquefied layer:

$$D = 0.075\, H^{0.5}\, \theta^{0.33}$$

Where,

D: *horizontal displacement [m]*

Θ: *slope of ground surface or base of liquefied soil [%]*

H: *thickness of liquefied soil [m] (the cumulated thickness of zones with N_{60}' smaller than 15)*

$D = 0.075 \times 30.3^{0.5} \times 4.10^{0.33}$

$D = 0.075 \times 5.50 \times 1.59$

D = 0.72 m

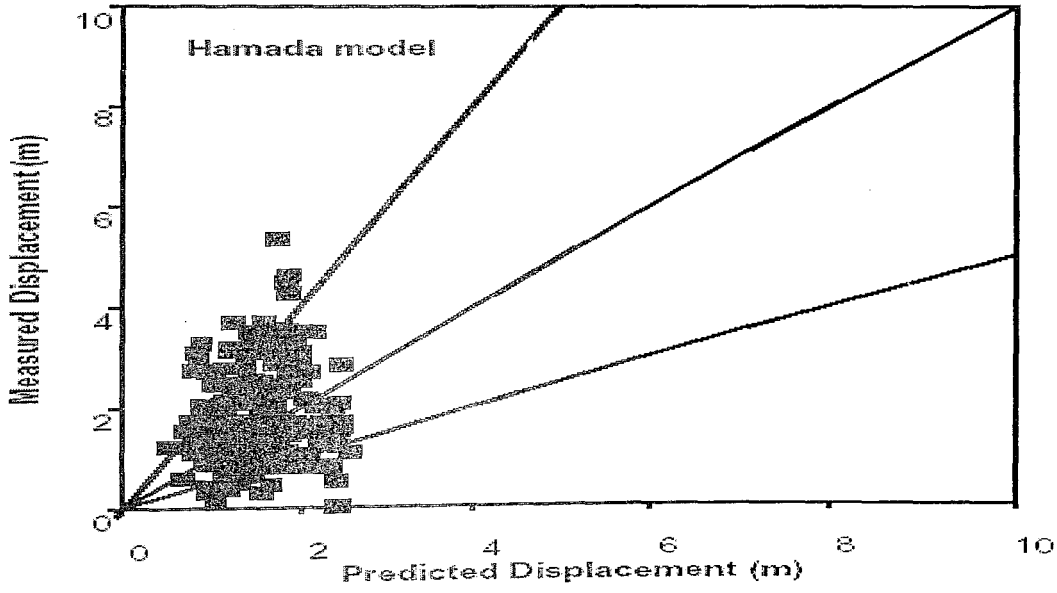

Figure 6-5 Hamada (1986) Model for Ground Slope

The Comparison between Predicted and the Measured Liquefaction-Induced Lateral Displacement

Although the Hamada model is only based on topographic and geotechnical parameters (i.e., S and H), and no seismic parameters (e.g., R and M_w) are used. The figure shows the comparison of measured displacement with those calculated in the equation for the ground-slope entries in the Bartlett and Youd (1992) database. In this comparison, it is seen that Hamada Model is quite successful in evaluating the liquefaction-induced lateral displacement. Thus, thus the model can be used for further calculations. **D = 0.72 m**

6.2. Spectral Analysis for TSC-98

Spectral analysis is an approach to examine the structural dynamics to the design of structures and development of lateral force requirements in building codes. This method summarizes the peak response of all possible linear SDF systems by the means of response spectra. It also provides a practical way of solution in characterizing ground motions and their effects on structures, with the consideration of distance to fault line and the conditions of the soil.

Nevertheless, in this method the engineer assumes as if the structure responds linearly to a strong ground motion. Since it is a linear assumption, many argue that this analyze method is insufficient to examine a structure's seismicity. Not to mention the fact that, all the analysis methods have some defects of acceptations, which are not the same in reality. Thus, the engineer must accept the method as a way of approach and consider making the best approach to obtain most actual results.

6.2.1. Determination of SPA Coefficients

6.2.1.1. Determination of Ductility Level R

Apart from that, the engineers use many reduction factors and coefficients in spectral analysis to simulate the non-linearity such as structural behavior factor (R). By the means of this factor, it is assumed that, the structure will encounter only $1/R_a$ (seismic load reduction factor) of the ground motion with its stiffness, and the exceeding force will be overwhelmed by displacement (ductility). The structural behavior factor (R), is found from the table below:

BUILDING STRUCTURAL SYSTEM	Systems of Nominal Ductility Level	Systems of High Ductility Level
(1) CAST-IN-SITU REINFORCED CONCRETE BUILDINGS		
(1.1) Buildings in which seismic loads are fully resisted by frames	4	8
(1.2) Buildings in which seismic loads are fully resisted by coupled structural walls	4	7
(1.3) Buildings in which seismic loads are fully resisted by solid structural walls	4	6
(1.4) Buildings in which seismic loads are jointly resisted by frames and solid and/or coupled structural walls	4	7

Table 6-1 Structural Behavior Factors (R) (TSC-98, P.13)

This factor carries the engineer to seismic load reduction factor (R_a), by means of the equations below:

$$R_a(T) = 1.5 + (R-1.5)\,T / T_A \quad 0 < T < T_A$$

$$R_a(T) = R \qquad T_A < T \text{ (TSC-98, P.12)}$$

$$R = 7 \qquad \text{"from table 6-1"}$$

The load reduction factor R_a will be computed in the following chapter. After the determination of R, the other coefficients are computed in the following notes.

6.2.1.2. Seismic Zone and A_0

The A_0 also known as effective ground acceleration coefficient is the possible PGA of the considered region. Since the structure being only 5 km away from currently active fault line the seismic zone is found as 1. And the corresponding A_0 is 0.4

6.2.1.3. Local Site Class and T_A & T_B

Due to the existence of the piles underneath the building, the structure will mostly be affected by the motion, which comes from the substructure and obviously the properties of only that soil layer must be taken into account. Since the piles are anchored to bedrock (which is a soft rock), soil group B is chosen. And since the bedrock is considered as the soil layer, the thickness of the topmost layer is taken as 0.

According to the facts that are stated above, local site class is chosen as Z1.

Soil Group	*Description of Soil Group*	*Stand. Penetr. (N/30)*	*Relative Density (%)*	*Unconf. Compres. Strength (kPa)*	*Shear Wave Velocity (m/s)*
(A)	1. Massive volcanic rocks, unweathered sound metamorphic rocks, stiff cemented sedimentary rocks	—	—	> 1000	> 1000
	2. Very dense sand, gravel...	> 50	85—100	—	> 700
	3. Hard clay, silty lay.....	> 32	—	> 400	> 700
(B)	1. Soft volcanic rocks such as tuff and agglomerate, weathered cemented sedimentary rocks with planes of discontinuity.....	—	—	500—1000	700—1000
	2. Dense sand, gravel.....	30—50	65—85	—	400—700
	3. Very stiff clay, silty clay..	16—32	—	200—400	300—700
(C)	1. Highly weathered soft metamorphic rocks and cemented sedimentary rocks with planes of discontinuity	—	—	< 500	400—700
	2. Medium dense sand and gravel.....	10—30	35—65	—	200—400
	3. Stiff clay, silty clay.....	8—16	—	100—200	200—300
(D)	1. Soft, deep alluvial layers with high water table.....	—	—	—	< 200
	2. Loose sand.....	< 10	< 35	—	< 200
	3. Soft clay, silty clay.....	< 8	—	< 100	< 200

Table 6-2 Soil Groups (TSC-98, P.78)

Local Site Class	*Soil Group according to Table 12.1 and Topmost Layer Thickness* (h_1)
Z1	Group (A) soils Group (B) soils with $h_1 \leq 15$ m
Z2	Group (B) soils with $h_1 > 15$ m Group (C) soils with $h_1 \leq 15$ m
Z3	Group (C) soils with $15 \text{ m} < h_1 \leq 50$ m Group (D) soils with $h_1 \leq 10$ m
Z4	Group (C) soils with $h_1 > 50$ m Group (D) soils with $h_1 > 10$ m

Table 6-3 Local Site Classes (TSC-98, P.78)

Local Site Class acc. to Table 12.2	T_A (second)	T_B (second)
Z1	0.10	0.30
Z2	0.15	0.40
Z3	0.15	0.60
Z4	0.20	0.90

Table 6-4 Spectrum Characteristic Periods (TSC-98, P.11)

$T_A = 0.10$ s

$T_A = 0.30$ s

6.2.1.4. Importance Factor I

The building codes desire to analyze the response spectrum of important buildings much more conservatively to prevent a massive life loss during an earthquake. Obviously the Turkish Earthquake Code also has a requirement of increasing the assumed lateral force to buildings, which are important. This factor is determined by the building's service purpose, for instance the communication facilities that will be needed after an earthquake to command the rescue teams and etc. This factor also depends on the amount of people that the building holds at a time, just like schools, hospitals and prisons. Since the project structure is an industrial building, the importance factor *I* is found as 1.

4. Other buildings Buildings other than above defined buildings. (Residential and office buildings, hotels, building-like industrial structures, etc.)	1.0

Table 6-5 The Importance Factor, *I* (TSC-98, P.11)

6.2.2. Response Spectra

With the development of earthquake analysis procedures with the availability of modern computers, it is now possible to determine the linearly elastic response of any structure to a possible ground motion. How well the computed response agrees with actual response of a structure during an earthquake depends primarily on the quality of the structural idealization.

The response spectrum analysis provides a structural response based on the peak values of forces and deformations over the duration of the earthquake-induced response. Now the question is that if the peak response can be determined directly from the response spectrum for the ground motion without carrying out a time-history analysis. For single degree of freedom systems, the answer is "yes", but for MDF (Multi Degree of Freedom) systems the answer is a "qualified yes".

The peak responses of MDF systems can be computed from the response spectrum, but the results are not exact unless, the engineer makes the best assumptions for both the soil and the structure. During the spectral analysis, the MDF system's modes will be integrated with respect to their participation factors. TSC-98 requires obtaining at least 90% of the total mass of the structure. Since the model's mass is distributed between the super and the substructure, very small modes with short periods take about 35% of the total mass. Thus 90% modal participation cannot be provided. This case will also be shown in the following notes.

6.2.3. Modal Analysis

Modal analysis is one of the important steps to achieve a spectral analysis. Since the substructure is combined with the superstructure in the evaluation, the modal analysis will be computed together as a unified structure.

The following steps are applied during the computation of the dynamic response of an MDF system to external forces *p(t)* (Chopra, 1995):

- *Define the structural properties*
  - *Determine the mass matrix* ***m*** *and stiffness matrix* ***k***
  - *Estimate the modal damping ratios* ζ *(=0.05)*

- *Determine the natural frequencies* ω_n *and modes* $\boldsymbol{\emptyset_n}$

- *Compute the response in each mode by the following steps*
  - *Compute* $\boldsymbol{q_n(t)}$ *by the following equations*
    - $M_n q_n^{oo} + C_n q_n^{o} + K_n q_n = P_n(t)$
    - $q_n^{oo} + 2\,\zeta_n\,\omega_n\,q_n^{o} + \omega_n^{2}\,q_n = \dfrac{\mathrm{Pn(t)}}{\mathrm{Mn}}$
  - *Compute the nodal displacements* $\boldsymbol{u_n(t)}$ *from the eq. below*
    - $u_n(t) = \emptyset_n\, q_n(t)$
  - *Compute the element forces associated with the nodal displacements* $\boldsymbol{u_n(t)}$ *for the desired values of* ***T*** *and the element forces of interest.*

- *Combine the contributions of all modes to determine the total response. The nodal displacements and element forces are given sequently in the equations below:*
  - $u(t) = \sum_{n=1}^{N} u_n(t) = \sum_{n=1}^{N} \emptyset_n q_n(t)$
  - $r(t) = \sum_{n=1}^{N} r_n(t)$

By following the procedure that is stated above, the mode shapes are obtained by means of the SAP2000 computer program. The modal analysis output of the system is defined below:

M O D A L P A R T I C I P A T I N G M A S S R A T I O S

MODE	PERIOD	INDIVIDUAL MODE (PERCENT)			CUMULATIVE SUM (PERCENT)		
		UX	UY	UZ	UX	UY	UZ
1	**0.533744**	**2.3148**	**49.1568**	**0.0111**	**2.3148**	**49.1568**	**0.0111**
2	**0.494054**	**52.0349**	**3.2264**	**0.1544**	**54.3497**	**52.3832**	**0.1655**
3	**0.255023**	**6.9279**	**3.8613**	**16.0452**	**61.2777**	**56.2445**	**16.2107**
4	0.170073	0.6420	2.1626	0.6093	61.9196	58.4072	16.8200
5	0.114324	2.4876	3.0335	2.7807	64.4073	61.4407	19.6007
6	0.072376	1.0180	0.2066	3.5941	65.4252	61.6473	23.1948
7	0.063738	0.1528	1.4827	0.0090	65.5781	63.1300	23.2038
8	0.053810	0.0034	0.7874	0.0183	65.5815	63.9174	23.2221
9	0.052164	0.2168	0.0001	3.7713	65.7983	63.9175	26.9934
10	0.049856	0.0213	0.0160	2.2124	65.8196	63.9335	29.2058
11	0.048951	0.0028	0.0013	0.0027	65.8224	63.9347	29.2085
12	0.048650	0.0000	0.0002	0.0004	65.8224	63.9350	29.2089
13	0.048507	0.0071	0.0000	0.0479	65.8295	63.9350	29.2568
14	0.048442	0.0000	0.0000	0.0630	65.8295	63.9350	29.3198
15	0.048323	0.0064	0.0003	0.1053	65.8359	63.9353	29.4251
16	0.048081	0.0001	0.0012	0.0002	65.8359	63.9365	29.4253
17	0.047945	0.0012	0.0079	0.0000	65.8371	63.9444	29.4253
18	0.047826	0.0008	0.0005	0.0030	65.8379	63.9449	29.4283
19	0.047794	0.0000	0.0052	0.0081	65.8379	63.9501	29.4365
20	0.047606	0.0016	0.0048	0.0136	65.8396	63.9548	29.4501
21	0.047567	0.0005	0.0046	0.0090	65.8400	63.9595	29.4591
22	0.047515	0.0020	0.0004	0.0215	65.8420	63.9599	29.4806
23	0.047431	0.0000	0.0021	0.0049	65.8420	63.9620	29.4854
24	0.047338	0.0000	0.0005	0.0066	65.8420	63.9625	29.4921
25	0.047275	0.0001	0.0000	0.0017	65.8422	63.9625	29.4937
26	0.047197	0.0008	0.0011	0.0300	65.8429	63.9636	29.5237
27	0.047134	0.0010	0.0012	0.0288	65.8439	63.9647	29.5525
28	0.047005	0.0001	0.0093	0.0878	65.8440	63.9741	29.6403
29	0.046943	0.0017	0.0004	0.0072	65.8457	63.9745	29.6475
30	0.046826	0.0000	0.0012	0.0000	65.8457	63.9757	29.6475
31	0.046805	0.0007	0.0000	0.0249	65.8464	63.9757	29.6725
32	0.046739	0.0001	0.0004	0.0042	65.8465	63.9762	29.6766
33	0.046693	0.0000	0.0019	0.0008	65.8465	63.9781	29.6774
34	0.046581	0.0002	0.0004	0.0037	65.8467	63.9785	29.6811
35	0.046461	0.0001	0.0001	0.0040	65.8468	63.9786	29.6851
36	0.046403	0.0013	0.0003	0.0507	65.8482	63.9789	29.7357
37	0.046117	0.0001	0.0005	0.0000	65.8483	63.9794	29.7358
38	0.046038	0.0001	0.0001	0.0024	65.8484	63.9795	29.7382
39	0.045845	0.0085	0.0000	0.2298	65.8569	63.9795	29.9679
40	0.045724	0.0000	0.0006	0.0060	65.8569	63.9801	29.9739
41	0.045542	0.0048	0.0001	0.1045	65.8617	63.9802	30.0784
42	0.045205	0.0001	0.0001	0.0086	65.8619	63.9803	30.0869
43	0.044987	0.0004	0.0007	0.0179	65.8623	63.9810	30.1049
44	0.044714	0.0041	0.0032	0.0306	65.8663	63.9841	30.1355
45	0.044274	0.0008	0.0001	0.0316	65.8672	63.9842	30.1670
46	0.044033	0.0065	0.0006	0.2063	65.8737	63.9848	30.3733
47	0.043872	0.0004	0.0001	0.0448	65.8740	63.9849	30.4181
48	0.043574	0.0000	0.0015	0.0012	65.8740	63.9864	30.4193
49	0.043346	0.0003	0.0010	0.0132	65.8743	63.9874	30.4325
50	0.043050	0.0039	0.0007	0.0748	65.8783	63.9881	30.5073

The calculated three main mode shapes, with 3-d and X-Y view, are shown sequently below:

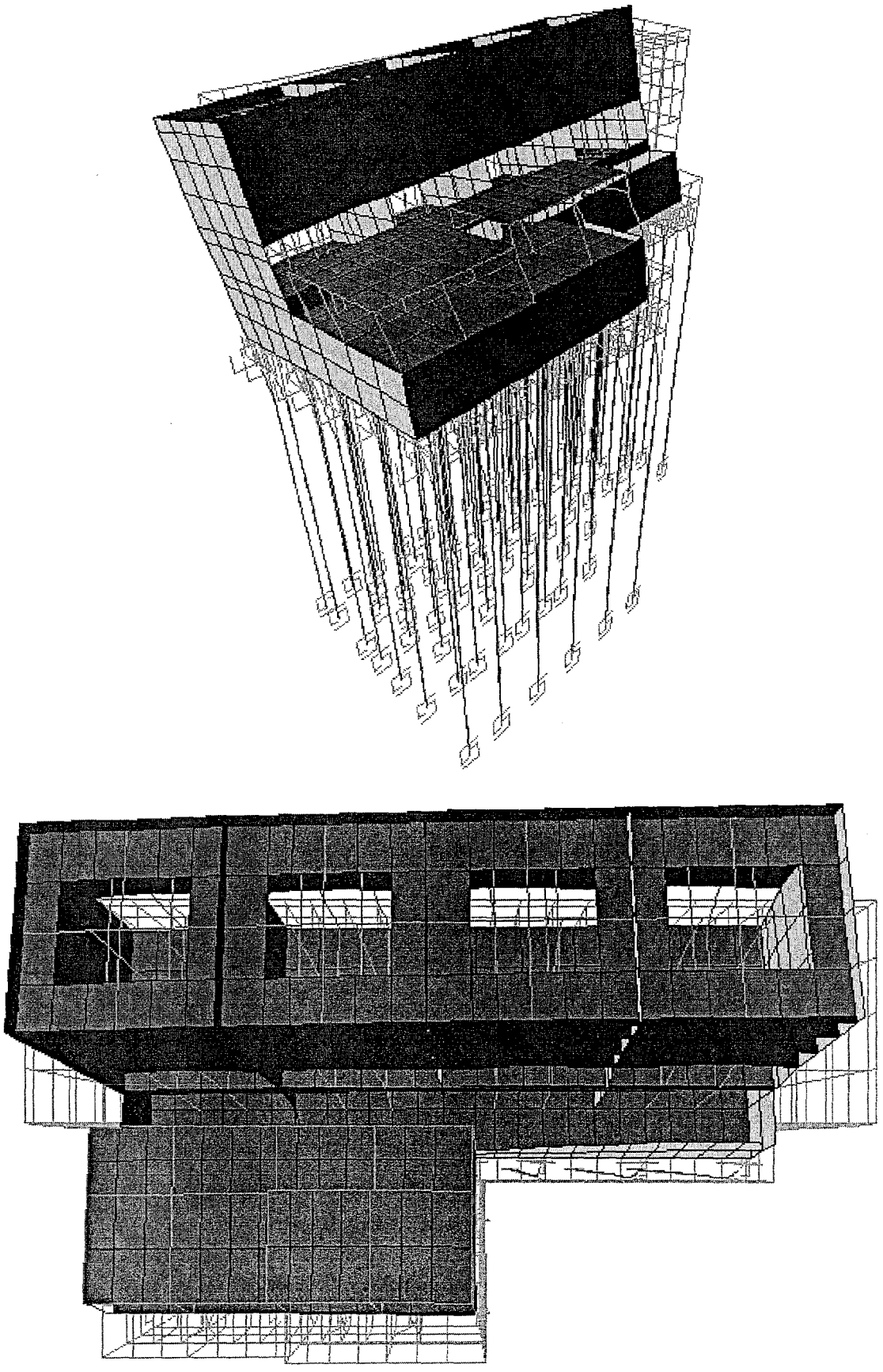

Figure 6-6 1st Mode, T = 0.53s, MPR = %2 - %49 - %0.01 "U(X,Y,Z)"

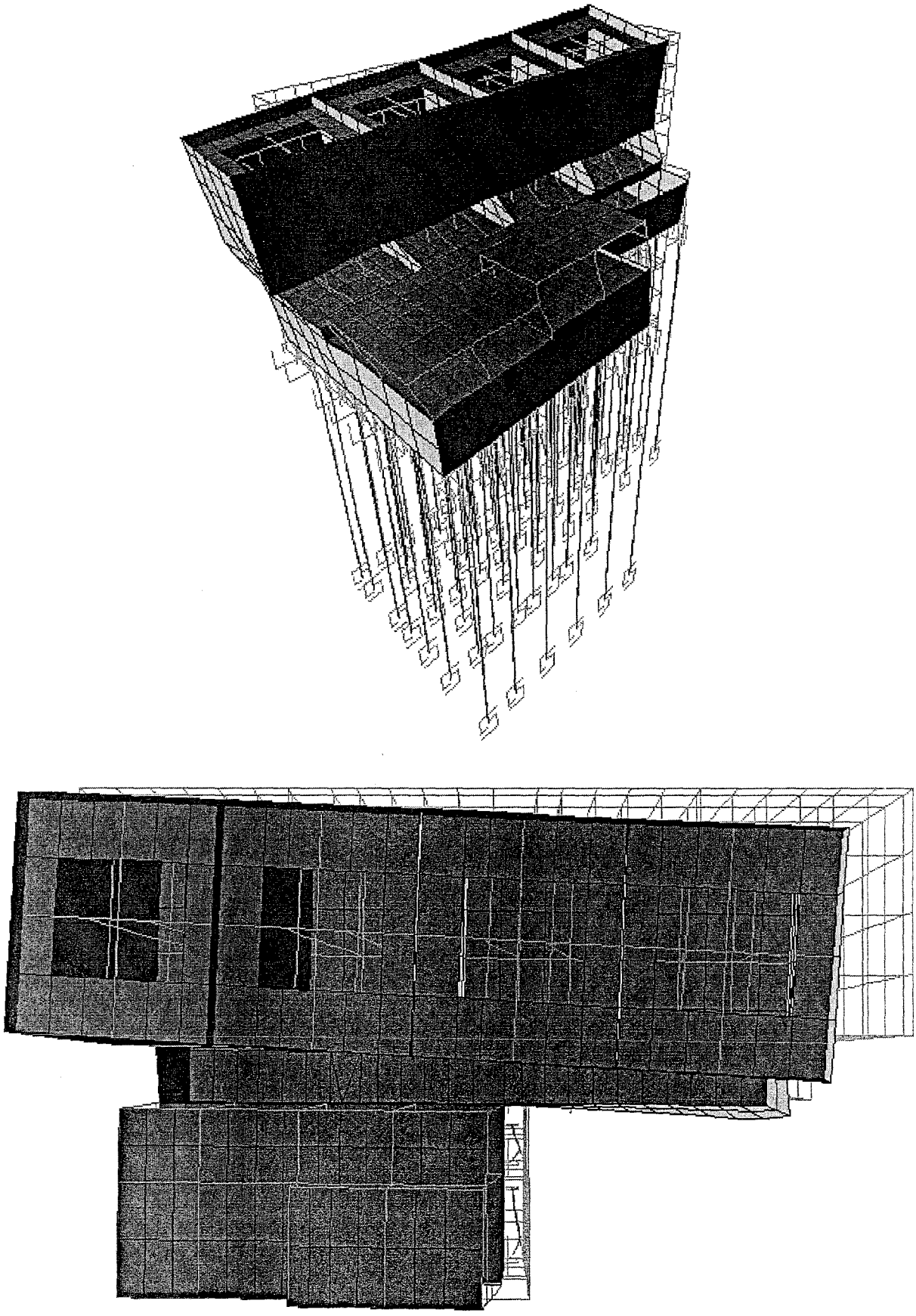

Figure 6-7 2nd Mode, T = 0.49s, MPR = %52 - %3 - %0.15 "U(X,Y,Z)"

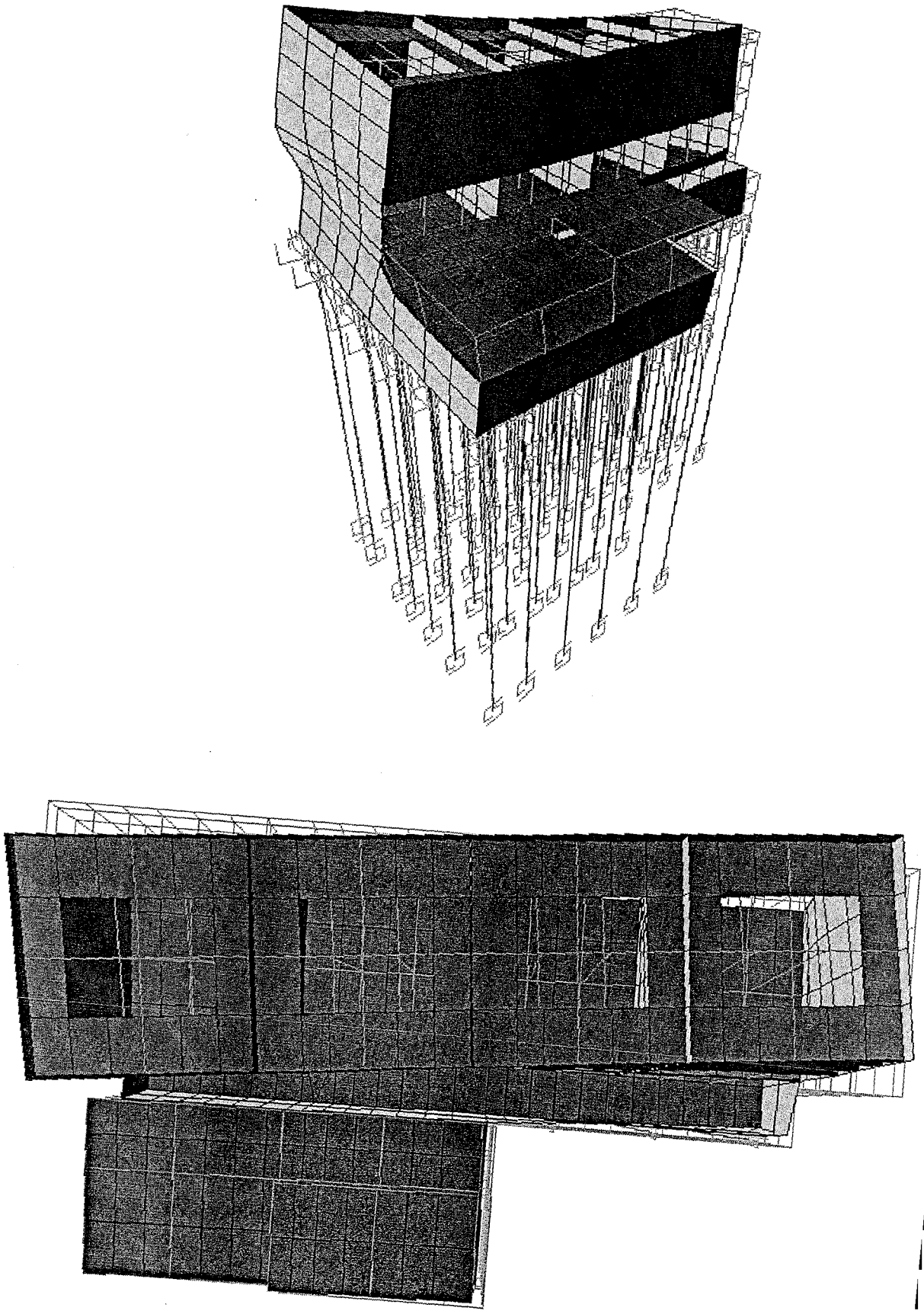

Figure 6-8 3rd Mode, T = 0.26s, MPR = %7 - %4 - %0.16 "U(X,Y,Z)"

6.2.4. Response Spectrum of the Structure

When all the coefficients that are computed above, now it is possible to define the response spectrum of the structure by the equations in the following:

$$Ra(T)=1,5+(R-1,5)*T/T_A \qquad (0=<T=<T_A)$$
$$Ra(T)=R \qquad (T>T_A)$$

$$S(T) = 1+1,5*T/T_A \qquad (0=<T=<T_A)$$
$$S(T) = 2,5 \qquad (T_A=<T=<T_B)$$
$$S(T) = 2,5*(T_B/T)^{0,8} \qquad (T>T_B)$$

$$A(T)=A_0*I*S(T)$$
$$Spa(T)=A(T)*g/Ra(T)$$

R = 7
A_o = 0.4
Z = Z1 (T_A = 0.10s, T_B = 0.30s)

Table 6-6 The Response Spectra Coefficients of the Site and the Structure

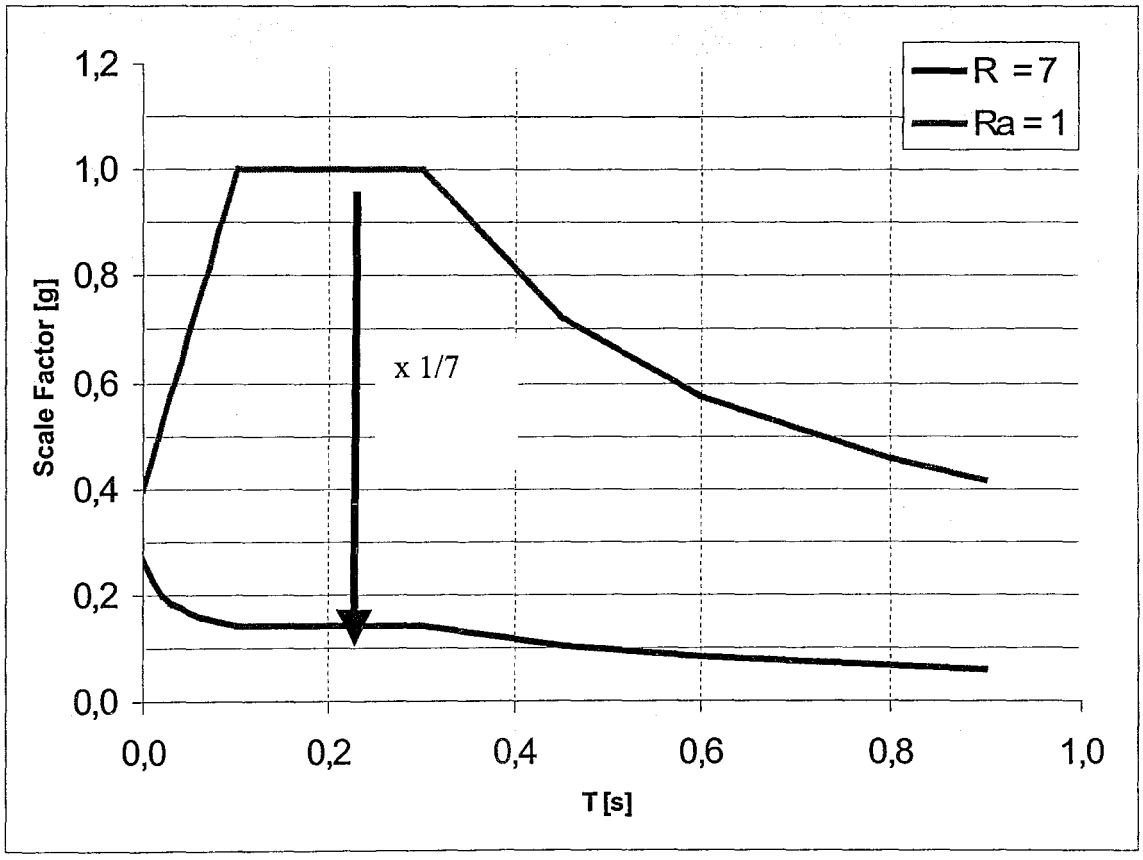

Figure 6-9 The Inelastic Response Spectrum of the Building

6.3. T-H Analysis

Time-history analysis has recently been recognized by engineers as a rational method to analyze structures under recorded/simulated earthquakes instant by instant. This analysis method has provided the observation of simulated movement of a structure under a desired a strong ground motion. Moreover the resisting forces of the structure can also be measured by this excellent method of analysis.

Even though, the analysis can simulate the structure's motion quite alike the motion under a real earthquake, this methodology has some defects such as assuming the soil to stay linear.

6.3.1. Target Spectrum & Earthquake Simulation

As a matter of analyzing a structure in time-history, the main problem is choosing the correct earthquake, for which the character and magnitude is alike, the one that may occur in the investigated building's site. To overcome this matter, the engineer must simulate an earthquake data that has specific PGA and S(A) values that fit with the probable earthquake.

Firstly S_s, S_1 and PGA values are obtained from Erdik (2003) for the structure located in Dilovası for which the coordinates are 40.78'N & 29.59'E for an earthquake with an occurrence probability of 10% in 50 years. They are as follows:

$S_s = 1.5891$ g $= 1558.90$ cm/s^2
$S_1 = 0.6969$ g $= 683.66$ cm/s^2
PGA $= 0.7104$ g $= 696.90$ cm/s^2
$M_w = 7.5$
R $= 4.83$ km

Table 6-7 The Determined SPA Values for M_w =7.5 (Erdik, 2003)

S_s and S_1 are the values of the spectral acceleration values for T=0.2 and 1.0 s respectively. Thus, the simulated motion's SPA graph must coincide with these data. The target spectrum is illustrated below:

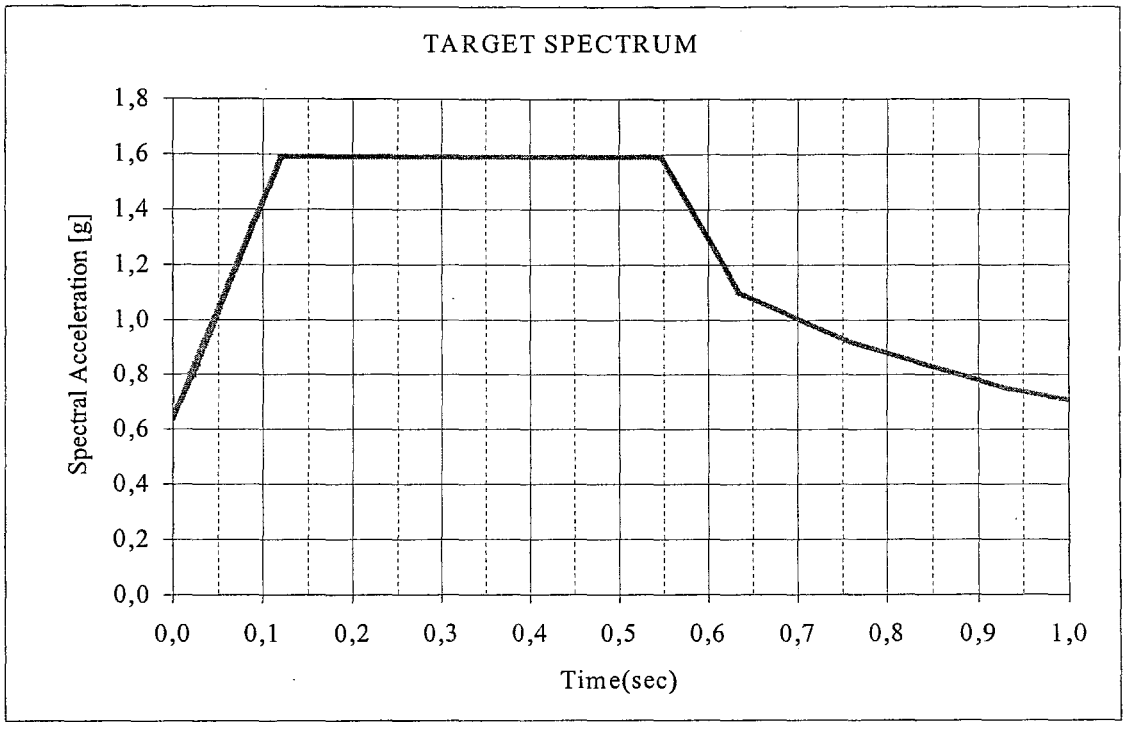

Figure 6-10 The Target Spectrum for the Site for M_w =7.5

With the means of the variables given in the table above, two probable ground motion data are simulated @ 100Hz and duration of 60s. The simulated data computed by the outputs of RSCTH (Response Spectra Compatible Time Histories) program, are shown below:

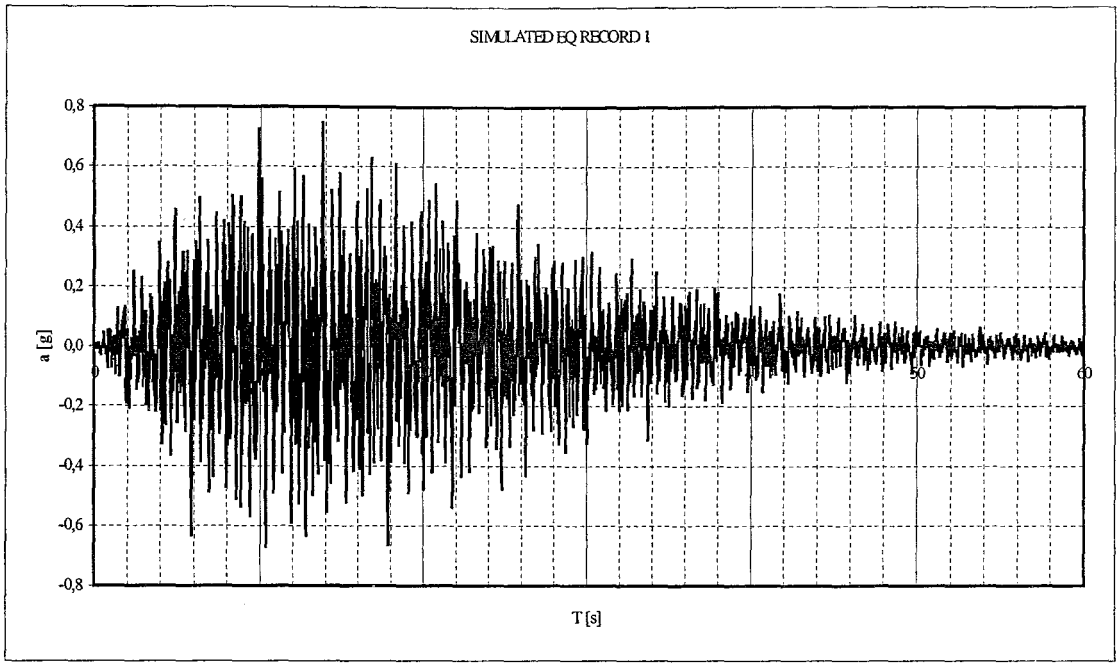

Figure 6-11 Simulated Earthquake Data 1

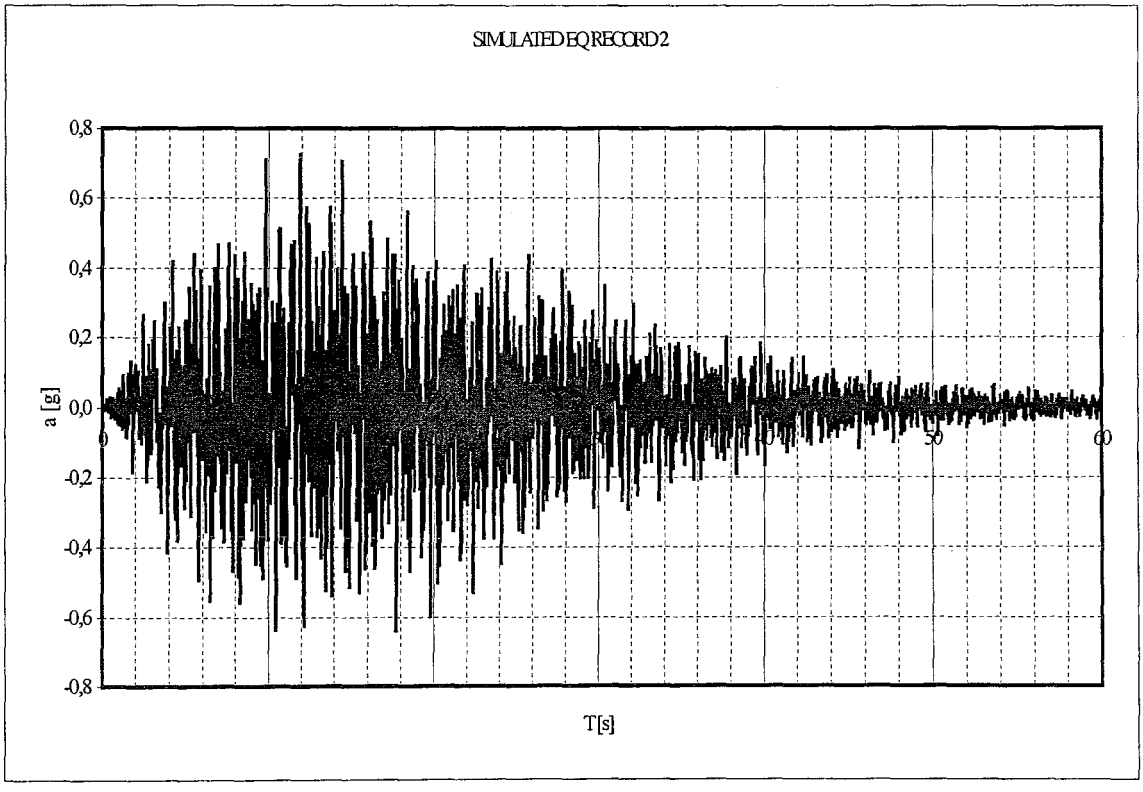

Figure 6-12 Simulated Earthquake Data 2

Now, it can be checked if the simulated data coincide with the target spectrum (Piece-wise Exact Method is used for calculation of SPA)

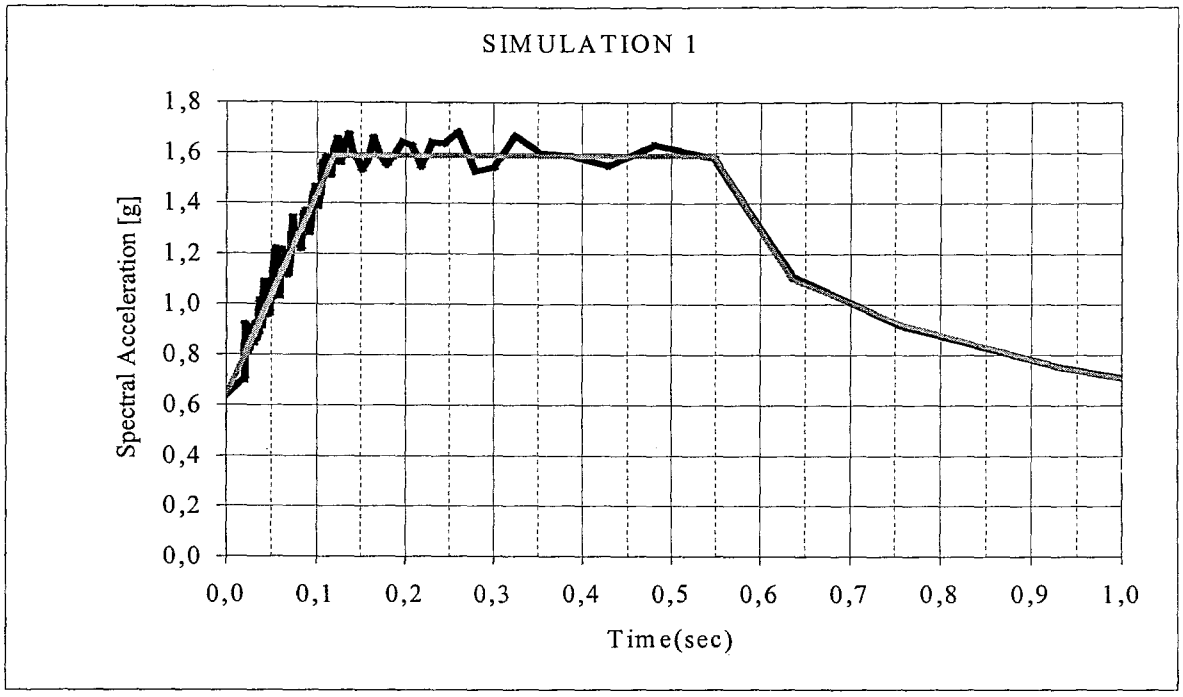

Figure 6-13 The Target and the Simulated SPA 1

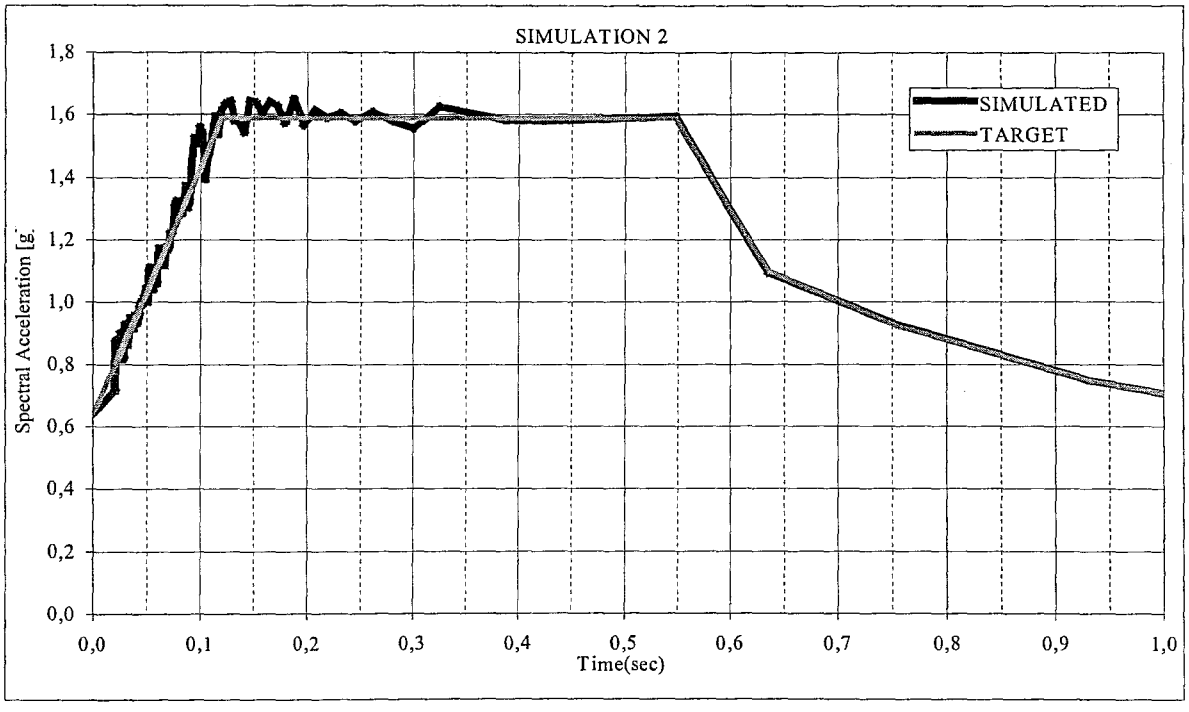

Figure 6-14 The Target and the Simulated SPA 2

As also seen in the figure, the simulated earthquake data perfectly fits the target spectrum. Now for the sake of conservatism, one more earthquake data's SPA will be computed, where it will be a recorded earthquake, in the next chapter.

6.3.2. Application of a Recorded Motion (YPT, 1999)

One of the main problems in time-history analysis is to choose the most appropriate ground motion data to imitate the case in reality. By means of the highly developed programs and computers, earthquake engineers try to simulate a strong ground motion data, which fits to the site conditions. Somehow, it may be an insufficient way to support the whole analysis to an imitation. Thus, just for the comparison of the results, it is necessary to utilize a recorded ground motion data, which has similar characteristics to a probable earthquake.

To provide this, the YPT data will be chosen for the T-H analysis because it is a near-field data and holds the same characteristics that Dilovasi may face. However, this is not an easy case to apply the record in a rational way. To overcome this, the following procedures will be followed

6.3.2.1. The Original Recorded Data

As stated above, YPT record will be used for the analysis. In addition, to get the exact results; E-W components of the data will be applied to the structure's X-X direction and N-S to the Y-Y direction, due to the structure's position in global coordinates. The original data are illustrated in order below:

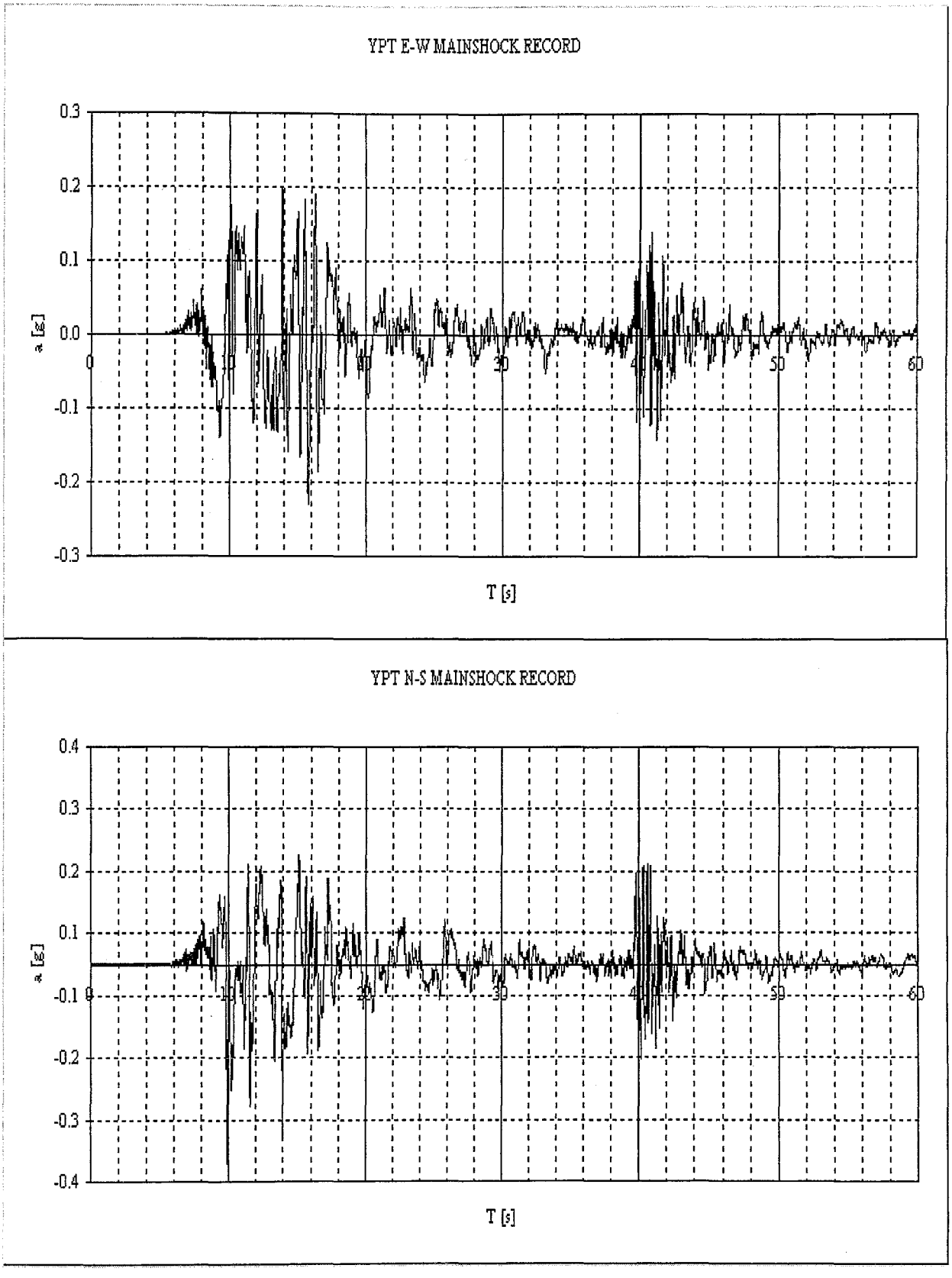

Figure 6-15 The Original YPT E-W and N-S Mainshock Data (BOUN, 1999 Kocaeli)

6.3.2.2. Matching the Data with the Target Spectrum

Since the original records have noise in the data, this must be eliminated before the application. The noise usually mixes with the ground motion data due to the non-availability of the instruments to distinguish the original ground shaking and the shaking that is affected by the facilities' vibrations in the environment. To overcome this problem, the records are filtered between 0.1 – 52 Hz. and trended by means of the MATLAB program. The comparison of filtered and the original data of YPT E-W and N-S records are illustrated in order as the following:

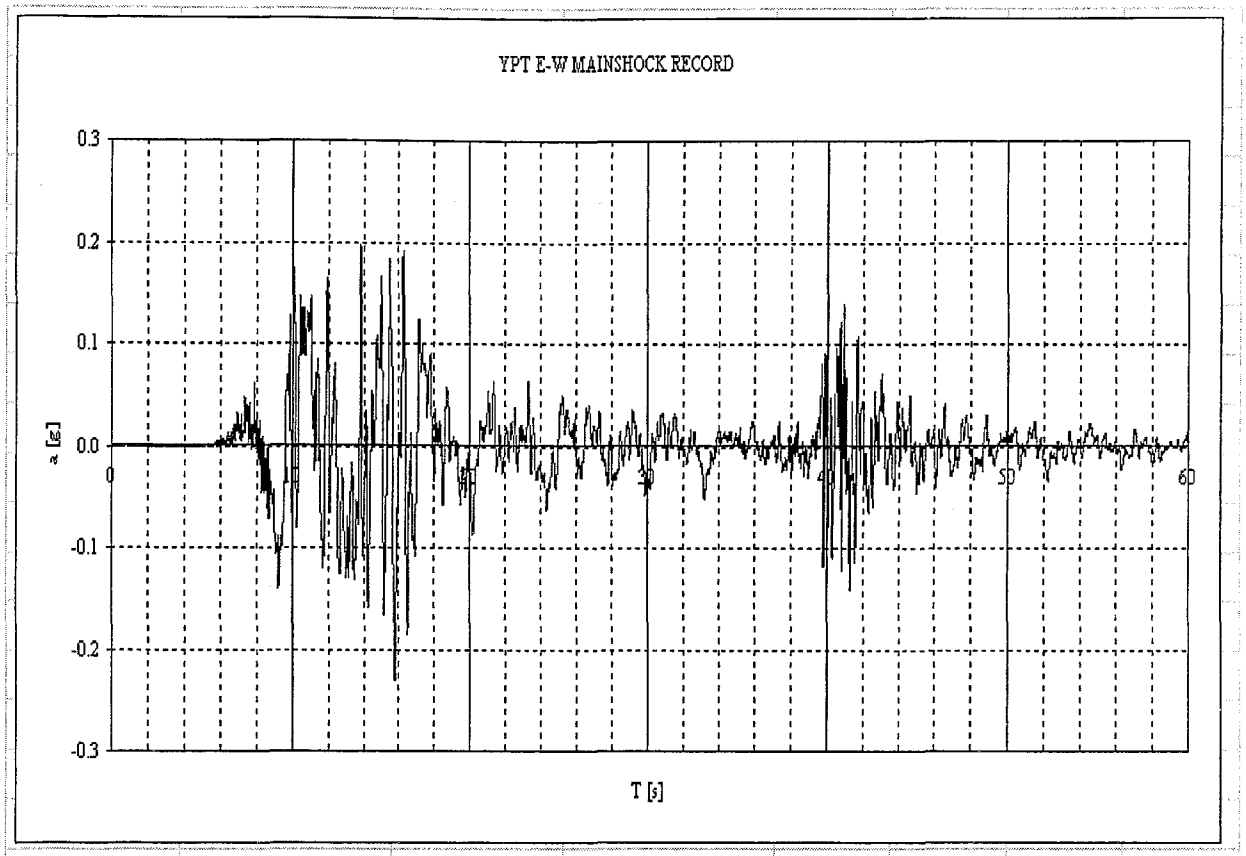

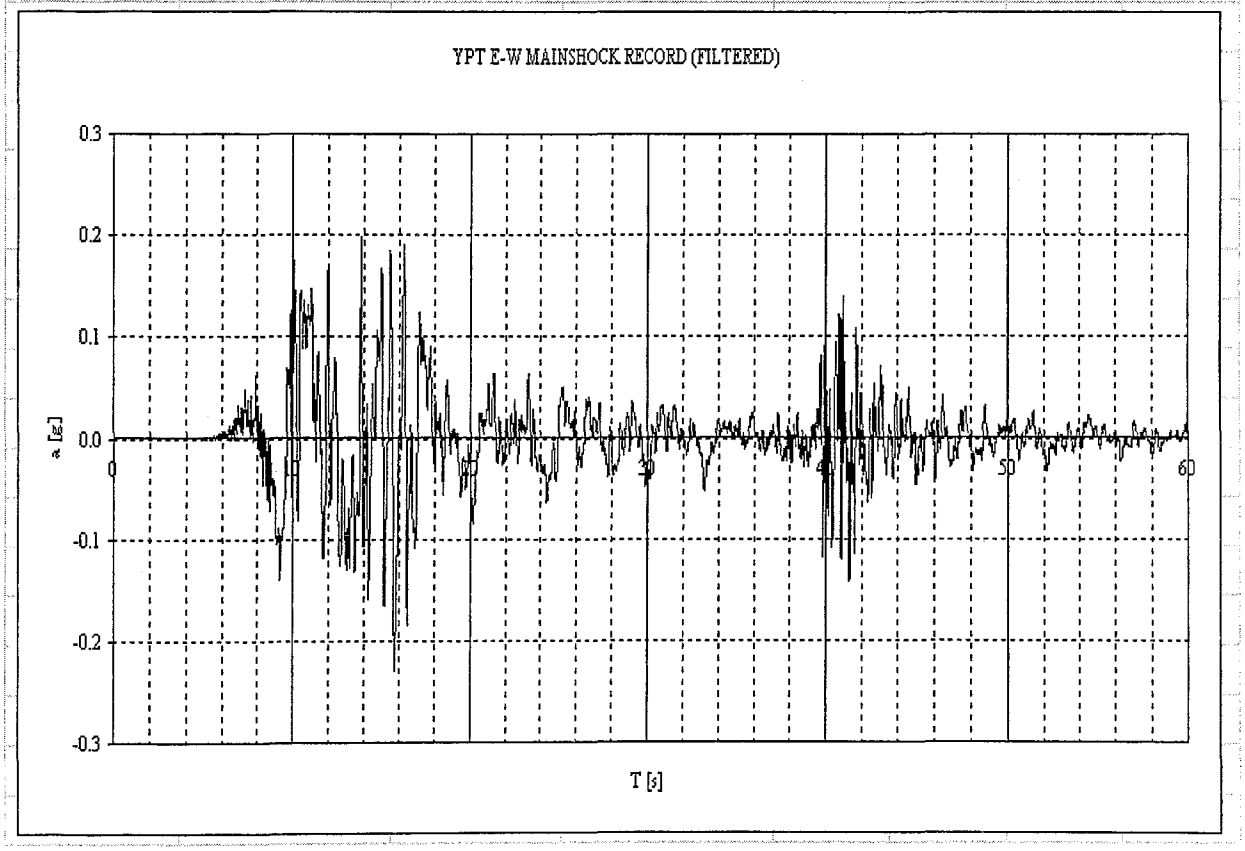

Figure 6-16 Before and After the Filtering of the Data YPT E-W (PGA = -0.23 g)

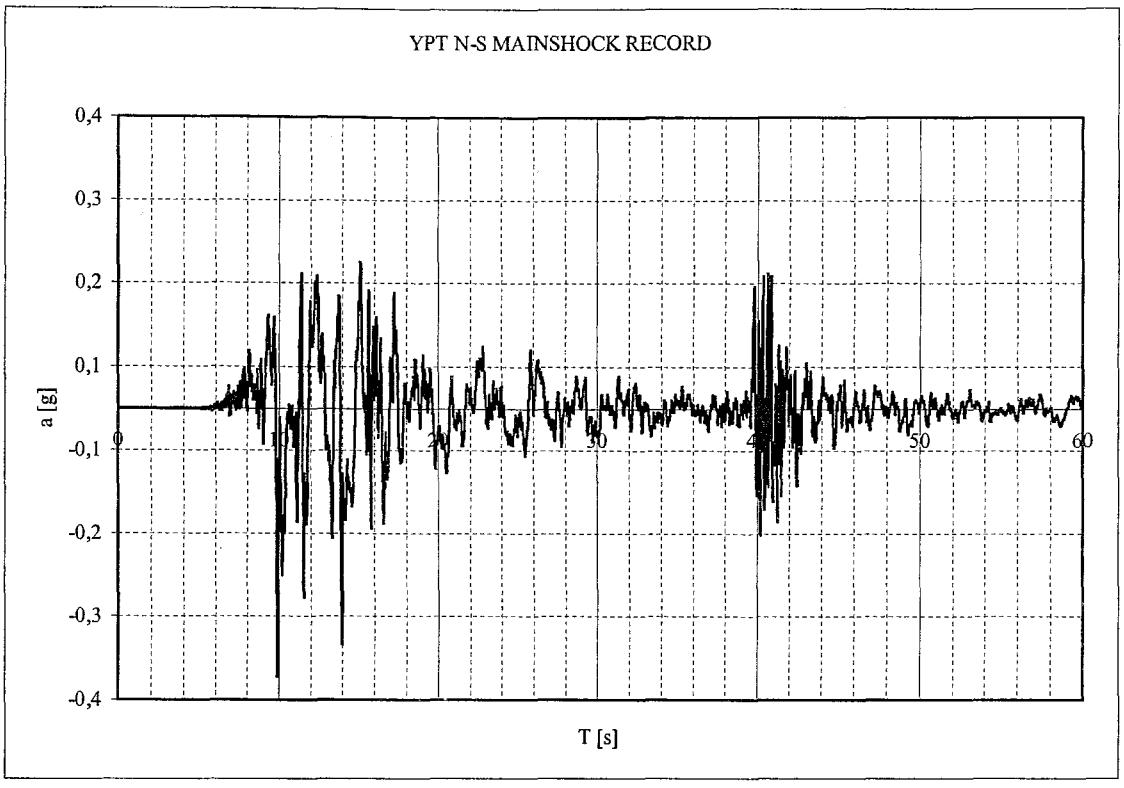

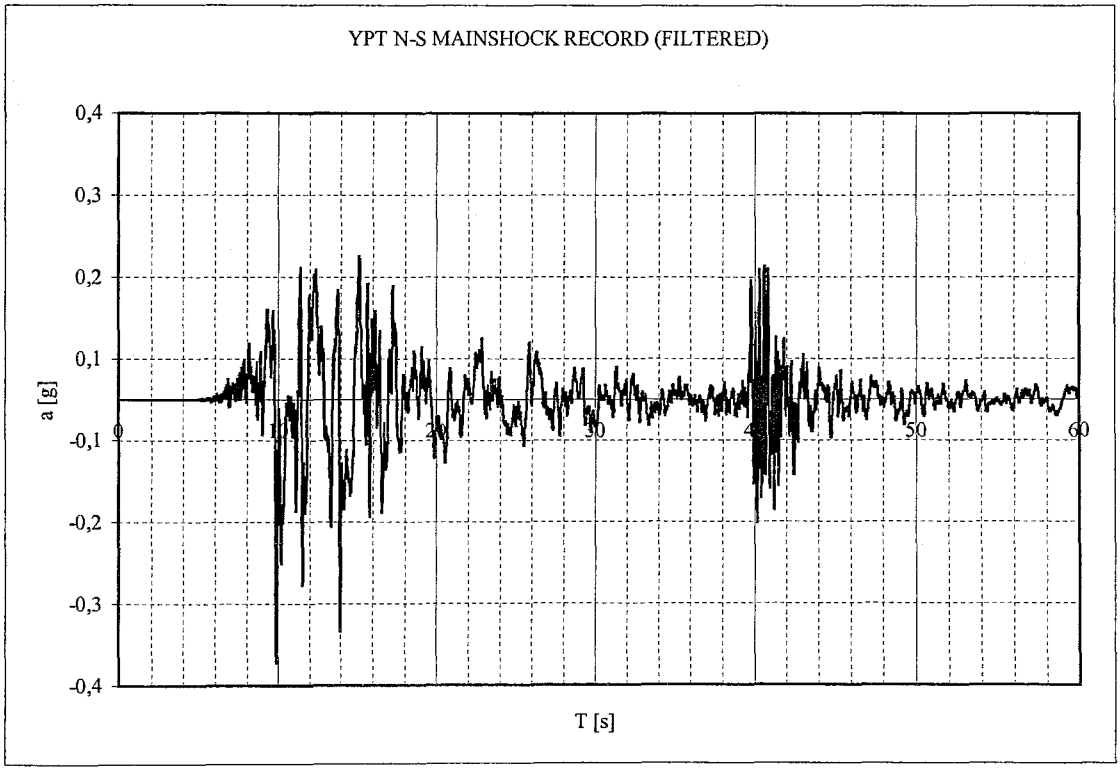

Figure 6-17 Before and After the Filtering of the Data YPT N-S (PGA = -0.32 g)

After the filtering and de-trending the data, it can be judged if the two data coincide with the desired SPA of the site as in the following:

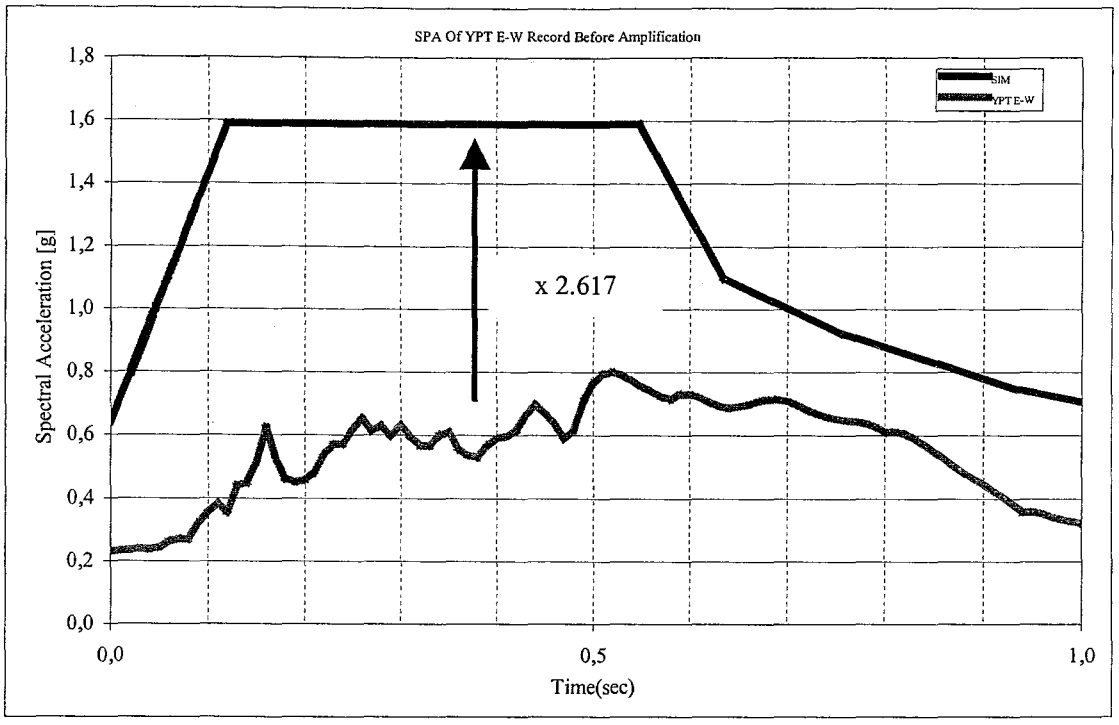

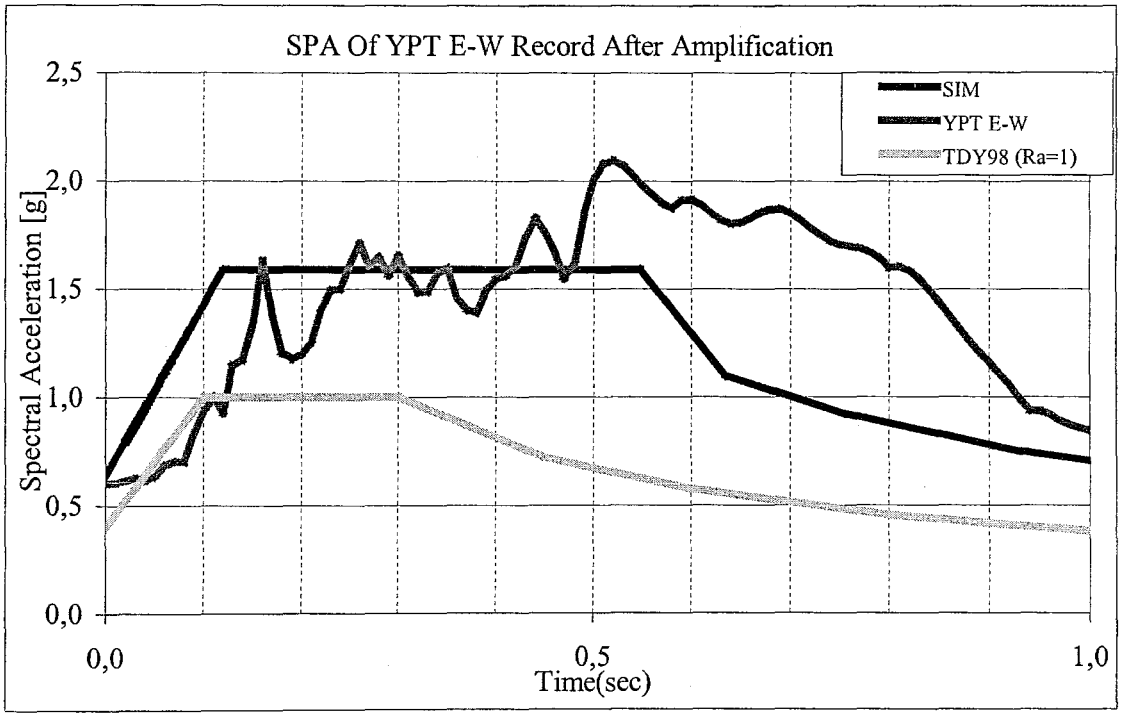

Figure 6-18Before & After the Amplification (x2.617) of SPA of YPT E-W Data

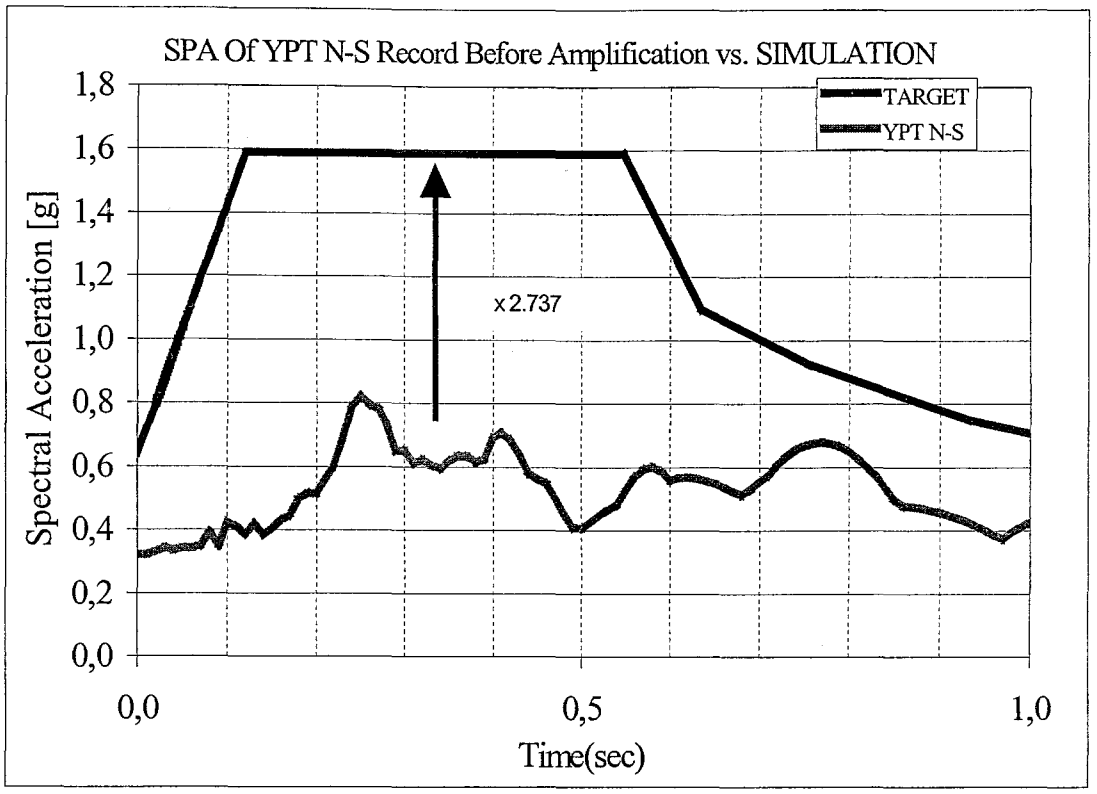

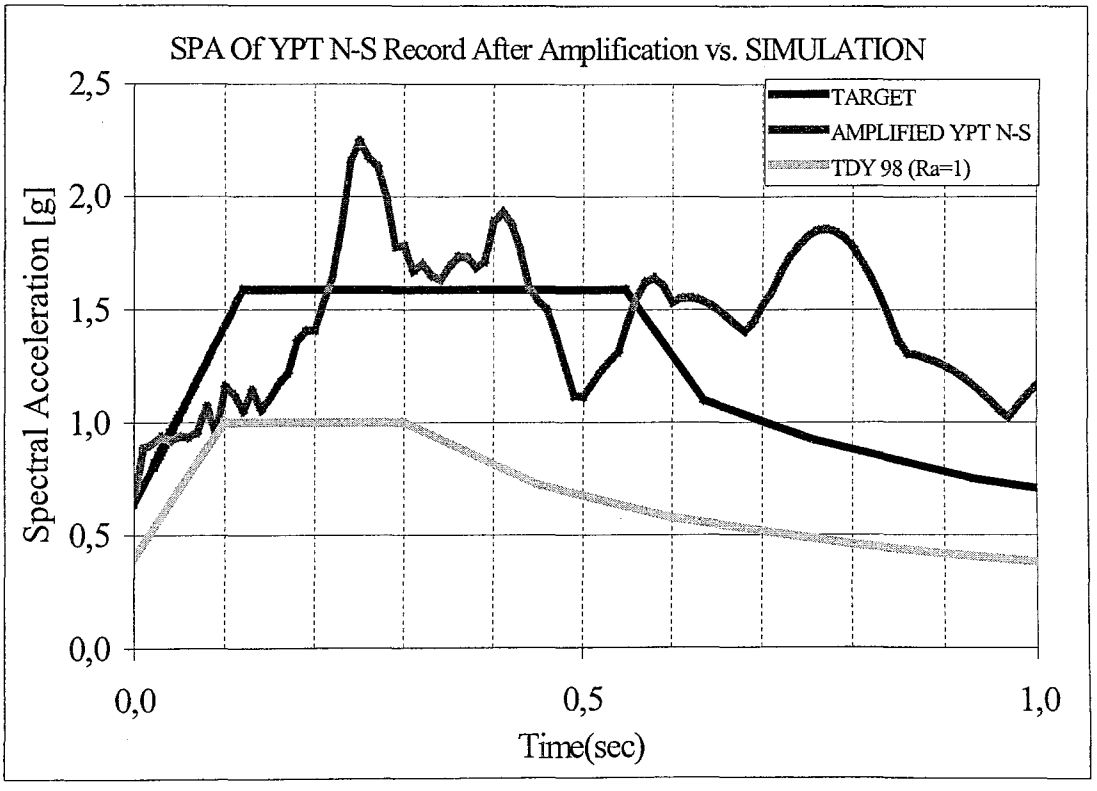

Figure 6-19Before & After the Amplification (x2.737) of SPA of YPT N-S Data

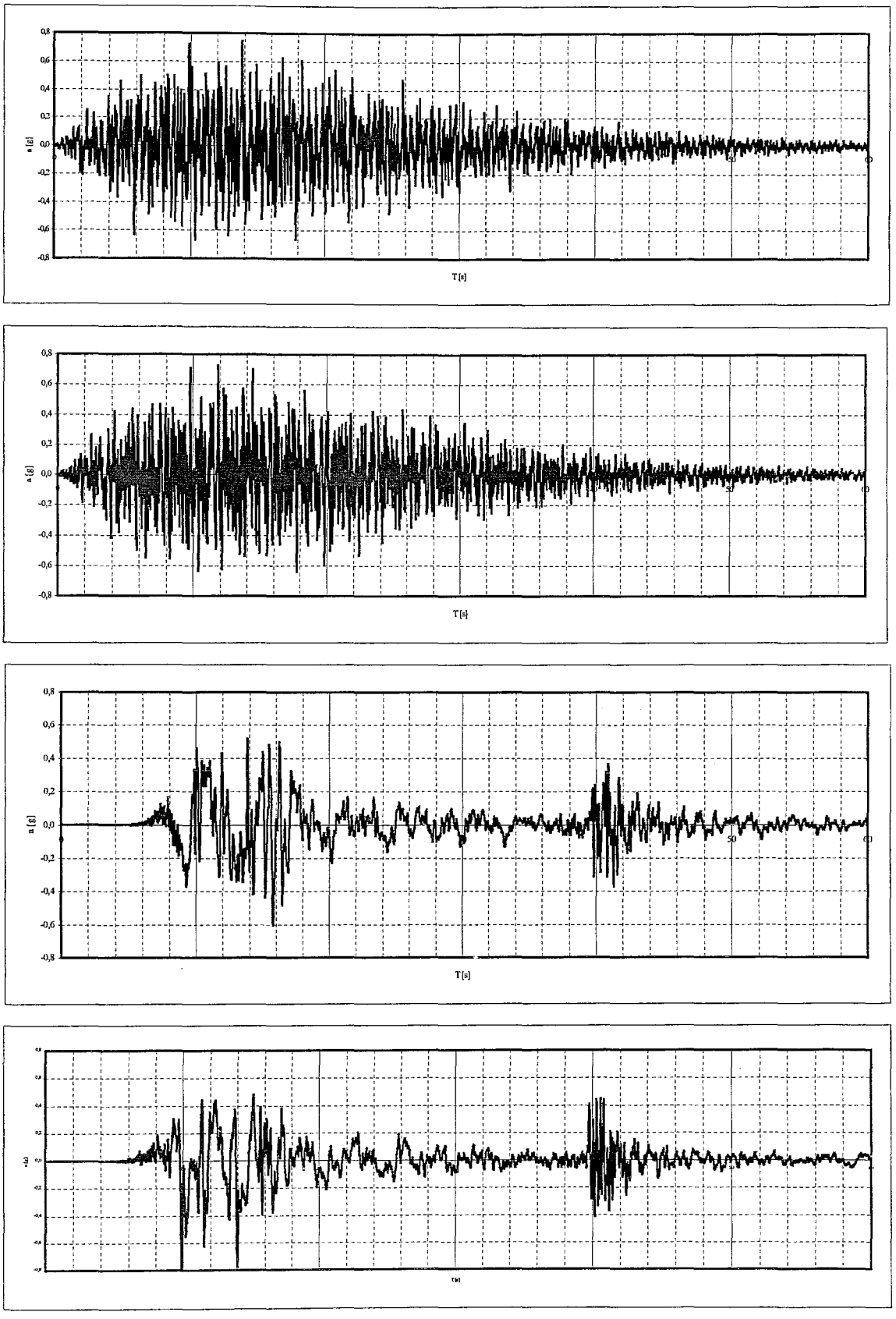

Figure 6-20 The Records SIMULATION 1, 2, YPT E-W and YPT N-S

7. RESULTS

7.1. Lateral Spreading Analysis

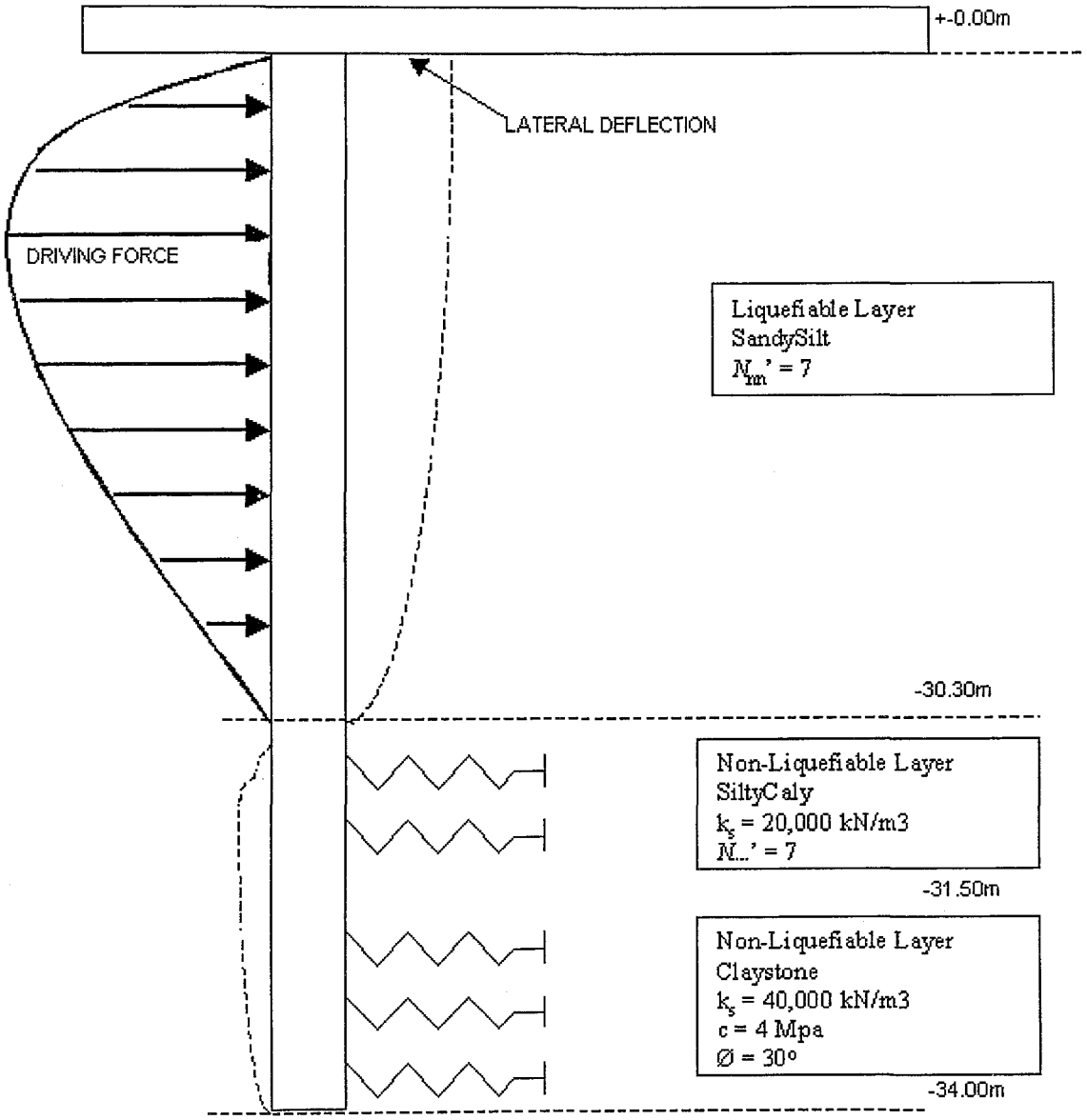

Figure 7-1 Schematic Illustration of the Lateral Spreading Model

The total lateral displacement was found to be 72 cm in the analysis. When this displacement is applied to the soil layer, which is between the pile and the liquefaction-induced driving force, the stress distribution is illustrated below.

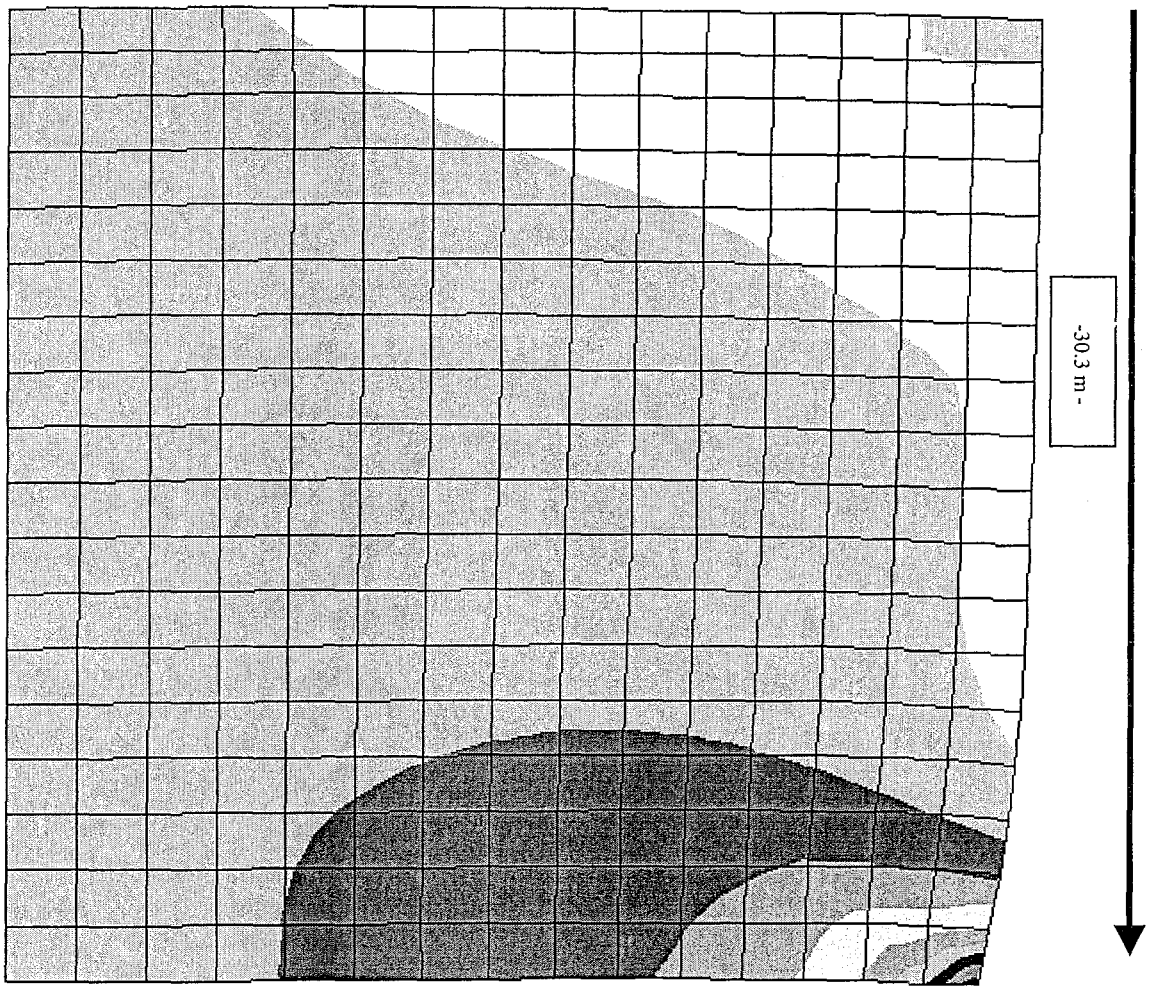

Figure 7-2 Stress Diagram of the Soil due to the Liquefaction-Induced Lateral Displacement towards to the Pile Group

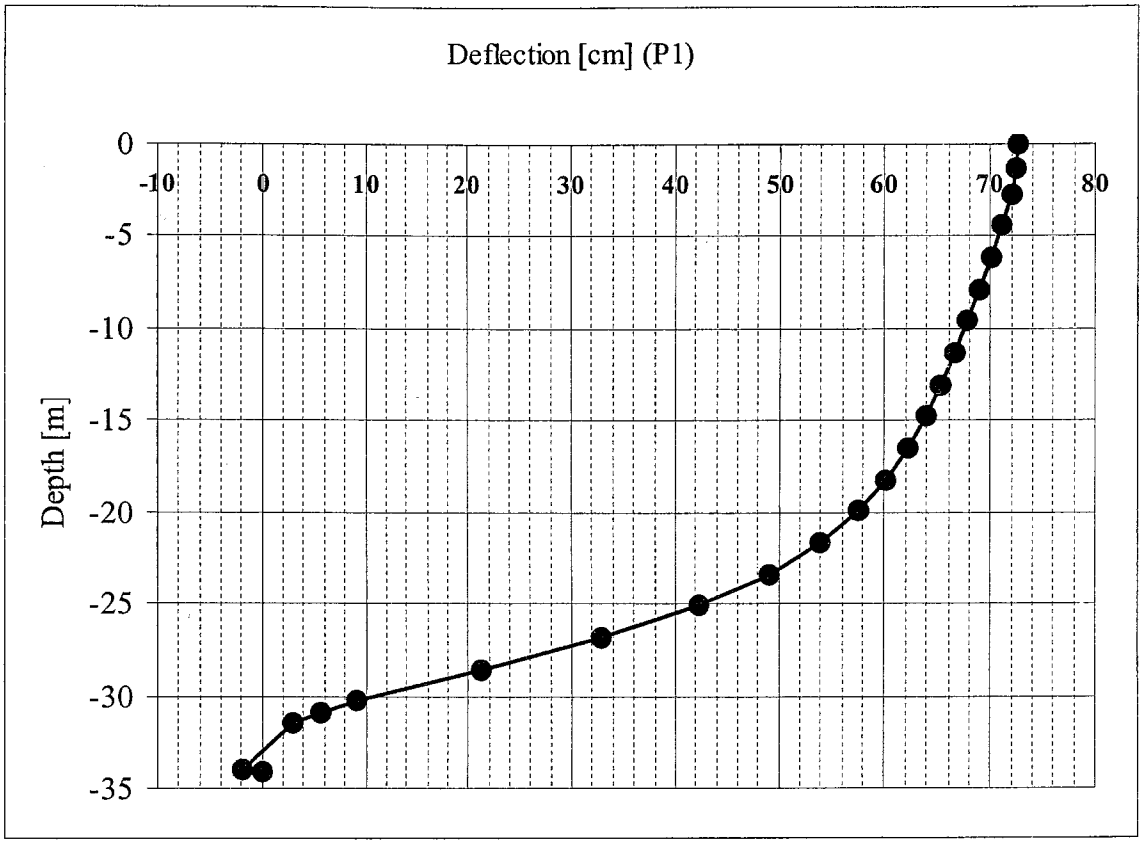

Figure 7-3 Lateral Spreading-Induced Deflection Curves of the Piles

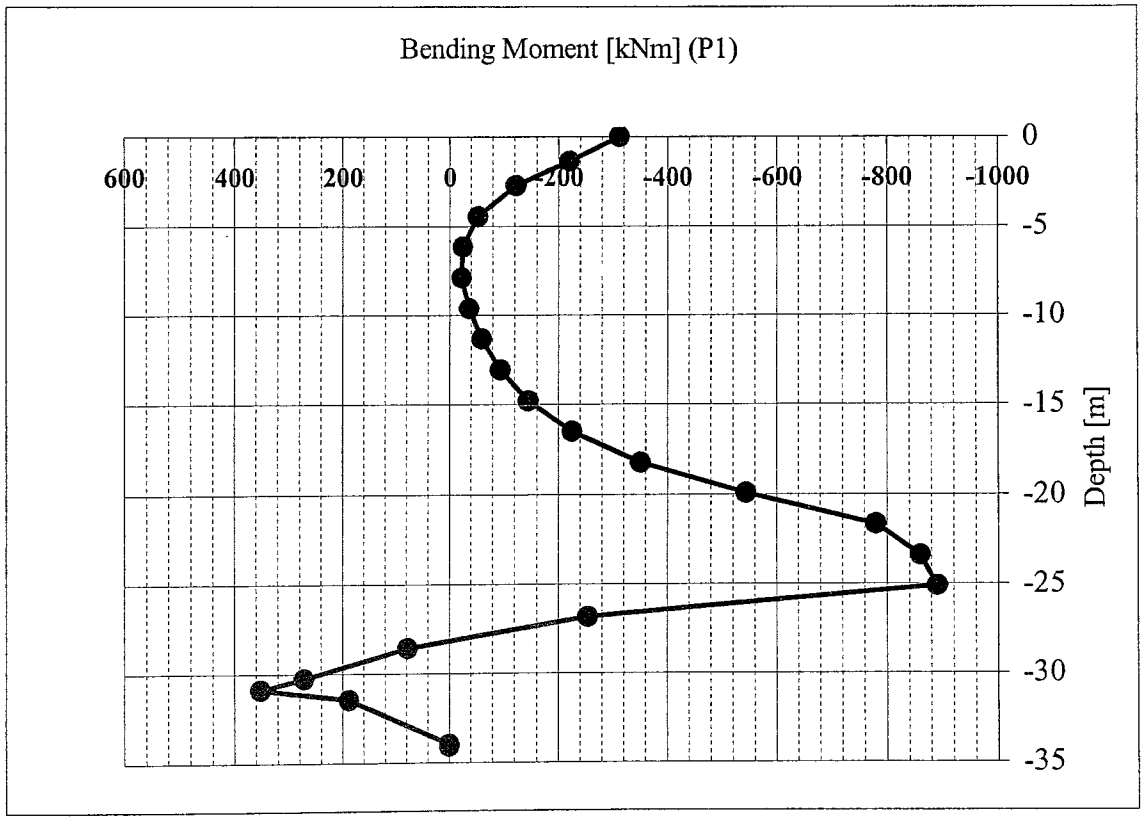

Figure 7-4 Lateral Spreading-Induced Bending-Moment Curves of the Piles

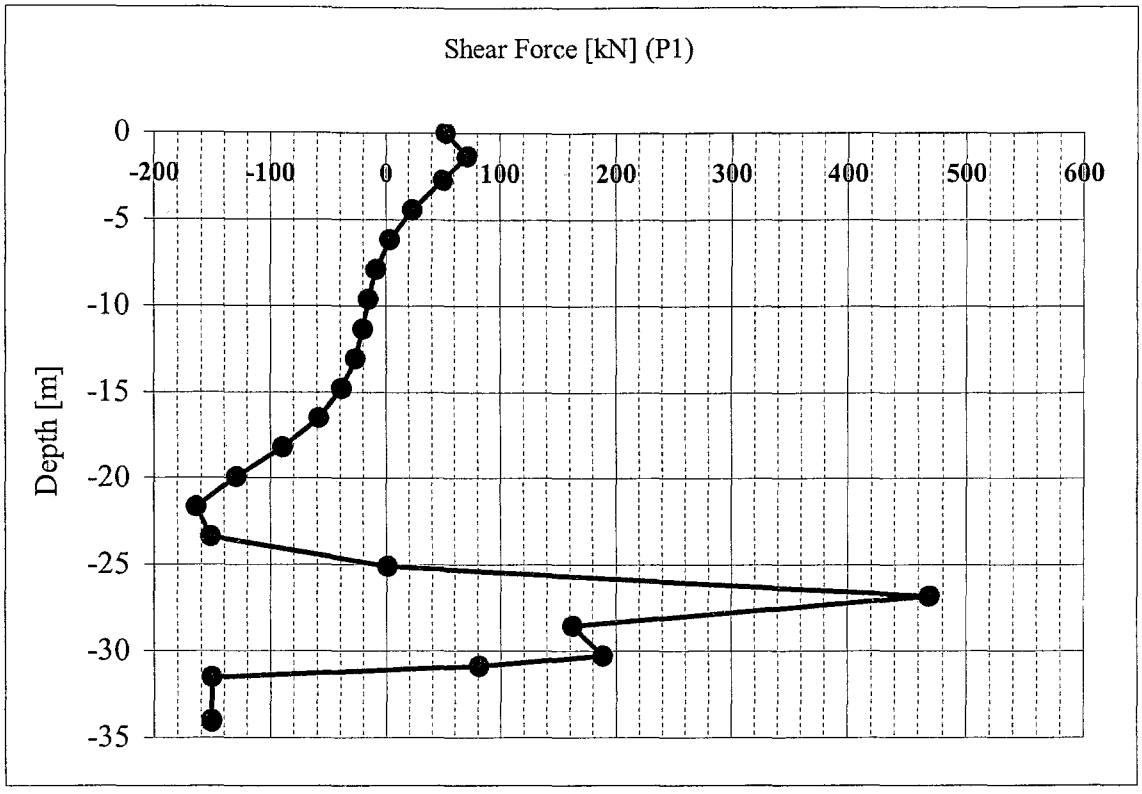

Figure 7-5 Lateral Spreading-Induced Shear Force Curves of the Piles

As seen in the figures above, the pile displacements and forces increase significantly near the spreading zone. The final computed lateral spreading-induced shear and bending moment values are as follows:

M = 1273 kNm ***V= 469 kN*** ***P = 553 kN (static)***

7.2. Spectral Analysis for TSC-98

For the sake of simplicity, not all of the 77 piles and their hinge forces will be shown. Instead, only one pile, which has the maximum bending moment and also shear force, will be illustrated in this results section. To obtain the weakest pile, all the spectral analysis results are checked and their average forces and their standard deviations are illustrated in the table below:

NL-LINK	P	V2	V3	M2	M3
MAX	*-1201*	*-48*	*-38*	*-82*	*-111*
MIN	*-82*	*45*	*40*	*89*	*100*
AVG	*-841*	*-1*	*0*	*1*	*-2*
SIGMA	*97*	*28*	*24*	*37*	*44*
AVG+-SIGMA	*-744*	*27*	*25*	*39*	*43*
ABS(MAX)	**1201**	**48**	**40**	**89**	**111**

Table 7-1 Non-Linear Link Element Forces from Spectral Analysis Results

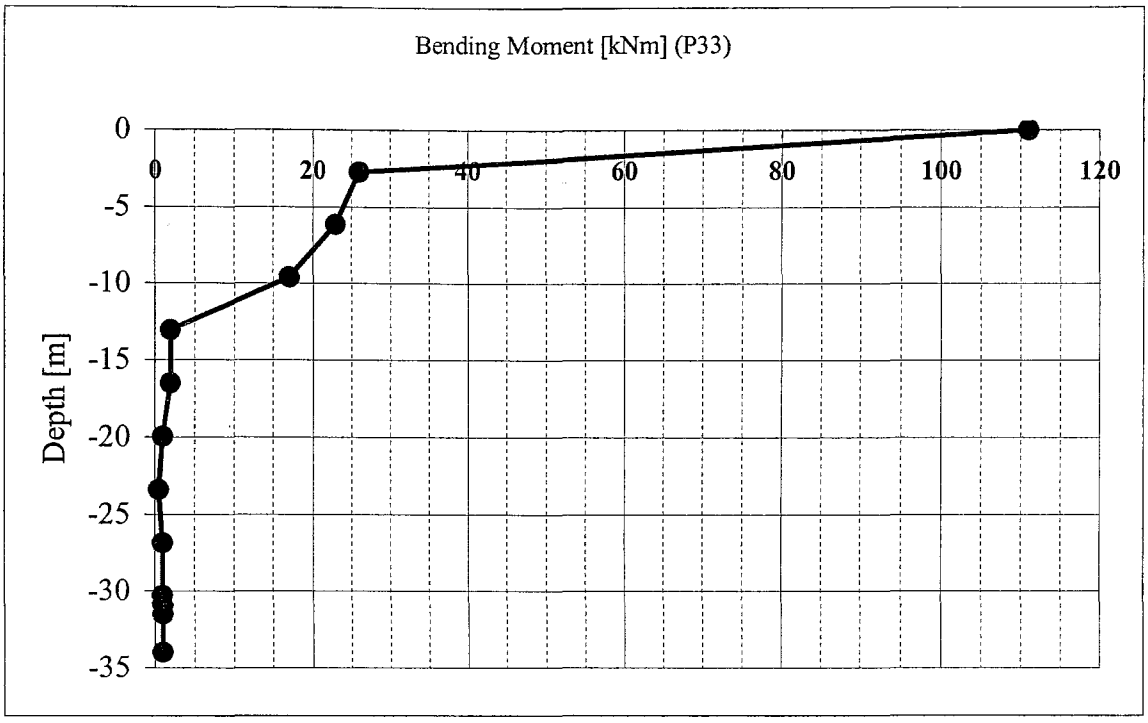

Figure 7-6Bending Moment & Depth Diagram According to TSC-98 (ID:NLL32)

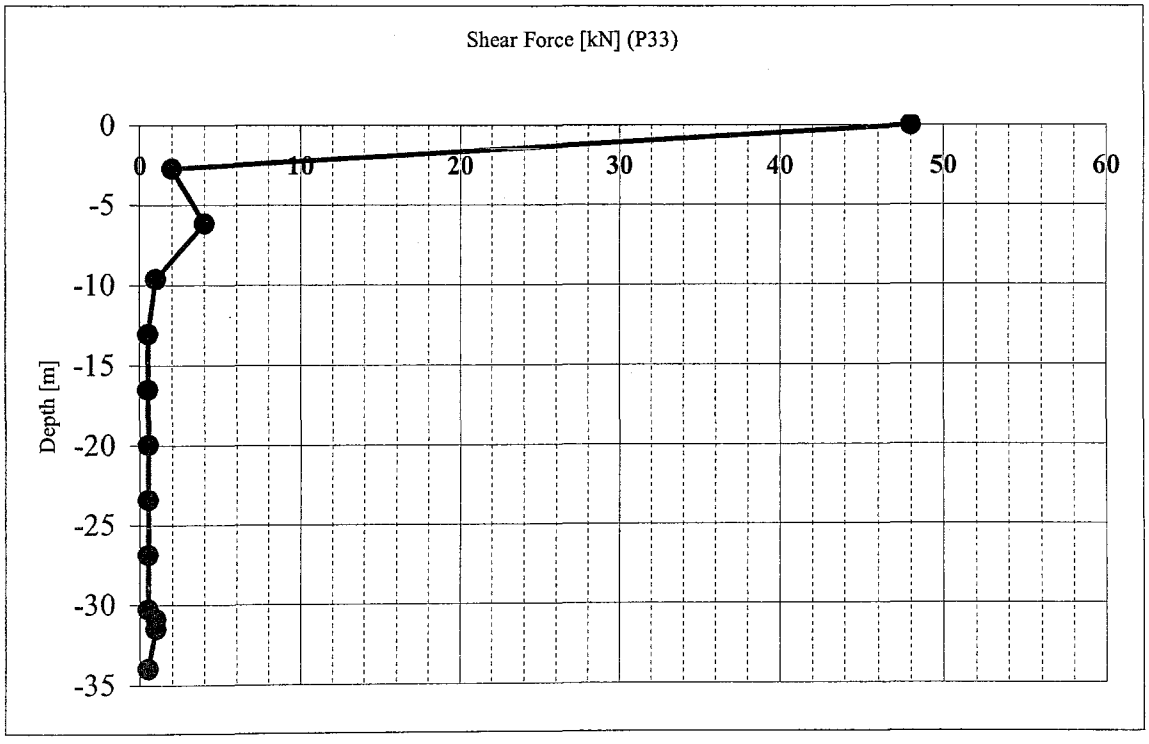

Figure 7-7 Shear Force & Depth Diagram According to TSC-98 (ID: NLL32)

M = 111 kNm ***V= 48 kN*** ***P = 825 kN (static)***

7.3. Time-History Analysis

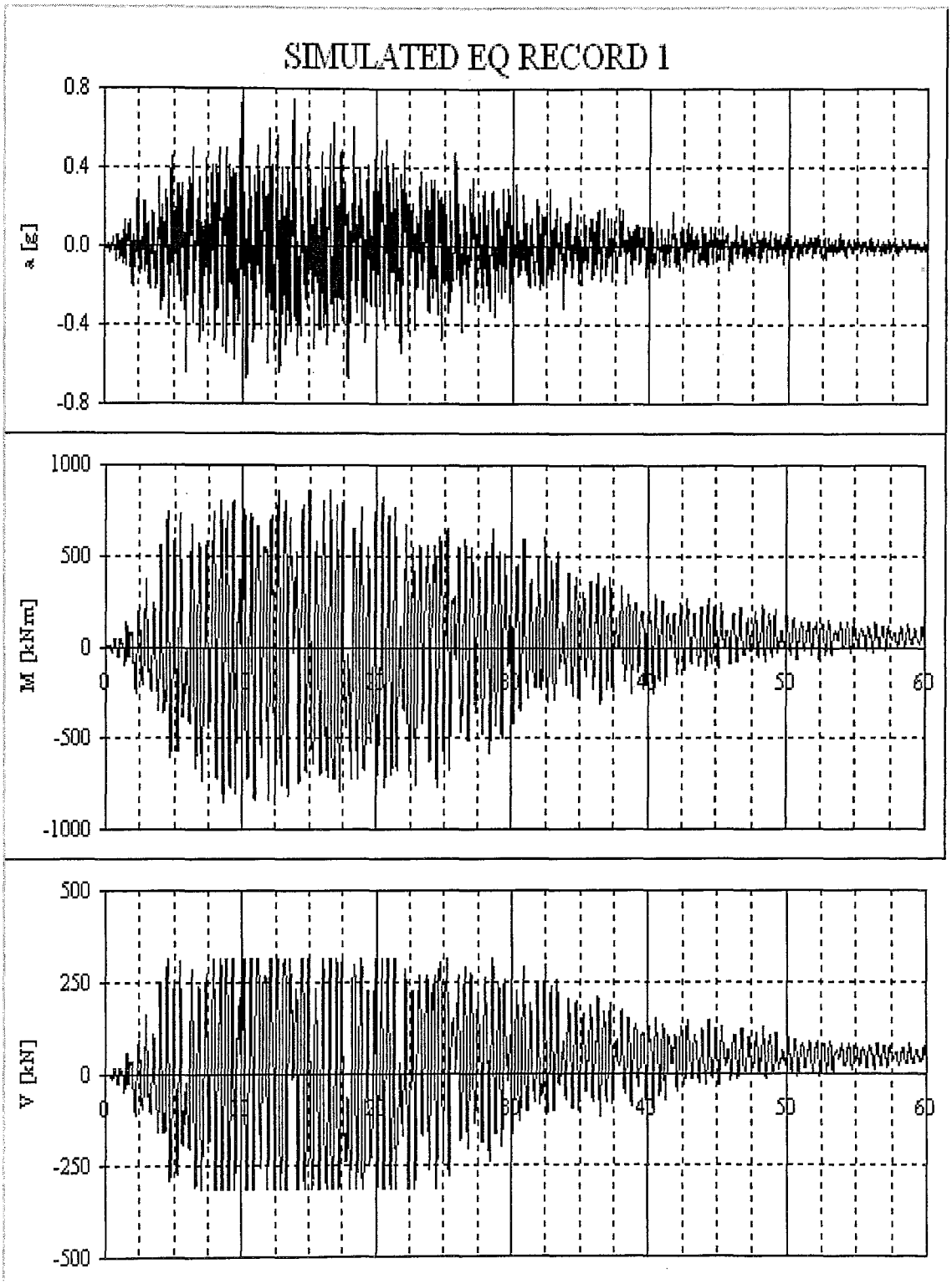

Figure 7-8 (1) Simulated Earthquake 1 (2) M33 (3) V22 (Element ID: 21)

$$\underline{M_{33} = 861\ kNm}$$

$$\underline{V_{22} = 317\ kN}$$

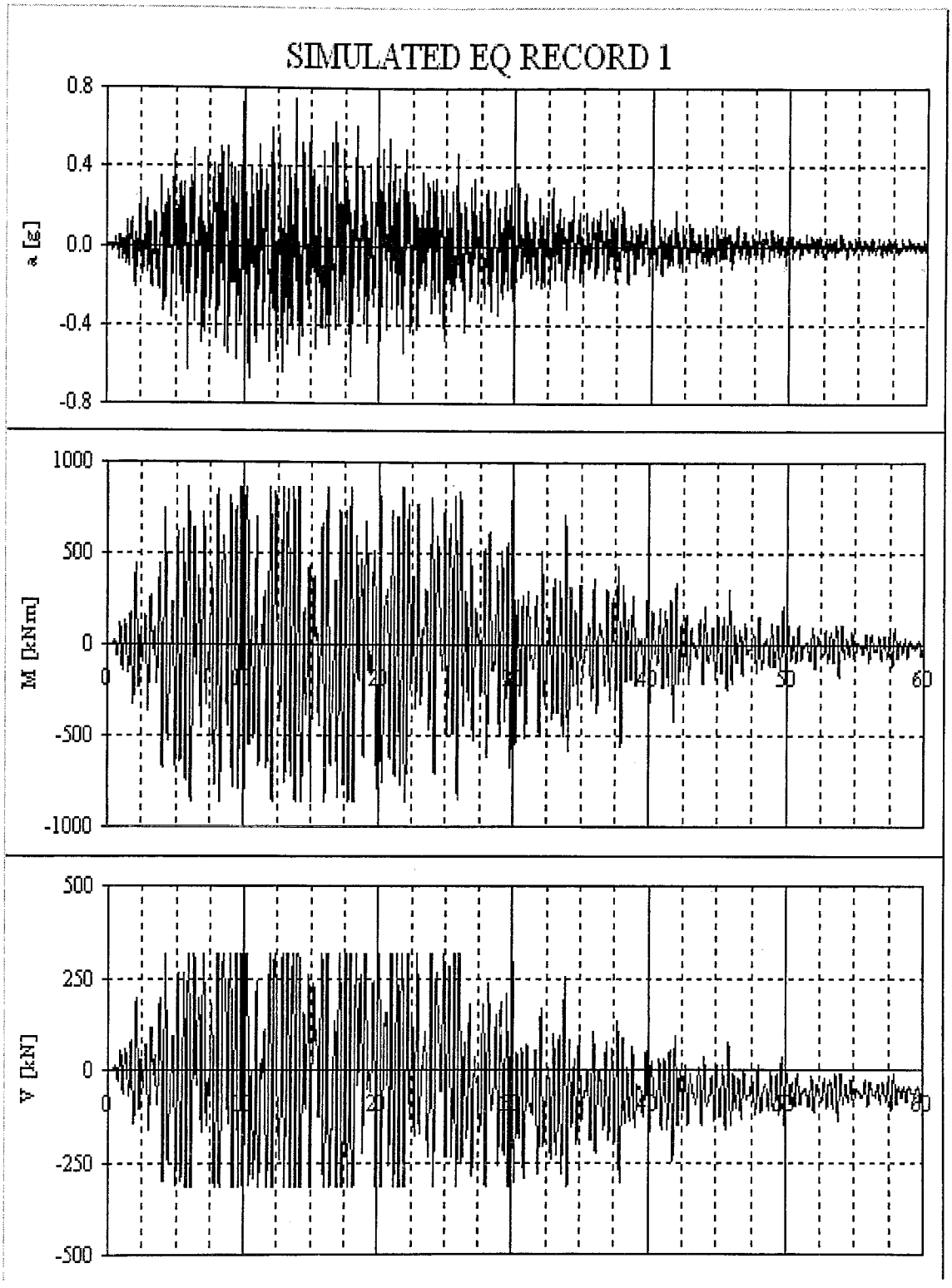

Figure 7-9 (1) Simulated Earthquake 1 (2) M33 (3) V22 (Element ID: 18)

$$\underline{M_{22} = 862\ kNm}$$

$$\underline{V_{33} = 317\ kN}$$

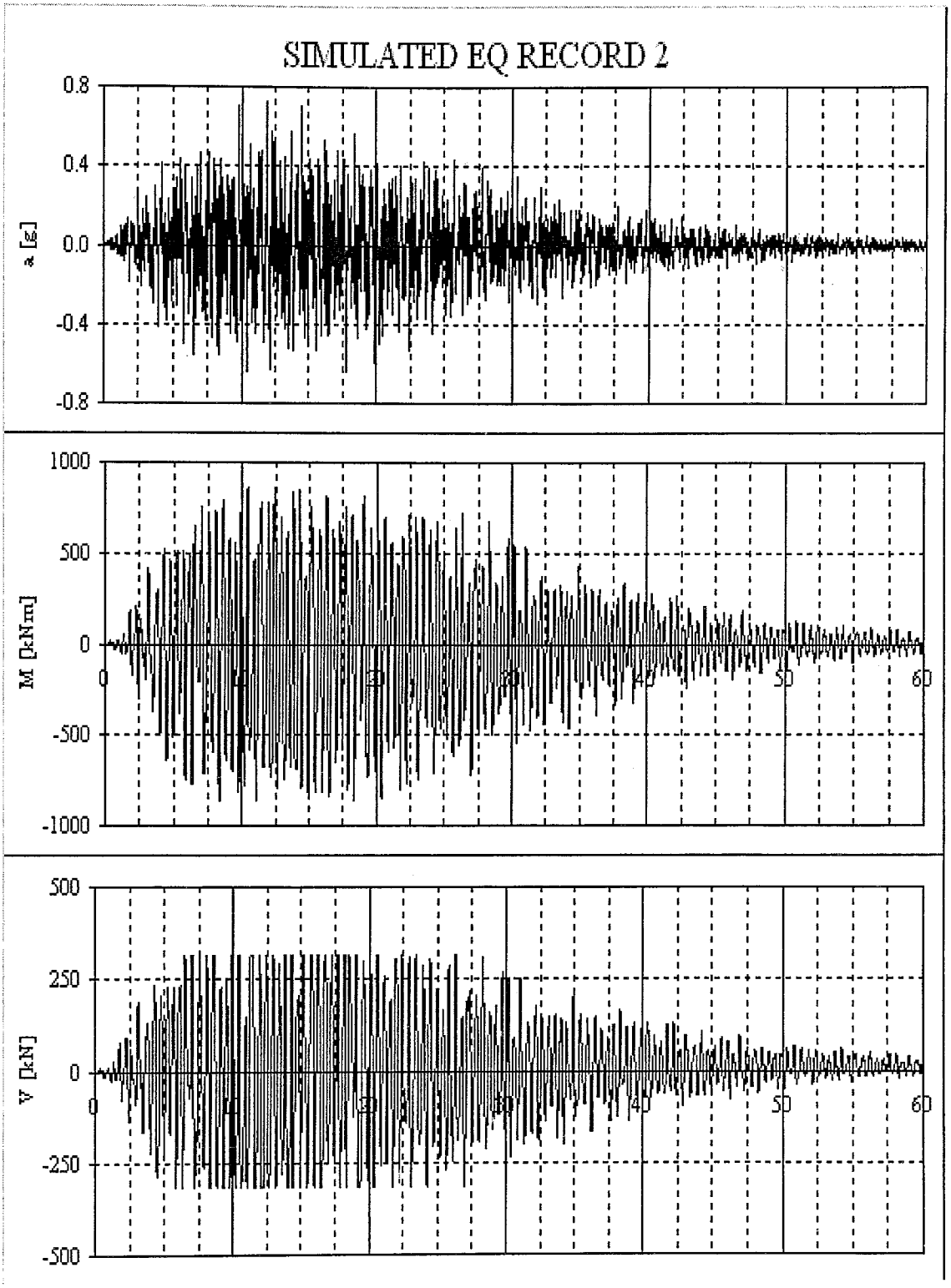

Figure 7-10 (1) Simulated Earthquake 2 (2) M33 (3) V22 (Element ID: 21)

$$\underline{M_{33} = 860\ kNm}$$

$$\underline{V_{22} = 316\ kN}$$

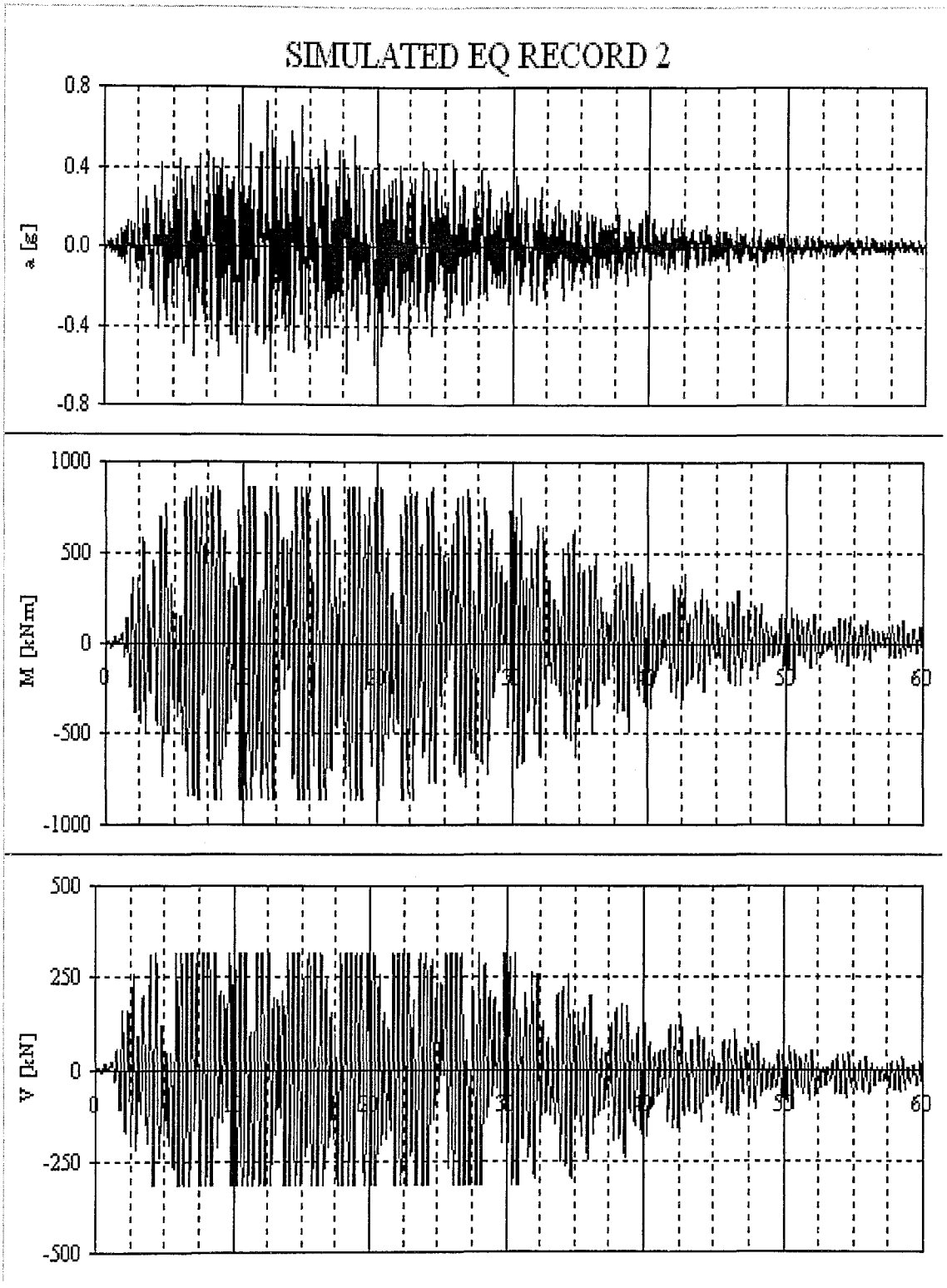

Figure 7-11 (1) Simulated Earthquake 2 (2) M33 (3) V22 (Element ID: 18)

$$\underline{M_{22} = 861\ kNm}$$

$$\underline{V_{33} = 317\ kN}$$

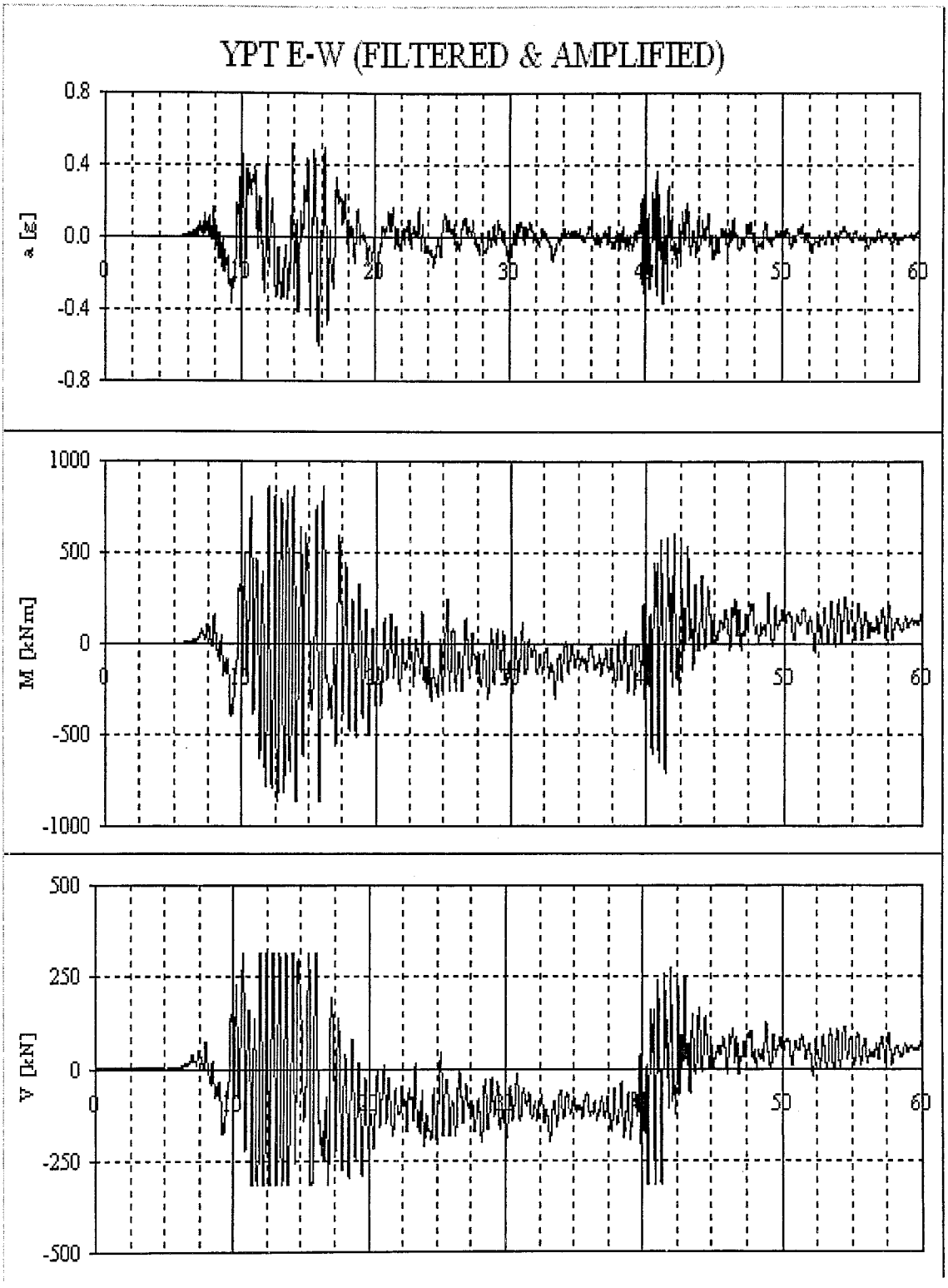

Figure 7-12 (1) YPT E-W (2) M33 (3) V22 (Element ID: 21)

$\underline{M_{33} = 861\ kNm}$

$\underline{V_{22} = 317\ kN}$

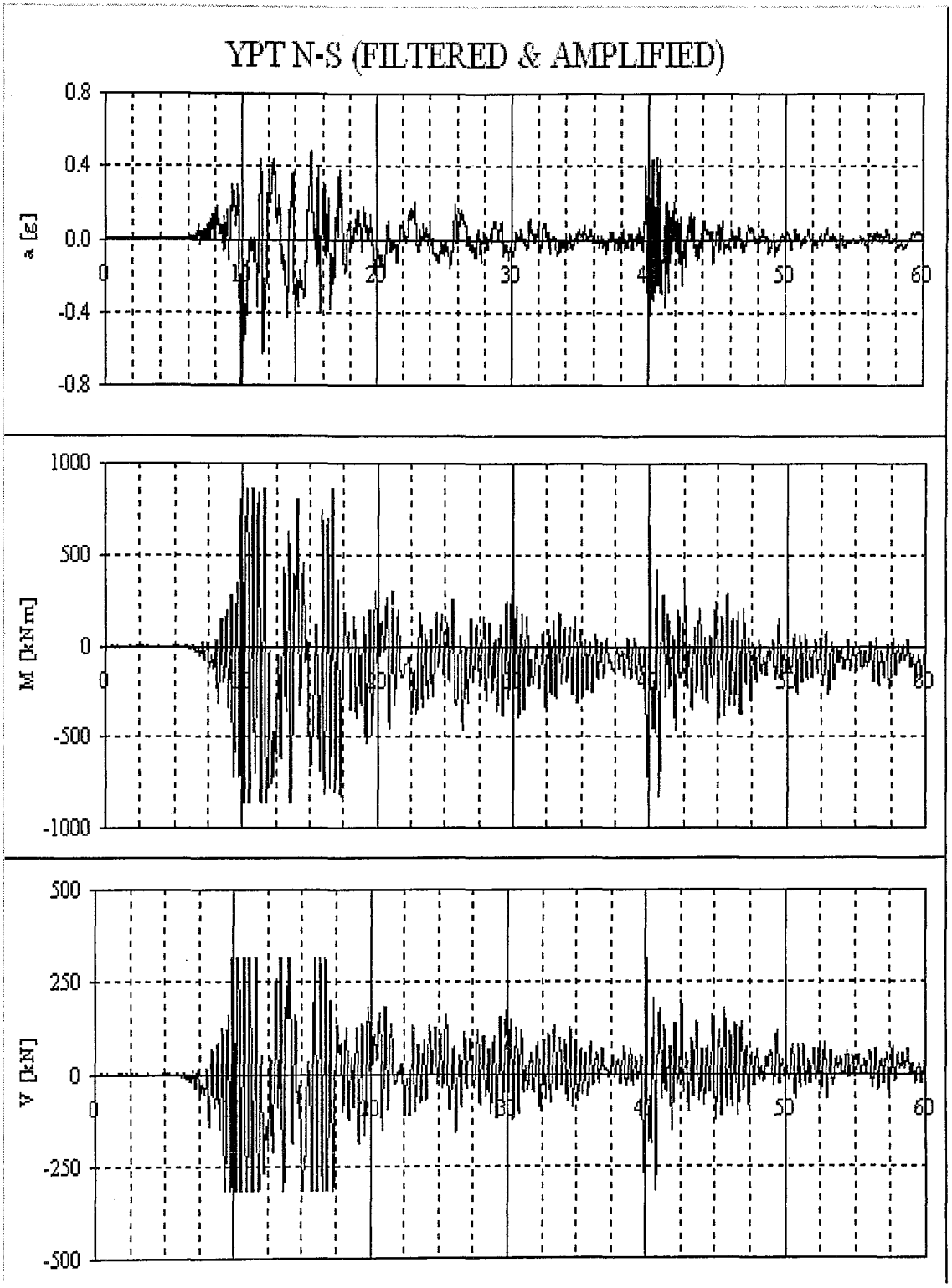

Figure 7-13 (1) YPT N-S (2) M33 (3) V22 (Element ID: 18)

$\underline{M_{22} = 862\ kNm}$

$\underline{V_{33} = 317\ kN}$

7.4. Comparison of the Results

	T.D.Y. 98 X-X	T.D.Y. 98 Y-Y	T-H SIM1 X-X	T-H SIM1 Y-Y	SHEAR CAPACITY
P [kN]	825	824	871	871	-
M [kNm]	111	89	861	862	-
V [kN]	48	40	317	317	908

	T-H SIM2 X-X	T-H SIM2 Y-Y	T-H YPT E-W X-X	T-H YPT N-S Y-Y	LATERAL SPRD.
P [kN]	871	871	871	871	553
M [kNm]	860	861	861	862	890
V [kN]	316	317	317	317	469

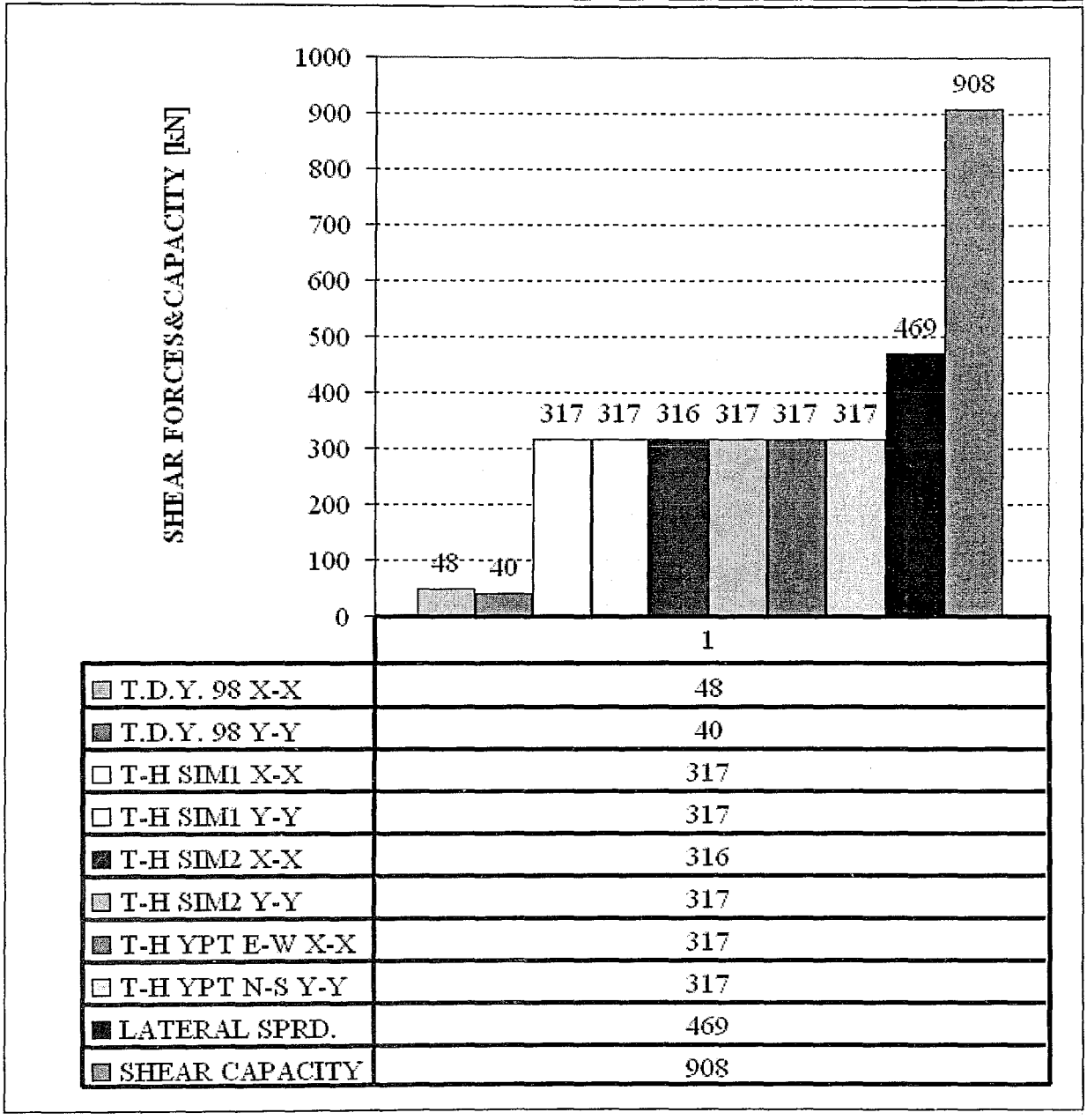

Table 7-2 The Shear Forces' Comparison Table of the Entire Analysis

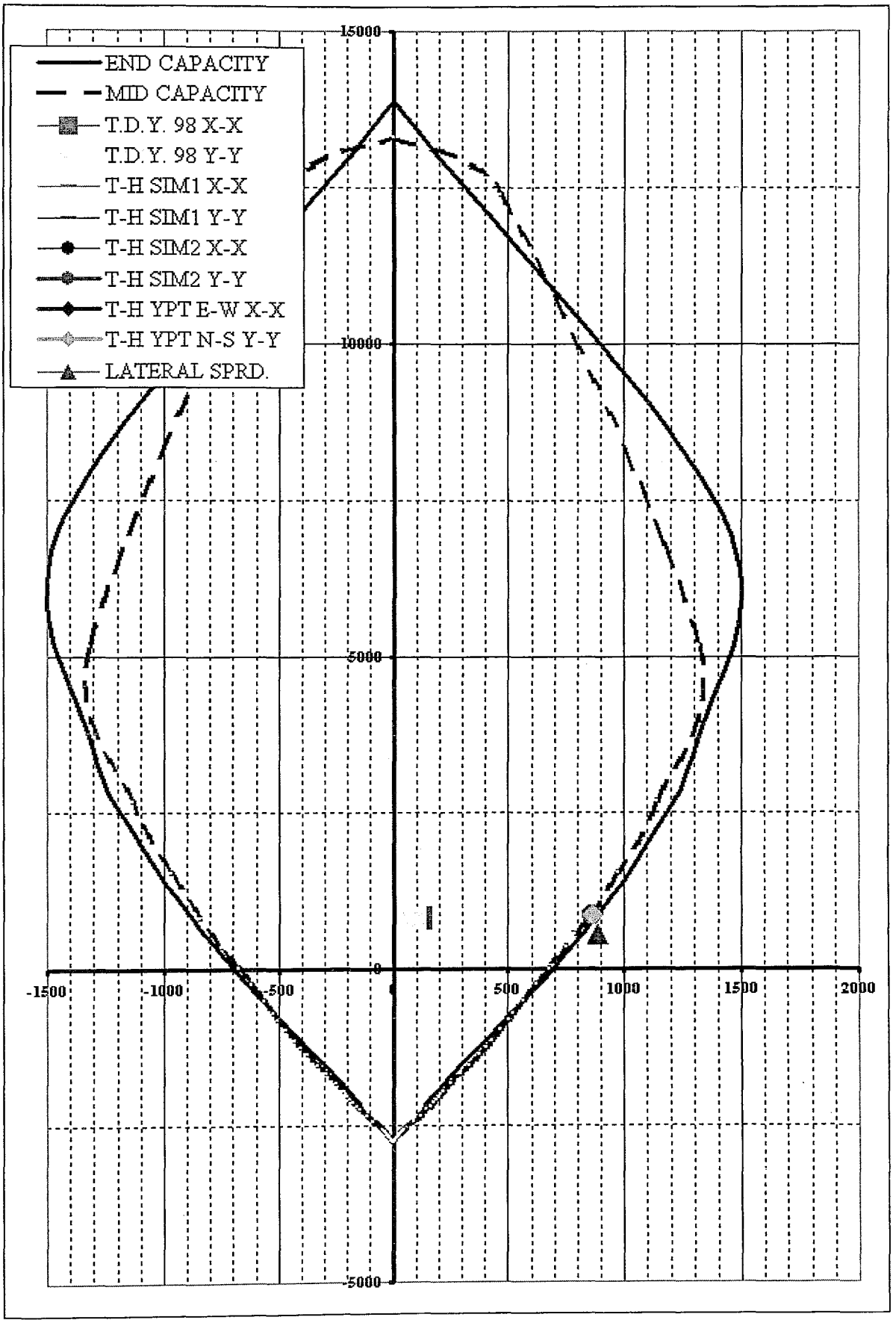

Table 7-3 The P-M Interactions' Comparison Table of the Entire Analysis

8. CONCLUSIONS

An analytical method for estimating the seismic response of piles by means of response spectra, time-history and lateral spreading analysis is presented. Results obtained from seismic evaluation of the pile groups at the site can be summarized as:

(1) A close estimation of liquefaction possibility of the site is evaluated from many empirical based methods, and the site is found likely to face liquefaction.

(2) Non-Linear Time-History and Lateral Spreading Analyses has shown that the piles may not be able to support the superstructure during a probable earthquake that has a moment magnitude of 7.5.

(3) Lateral Spreading demands extreme capacities from the pile groups. Thus, extra precautions must be considered to prevent the piles' failure. Increasing the quantity of piles or using much denser transverse reinforcement may cure the problem.

(4) The great distance between the results which are obtained from Time-History and Spectral Analyses for TSC-98 showed that while making an aseismic structure design within the vicinity of a fault line, the engineer must not be satisfied with only TSC-98 requirements and should amplify the PGA values (A_o) for the desired site according to the regional simulations with his judgment.

REFERENCES

1) Bowles, Joseph E., *Foundation Analysis and Design* (1990)

2) Kramer, Steven L., *Geotechnical Earthquake Engineering* (1996)

3) Chopra, Anil K., *Dynamics of Structures* (1995)

4) Priestly, M .J. N., *Seismic Design and Retrofit of Bridges* (1996)

5) Turkish Seismic Code, *Specification for Structures to be Built in Disaster Areas* (1998)

6) Turkish Standards 500, *Requirements for Design and Construction of Reinforced Concrete Structures* (2000)

7) Alpay, Hasan E., *Geotechnical Report of Diler Iron and Steel Industry Inc.* (1998)

8) Erdik, Mustafa Ö., *Earthquake Hazard in Marmara Region* (2003)

9) Seed, H.B. and Idriss, I.M., *Simplified Procedure For Evaluating Soil Liquefaction Potential* (1971)

10) Seed, H.B. and Idriss, I.M., *Evaluation of Liquefaction Potential Using Field Performance Data* (1983 - 1985)

11) Seed, H. B. and Harder, L. F., Jr., *Determination of Penetration Resistance for Coarse-Grained Soils Using the Becker Hammer Drill* (1986)

12) Seed, H. B., Harder, L. F., *Influence of SPT Procedures in Soil Liquefaction Resistance Evaluation* (1990)

13) American Society of Civil Engineers, *Journal of Geotechnical Engineering* (1996)

14) Bartlett, S.F. and Youd, T.L., *Empirical Analysis of Horizontal Ground Displacement Generated by Liquefaction-Induced Lateral Spread* (1992)

15) Bartlett, S.F. and Youd, T.L., *Empirical Prediction of Liquefaction-Induced Lateral Spread* (1995)

16) Robertson, P. K. et al., *SPT-CPT Correlations* (1983)

17) Robertson, P. K. and Fear, C. E., *Liquefaction of Sands and its Evaluation* (1996)

18) Hamada et al., *Report for the Association for the Development of Earthquake Prediction* (1986)

19) JNCDI (Japan Nuclear Cycle Development Institute), *Physical Rock Properties Used for Design Report A-03* (1999)

20) (NZSEE) New Zealand Society for Earthquake Engineering Inc., USGS and Steinbrugge, *Collection of Earthquake Damage Photos in Turkey* (1999)

21) Departments of The Army and The Air Force, *Soils and Geology Procedures for Foundation Design of Buildings and Other Structures* (1983)

22) Ishihara, K. and Takeuchi, M., *Flow Failure of Liquefied Sand in Large Scale Shaking Tables* (1991)

23) Lang B., Lang P., *www.mininglife.com* (2003)

24) NRC (National Research Council), *Publication* (1985)

25) Skempton A. W., *Standard Penetration Test Procedures and the Effects in Sand of Overburden Pressure, Relative Density, Particle Size, Aging, And Overconsolidation, Geotechnique* (1986)

26) Youd, T. L. and Noble, S. K., *Liquefaction Criteria Based on Statistical and Probabilistic Analyses* (1997)

27) Riggs, *Use of In-Situ Tests in Geotechnical Engineering* (1986)

28) Ishihara, K., *Stability of Natural Deposits During Earthquakes* (1985), *Liquefaction and Flow Failure During Earthquakes* (1993)

29) U.S. Army Corps of Engineers, *Evaluation of Embankment and Foundation Earthquake Resistance* (1986)

30) Stagg, K. G., and Zienkiewicz, D. C., *Rock Mechanics in Engineering Practice 2nd ed.* (1968)

1. **The sites SPT test's output data gathered from the borehole S3:**

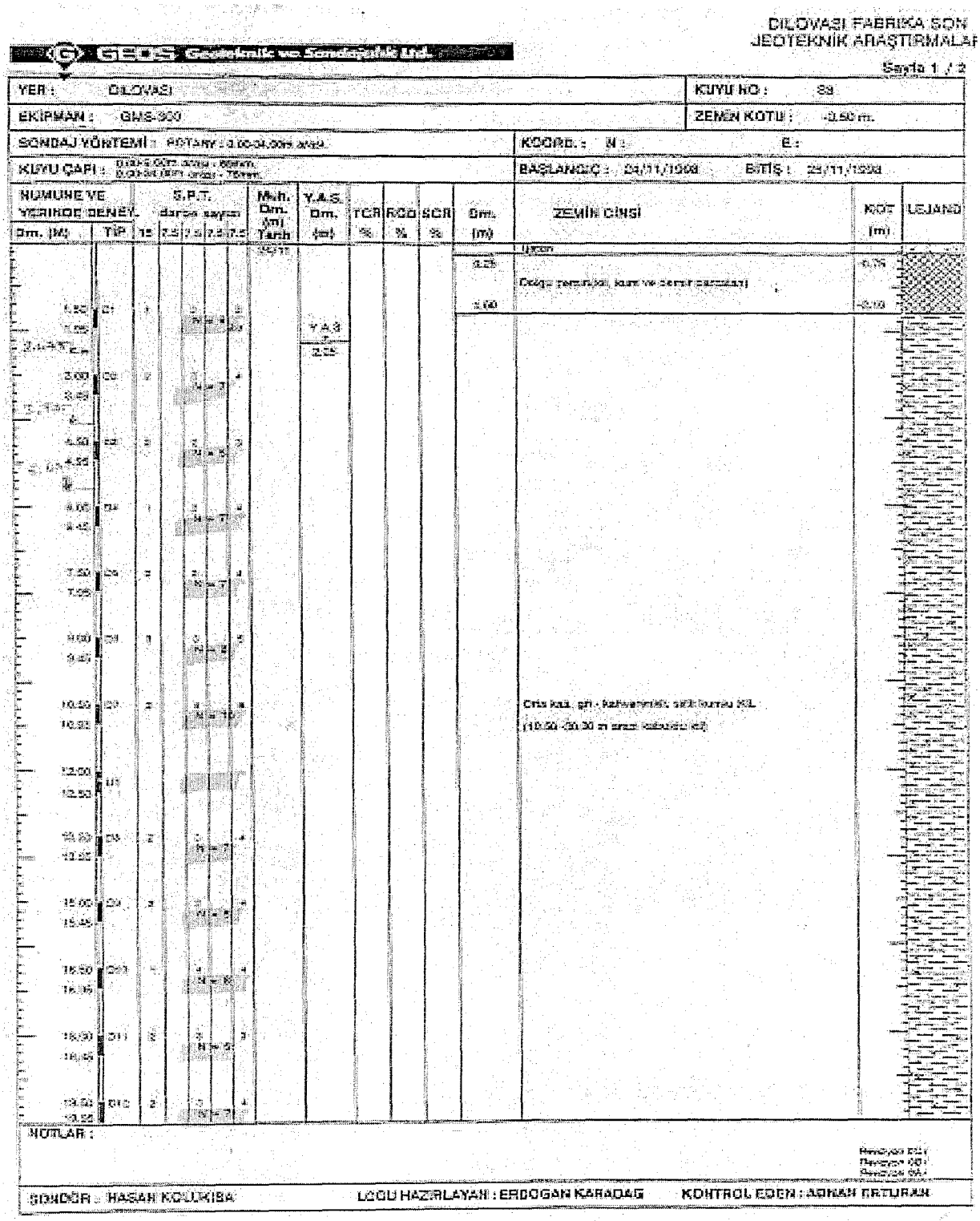

GEOS Geoteknik ve Sondajcılık Ltd.

YER : DİLOVASI	KUYU NO : S3
EKİPMAN : GMS-300	ZEMİN KOTU : -0.50 m.
SONDAJ YÖNTEMİ : ROTARY : 0.00-34.00m arası.	KOORD. : N : E :
KUYU ÇAPI : 9.00-34.00m arası - 76mm.	BAŞLANGIÇ : 24/11/1998 BİTİŞ : 25/11/1998

NUMUNE VE YERİNDE DENEY.		S.P.T. darbe sayısı					Muh. Drn. (m)	Y.A.S. Drn.	TCR	RQD	SCR	Drn.	ZEMİN CİNSİ	KOT	LEJAND
Drn. (M)	TİP	15	7.5	7.5	7.5	7.5	Tarih	(m)	%	%	%	(m)		(m)	
							24/11								
21.00	D13	2		2		4									
21.45				N = 6											
22.50	D14	3		3		3									
22.95				N = 6											
24.00	D15	2		3		3									
24.45				N = 6											
25.50	D16	3		3		3							Orta katı, gri - kahverenkli, siltli kumlu KİL		
25.95				N = 6									(10.50 -30.30 m arası kabuklu kil)		
27.00	D17	3		4		4									
27.45				N = 8											
28.50	D18	2		3		5									
28.95				N = 8											
30.00	D19	5		5		10									
30.45				N = 15											
												30.30		-30.80	
													Katı kıvamlı, gri-kahverenkli siltli KİL		
												31.50		-32.00	
32.00															
									15	0			Yeşil renkli, orta-ileri derecede ayrışmış KİLTAŞI		
												34.00	SONDAJ BİTİMİ	-34.50	
34.00															

NOTLAR :

Revizyon 0C/
Revizyon 0B/
Revizyon 0A/

SONDÖR : HASAN K@LUKISA LOGU HAZIRLAYAN : ERDOGAN KARADAG KONTROL EDEN : ADNAN ERTURAN

2. **The earthquake's SPA determination by piece-wise exact method with data filtering MATLAB code:**

```
**************************************************************************
clear all;
close all;

load C:\WINDOWS\Desktop\YPT_EW.txt;
dt=0.005;       % dt!!!!!
xx=YPT_EW;% g "mg, m/s^2"
x=xx*1;         % amplification factor

high=bpfilter(x,dt,52);                 % low-pass filter (52Hz.)
low=bpfilter(high,dt,0.1,'high');       % high-pass filter (0.1Hz.)

w=dtrend(high);                         % trending the data from noises
udd=w;
t=dt*(1:length(udd));

for p=1:100;
   T(p)=0.01*p;
   ksi=0.05;
   w=2*pi/T(p);
   wd=w*(sqrt(1-ksi^2));
   A11=( cos(wd*dt) + (ksi*w/wd)*sin(wd*dt) ) *exp(-ksi*w*dt);
   A12=( (1/wd)*sin(wd*dt) ) *exp(-ksi*w*dt);
   A21=( -w^2*A12 );
   A22=( cos(wd*dt) - (ksi*w/wd)*sin(wd*dt) ) *exp(-ksi*w*dt);
   D11=( A11-1 ) / w^2;
   D12=( A12-2*ksi*w*D11-dt ) / (w^2*dt);
   D21=( -A12 );
   D22=( D11/dt );

   ud(1)=0;
```

```
    u(1)=0;
    for k=1:length(udd)-1;
      ud(k+1)=A21*u(k)+A22*ud(k)+D21*udd(k)+D22*(udd(k+1)-udd(k));
      u(k+1)=A11*u(k)+A12*ud(k)+D11*udd(k)+D12*(udd(k+1)-udd(k));
    end
    Sd(p)=max(abs(u))*981;          % cm
    TT(p)=0.01*p;                   % *****
    Sv(p)=max(abs(u))*w*981;        % cm/s
    Sa(p)=max(abs(u))*w*w;          % g
end

Sa(1)=max(abs(udd));                % g
% subplot(3,1,3)
% plot(TT,Sd,'b')
% ylabel('Sd (cm)')
% grid
% subplot(3,1,2)
% plot(TT,Sv,'b')
% grid
% ylabel('Sv (cm/s)')
% subplot(3,1,1)
plot(TT,Sa,'b')
grid
ylabel('Sa (g)')
xlabel('T (s)')

gtext('YPT EW Spectral Acceleration For Damping Ratio = 0.05')
*****************************************************************
```

3. Shaft Program Output For Ø Piles